NTNU – Trondheim
Norwegian University of
Science and Technology

Synthesis of a Novel Tocopherol/Carotenoid Derivative

Marius Myreng Haugland

Chemistry

Supervisor: Vassilia Partali, IKJ
Co-supervisor: Richard Sliwka, IKJ

Norwegian University of Science and Technology
Department of Chemistry

Acknowledgements

I would like to thank my supervisor, professor Vassilia Partali, for her guidance and patience throughout the carrying-out of this work. Thank you for always being available, for your concern and for every pat on my back when things did not go well. I am also very grateful to my co-supervisor, dr. Hans-Richard Sliwka, for extremely rapid and thorough proofreading.

This work would not be the same, had it not been for the help of my fellow students and lab colleagues. I would like to thank Truc Mong Vo, Esther Blijleven, and Ph.D. candidate Asma Zaidi for all their encouragement and constructive suggestions. I am extra thankful to Ph.D. candidates Muhammad Zeeshan and Eugenia Sandru for their generous practical and theoretical assistance.

I would also like to thank my friend head engineer dr. Susana Villa Gonzalez for running MS analyses, for generous help with spectrum analysis and for all her cheer-up peptalks. I am also obliged to thank my friends Håkon and Ragnvald for their assistance with LaTeX.

It is a great pleasure to thank all my dear friends, too numerous to mention by name, for their encouragement during the course of this work. Thank you for all your smiles and hugs and for believing in me. Special thanks go to Erik and Stian for taking care of me during the hectical finishing stage of the project. And last, but not least, I would like to thank my family for their unconditional love and support. I could not have done this without you.

Marius Myreng Haugland
Trondheim, May 2012

Sammendrag

Målet med denne oppgaven er å syntetisere et tokoferol/karotenoid-derivat (**1**, figur I). Dette nye antioksidant-derivatet antas å utvise synergisme mellom sine kromanol- og polyen-bestanddeler. Syntesen av **1** ble fullført til og med den siste forløperen **12**.

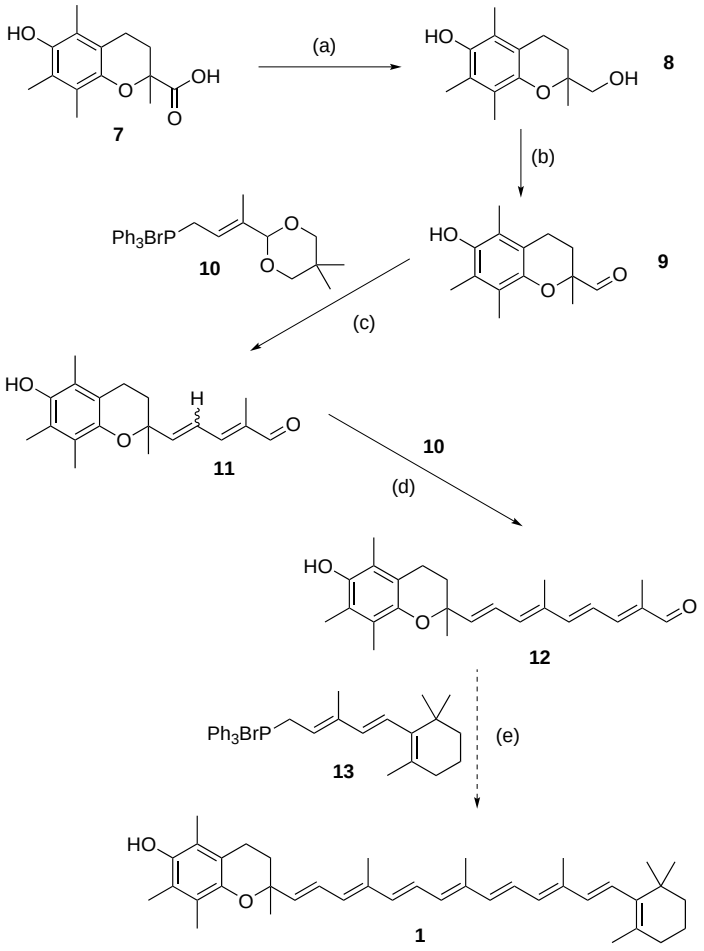

Figur I: Syntese av **1**.

Kommersielt tilgjengelig Trolox (**7**) ble redusert med Red-Al® til **8** (trinn *a*) med 95% utbytte. Kromanol-aldehyd **9** ble dannet ved Swern-oksidasjon av **8** med 65% utbytte (trinn *b*). En Wittig-reaksjon mellom **9** og fosfoniumsalt **10** ga **11** med 33% utbytte og varierende *cis* : *trans*-forhold (trinn *c*). Følgende forlengelse av polyenkjeden ga **12** (14% utbytte, trinn *d*). Wittig-reaksjonene ble gjennomført med refluks og bestråling med mikrobølger.

Flere forsøk på å beskytte fenol-gruppen i intermediatet **8** ved silylering eller benzylering førte kun til dannelse av **8B**. Oksidasjon av **8** ved Dess-Martin-oksidasjonen ga det uventede quinon-lignende derivatet **27**. Forsøk på å beskytte fenol-gruppen i intermediatet **9** ved benzoylering og silylering ga kun **9A**, som er uløselig i alle vanlige løsningsmidler.

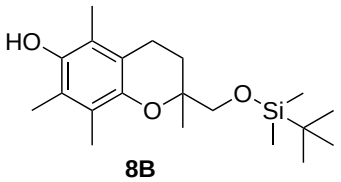

8B

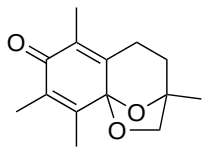

27

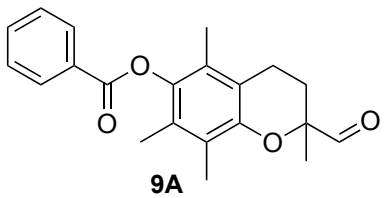

9A

Abstract

The goal of this work is the synthesis of a tocopherol/carotenoid hybrid derivative (**1**, figure II). The novel derivative is believed to exhibit synergistic antioxidant effects between its chromanol and polyene consituents. The synthesis of **1** was completed up to and including the immediate precursor **12**.

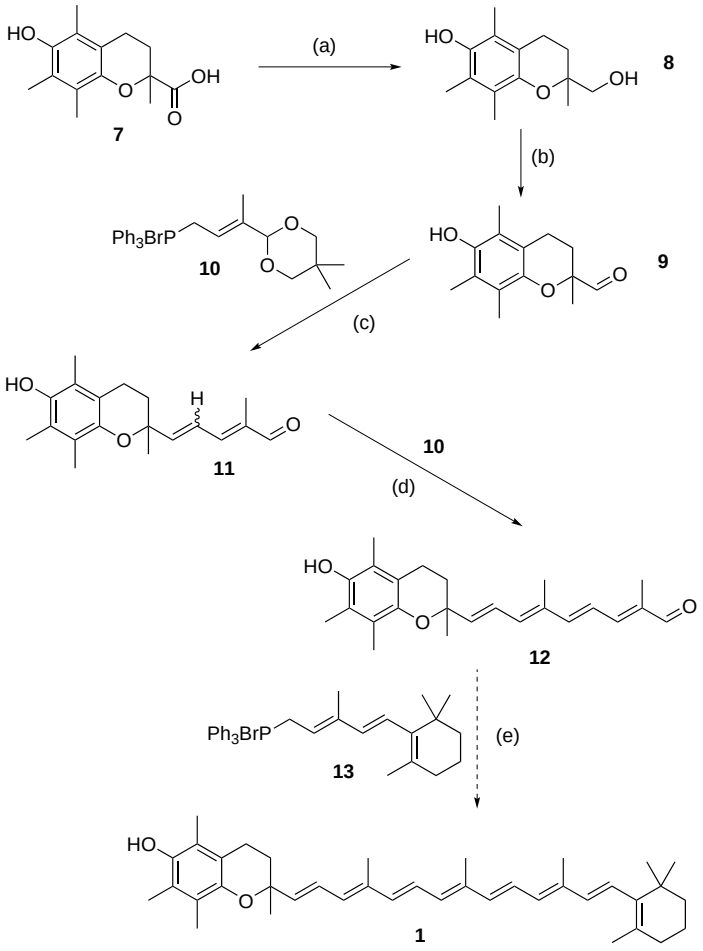

Figure II: Synthesis of **1**.

Commercially avaliable Trolox (**7**) was reduced by Red-Al® to **8** (step *a*) in 95% yield. Chromanol aldehyde **9** was formed by Swern oxidation of **8** in 65% yield (step *b*). Wittig reaction between **9** and phosphonium salt **10** afforded **11** in 33% yield and varying *cis* : *trans* ratio (step *c*), and subsequent elongation produced **12** (14% yield, step *d*). The Wittig reactions were performed with reflux and microwave irradiation.

Various attempts at protecting the phenolic group in intermediate **8** by silylation or benzylation did only lead to formation of **8B**. Oxidation of **8** by the Dess-Martin oxidation formed the unexpected quinone-like derivative **27**. Efforts to protect the phenolic group in intermediate **9** by benzoylation and silylation only produced **9A**, found to be unsoluble in all common laboratory solvents.

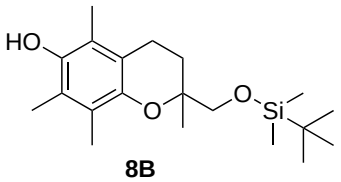

8B

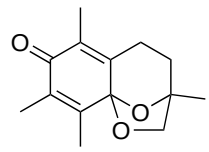

27

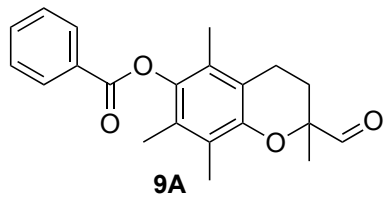

9A

Contents

List of Symbols and Abbreviations

2D Two-dimensional

A The pre-exponential constant in the Arrhenius equation

Ac Acetyl, CH_3CO

BHT Butylated hydroxytoluene, 2,6-di-*tert*-butyl-4-methylphenol

Bn Benzyl

Bz Benzoyl

c The speed of light in vacuum, 299,792,458 m/s.[1]

COSY (H,H)-correlated spectroscopy

DCC *N*,*N*′-Dicyclohexylcarbodiimide

DEPT Distortionless enhancement polarization transfer spectr.

DMAP 4-(Dimethylamino)pyridine

DMF *N*,*N*-Dimethylformamide

DMSO Dimethyl sulfoxide

E Energy

$\mathbf{E_a}$ Activation energy

eq Equivalents (by mol)

Et Ethyl, CH_3CH_2

EtOH Ethanol, CH_3CH_2OH

eV Electron volt

$\boldsymbol{h}$ Planck's constant, $6.62606896 \times 10^{-34}$ J s.[1]

HDL High-density lipoproteins

HMBC Heteronuclear multiple bond correlation spectroscopy

HPLC High-performance liquid chromatography

HRMS High resolution mass spectrometry

HSQC Heteronuclear single quantum coherence spectroscopy

IR Infrared spectroscopy

$\boldsymbol{k}$ The rate constant of a chemical reaction

$\boldsymbol{\lambda}$ Wavelength

$\boldsymbol{\lambda}_{\text{max}}$ Wavelength of maximum absorption

LDL Low-density lipoproteins

LRMS Low resolution mass spectrometry

Me Methyl, CH_3

MeOH Methanol, CH_3OH

MS Mass spectrometry

MW Microwave

NMR Nuclear magnetic resonance spectroscopy

Ph Phenyl, C_6H_5

R The Universal gas constant, 8.3144621 J mol^{-1} K^{-1}.[1]

ROS Reactive oxygen species

RT Room temperature

siRNA Small interfering ribonucleic acid

T Temperature

TBAF Tetrabutylammonium fluoride

TBDMS *tert*-Butyldimethylsilyl

THF Tetrahydrofuran

TLC Thin layer chromatography

***p*-TsOH** *p*-Toluenesulfonic acid

UV/Vis Ultraviolet-visible spectroscopy

VLDL Very low-density lipoproteins

List of Figures

List of Tables

Chapter 1

Introduction

Numerous attempts have previously been made at the synthesis of a polyunsaturated analogue of vitamin E (α-tocopherol).[2–4] By replacing the saturated alkyl moiety of α-tocopherol with a fully unsaturated polyene, one hopes to increase the antioxidant activity of the molecule. Though some authors do not agree,[5,6] most experiments show that mixtures of antioxidants like α-tocopherol and carotenoids (e.g. β-carotene) show a synergistic increase in antioxidant activity.[7–13] Synergism means that the total antioxidant activity of the mixture is greater than the sum of the contributions from each component. Chemically combining the key structural elements of different antioxidants in one molecule has also been reported to increase antioxidant activity.[14,15] Tocopherols, carotenoids and their antioxidant activity are discussed more thoroughly in the following chapter.

This synergism is the origin of the interest in a fully unsaturated analogue of α-tocopherol. The polyene chain intended to replace the alkyl chain of α-tocopherol is also the key structural element of carotenoids. It is thought to be responsible for the antioxidant properties of carotenoids. Taking this one step further, it would also be interesting to investigate the antioxidant properties of a compound combining full structural elements of carotenoids and α-tocopherol. One example of such a compound is **1**, the target molecule of this work. Its structure is shown in figure 1.1. **1** combines structural elements from α-tocopherol (**2**) and β-carotene (**3**).

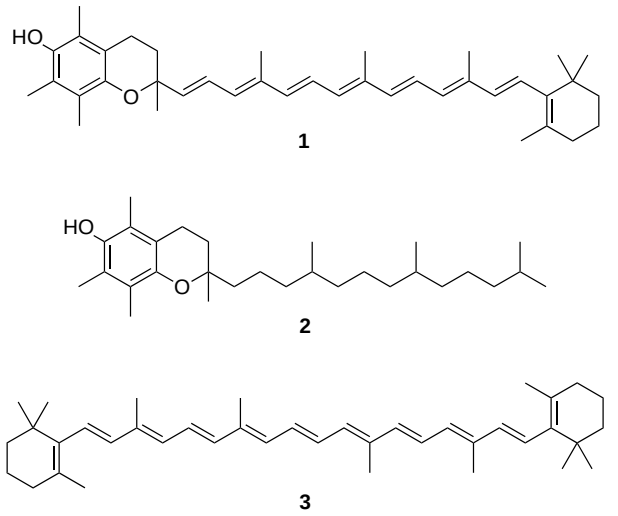

Figure 1.1: **1** combines structural elements from the natural antioxidants α-tocopherol (**2**) and β-carotene (**3**).

Other compounds combining α-tocopherol and carotenoids have been synthesized previously.[2,16,17] These are based on ester and ether linkages of carotenoic acids or alcohols and the chromanol acid Trolox (**7**, figure 1.3), with or without a glycerol linker and additional antioxidant moieties. However, the resulting compounds, though some have not been tested, have proven to have at best additive antioxidant effects. Even if no synergism is observed, these compounds still advantageously provide the body with several different antioxidants as post-absorptive metabolism may cleave the derivatives into their constituents. Thus the body is provided with several antioxidants by the absorption of a single molecule.[16] By designing target molecule **1**, the polyene chain and the chromanyl system are brought into closer proximity. This will hopefully intensify the synergistic interactions between the two systems. Additionally, the phenolic hydrogen, instrumental to the antioxidant activity of the chromanol moiety, is left unesterified.

In gene therapy, the delivery of new genetic material into the

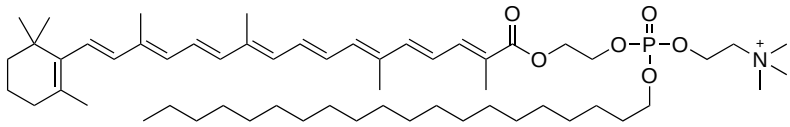

4

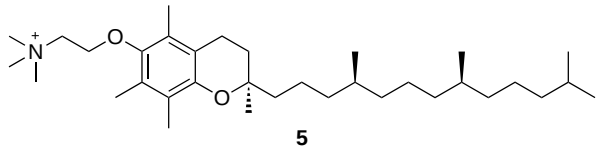

5

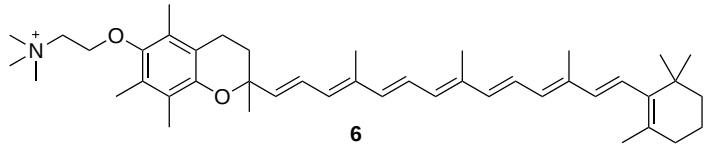

6

Figure 1.2: Gene transfection agents based on carotenoids (**4**), α-tocopherol (**5**) and target molecule **1** (**6**).

target cells depends on an efficient delivery system. Recently, a new class of vectors suitable for siRNA delivery based on carotenoids was reported.[18,19] An example of such a compound (**4**) is shown in figure 1.2. These novel, single-chain rigid cationic carotenoid lipids show promising delivery efficiency, among with low cytotoxic side effects. Tocopherols have also recently been derivatized into cationic lipids like **5** suitable for application as gene vectors.[20] Similarly, **1** may be derivatized into a cationic lipid (**6**). This derivative may represent another novel class of gene transfer molecules, unifying the novel carotenoid and tocopherol cationic lipids.

1.1 Strategy

Several strategies have been employed in the pursuit of an unsaturated α-tocopherol analogue. Størseth[2] attempted to directly couple an apocarotenoid based Wittig salt with an aldehydic derivative **9** (figure

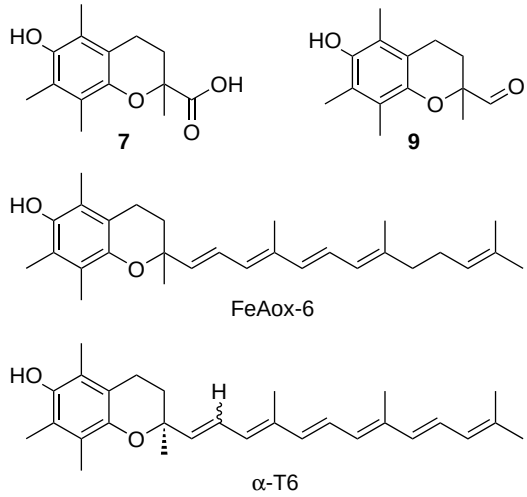

Figure 1.3: The structures of Trolox (**7**), chromanol aldehyde **9**, FeAox-6[3] and α-T6.[4]

1.3) of the chromanol ring system of α-tocopherol, and vice versa. These attempts failed.

Palozza *et al.*[3] successfully coupled a shorter polyene Wittig salt with the same chromanol aldehyde **9**, though without full conjugation of the polyene moiety. This unsaturated α-tocopherol analogue called FeAox-6 also lacks the functionality for further elongation.

Atkinson *et al.*[4] succeeded in producing an unsaturated α-tocopherol analogue in 2010, the year this work was commenced. Their strategy was to couple the chromanol aldehyde **9** with a Wittig salt containing additional functionality, allowing subsequent elongation to form a polyenic tocopherol analogue α-T6. The synthesis of α-T6 involves an intermediate common to the strategy employed in this work.

The synthesis of tocopherol-carotenoid **1** was based on coupling chromanol aldehyde **9** with Wittig salt **10** containing a short polyene chain and a protected aldehyde functionality. After deprotection, corresponding Wittig elongation of the polyene chain and coupling

with Wittig salt **13** should lead to **1**. This is summarized in figure 1.4.

The use of protection groups when working with carotenoids is complicated by the sensitivity of these compounds. Many deprotection methods would decompose the target **1**. With step economy also taken into consideration, the Wittig reaction was performed without protection of the phenol group. A similar step without protection was employed by Palozza *et al.*[3] in their synthesis of FeAox-6. Nevertheless, the Wittig reaction could also be attempted with benzoyl protection of the phenol group. A mild reductive deprotection of this group has been reported to leave the polyene chain intact.[26]

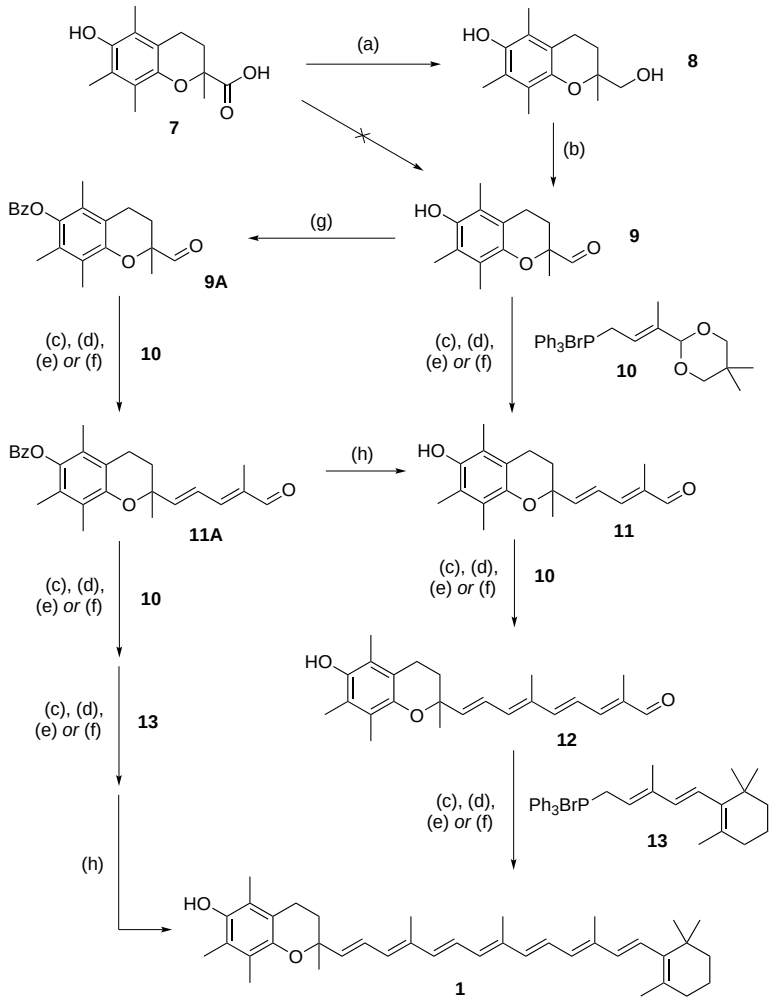

Figure 1.4: The synthesis of **1**. (a) $NaAlH_2(OCH_2CH_2OCH_3)_2$, THF, 0 °C.[2] (b) DMSO, $(COCl)_2$, NEt_3, CH_2Cl_2, -78 °C.[21] (c) 1. CH_3OK, CH_3OH, CH_2Cl_2, MW. 2. *p*-TsOH, CH_2Cl_2, 30 min.[22,23] (d) 1. CH_3OK, CH_3OH, CH_2Cl_2, reflux. 2. *p*-TsOH, CH_2Cl_2, 30 min.[22,23] (e) 1. EtOH, 1,2-epoxybutane, MW. 2. *p*-TsOH, CH_2Cl_2, 30 min.[24] (f) 1. EtOH, 1,2-epoxybutane, reflux. 2. *p*-TsOH, CH_2Cl_2, 30 min.[24] (g) BzCl, pyridine, CH_2Cl_2.[25] (h) DiBAlH, CH_2Cl_2.[26]

Chapter 2

Theory

This chapter will give a general survey of the theoretical background of this work. This includes some background information on carotenoids and tocopherols, and a general introduction to antioxidants and the antioxidative properties of carotenoids and tocopherols. Gene transfection vectors will also be discussed briefly. The final sections will discuss the use of microwave technology in organic synthesis, and consider reaction theory and mechanisms in somewhat more detail.

2.1 Carotenoids[27,28a]

Carotenoids are naturally occuring pigments and antioxidants distributed widely throughout Nature. Structurally they are classified as terpenoids, composed of several isoprene units. Carotenoids are distinguished by a long, conjugated polyene system, acting as a chromophore. This gives carotenoids bright colours, typically in the orange to red part of the spectrum. In their naturally occuring environment carotenoids are quite stable, but when isolated they become sensitive to light, heat and oxygen. Their limited solubility in common laboratory solvents is another challenge in carotenoid chemistry.

Carotenoids constitute a large and varied class of natural products. They occur as hydrocarbons, or *xanthophylls* containing functionalized carotenoids with hydroxy, carbonyl, ether and epoxy groups. Some examples of carotenoids are given in figure 2.1. The Greek let-

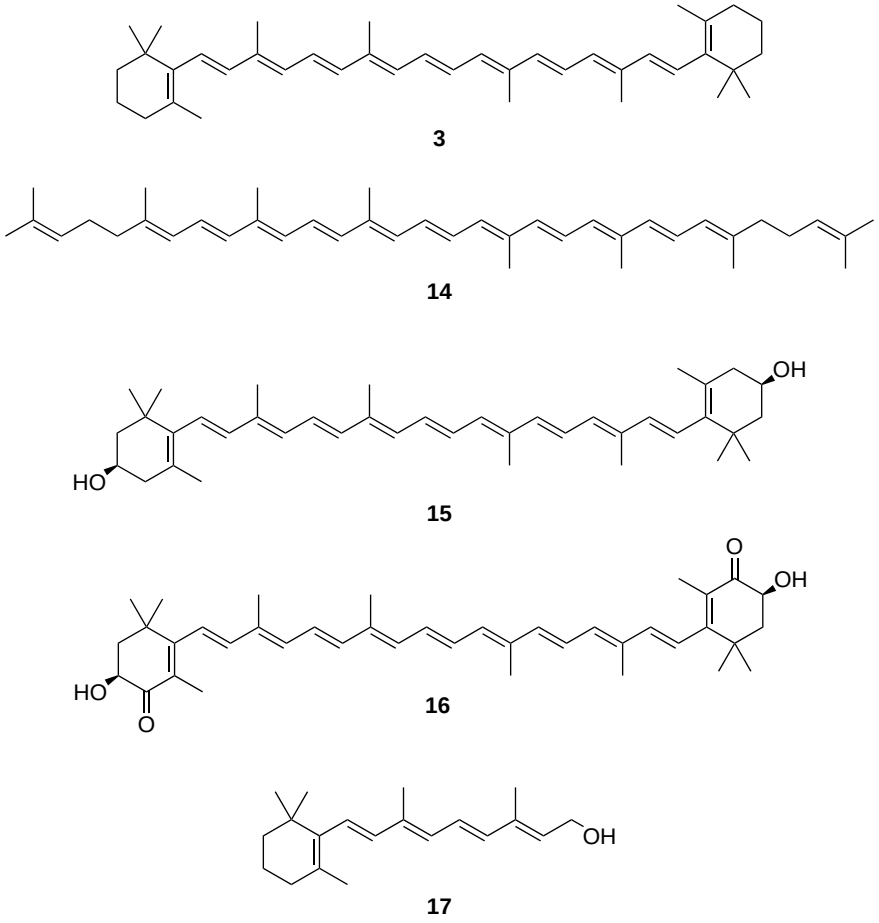

Figure 2.1: Structures of selected example carotenoids and apocarotenoids.

ter suffix specifies the structure of the cyclohexene moieties, thus **3** is β,β'-carotene. The acyclic lycopene (**14**) carotene may be formally derived into all other tetraterpenoid (C_{40}) carotenoids by modification or cyclization of one or both ends of the chain. It is found in red tomatoes, as well as in many kinds of fruit and berries. Zeaxanthin (**15**) is a common pigment in algae and plants, while astaxanthin (**16**) accounts

for red colours in many animals, e.g. salmon and crustaceans.

2.1.1 Absorption and distribution

The oral bioavailability of carotenoids is typically in the range of 10–30%.[29] Absorption is complex and among other factors depends on the geometry of the double bonds, the hydrophilicity of the carotenoid and co-formulation with dietary lipids. In general, increased hydrophilicity of the carotenoid increases bioavailability. All-*trans* isomers may have higher bioavailability than *cis* isomers, but this conclusion is under debate.[28b] Intestinal uptake of carotenoids is aided by formation of bile acid lipid micelles, and increased lipid content of the diet is seen to increase the uptake of carotenoids.

Transportation of carotenoids in the blood is performed by lipoproteins. Carotenes are mainly transported in low-density lipoproteines (LDL), while more polar carotenoids are transported in high-density lipoproteins (HDL). Adipose tissue is the main storage site for carotenoids, though high concentrations are also found in hepatic, adrenal and reproductive tissues. High concentrations of carotenoids and apocarotenoids are also found in the retina, as they have an important function in the mechanics of vision (see section 2.1.2).

2.1.2 Metabolism and bioactivity

Apocarotenoids are formed by oxidative cleavage of carotenoids, and frequently contain functionalities like hydroxy, aldehyde, carboxyl and ester groups. One important group of apocarotenoids are the vitamin A retinoids. Retinol (**17**, figure 2.1), is formed in mammals via the corresponding aldehyde retinal (β-apo-15-carotenal) by enzymatic cleavage with *βcarotene 15,15′-dioxygenase*. Notably, α-tocopherol is required in this biotransformation.[30] Carotenoids containing at least one β-ionone ring (like β-carotene) are considered pro-vitamin A compounds. Other apocarotenoids may also be formed by similar oxidative degradation. The vitamin A retinoids are instrumental to scoptic and colour vision. The oxidized form retinoic acid also finds importance as a hormon-like growth factor for epithelial cells.[31]

The conjugated polyene chain also imposes antioxidant properties

on carotenoids. These are treated in section 2.3.1. In combination with the presence of carotenoids in key tissues, potential beneficial health effects and disease prevention has been suggested from a diet high in carotenoids. These include protection against cancer, eye diseases, UV-induced skin damage, cardiovascular disease and enhancement of immune system function. Some of these effects may be attributed to the antioxidant properties of carotenoids, while others may be caused by regulatory effects on gene expression.

2.2 Vitamin E[28c,32a]

Vitamin E is a group of eight compounds, all exhibiting the same activity to larger or lesser extent. They all feature a chroman ring system with a phenol functionality and various degrees of aromatic ring substitution. Position 2 is also substituted with a long alkyl chain, either saturated or partly unsaturated. The compounds can be divided into two classes according to saturation: *Tocopherols* have a saturated hydrocarbon phytyl tail, while *tocotrienols* have three double bonds in the chain. The structures of tocopherols and tocotrienols are shown in figure 2.2.

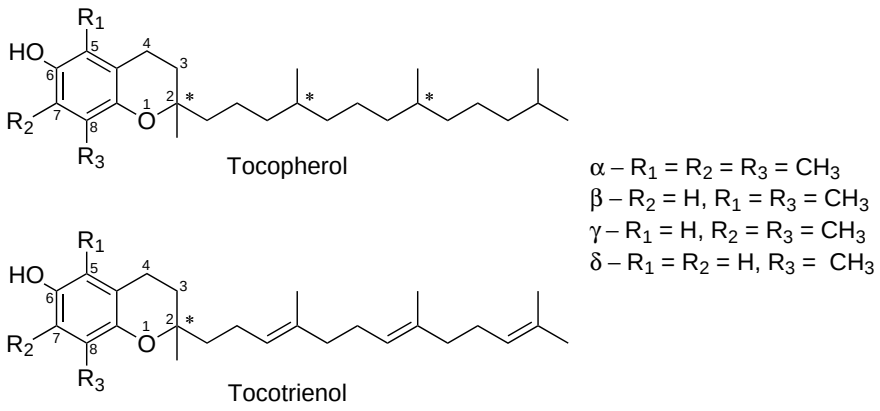

Figure 2.2: Structures of vitamin E tocopherols and tocotrienols.

Note that tocopherols have three stereogenic centers, while tocotrienols have only one. All natural forms of vitamin E have $2R$ configuration, which is required for vitamin activity. Activities differ according to configurations and substitution pattern. (R,R,R)-α-Tocopherol has the highest vitamin E activity, and the highest natural abundance. The chromanol head moiety is the active part of the molecule; compounds without the hydrocarbon tail also exhibit activity. A previously mentioned example is Trolox (**7**). The function of the hydrocarbon tail is to increase the lipophilicity of the vitamin, allowing incorporation into biological lipid membranes.

2.2.1 Absorption, distribution and metabolism

Plant seed oils are rich in Vitamin E, which is normally supplied through the diet. Similar to carotenoids, the absorption of vitamin E depends on the formation of lipid micelles aided by bile acid salts. The bioavailability of α-tocopherol is typically around 15–45%. Esterase and lipase enzymes from the pancreas hydrolyze common esters of tocopherols and tocotrienols into their active form. The vitamin is transported to the liver via lipids and carotenoids in chylomicrons.

The liver preferentially secretes the most active (R,R,R)-α-tocopherol in very low-density lipoproteins (VLDL) for redistribution to VDL and HDL, and further distribution to tissues. Targets for distribution include erythrocytes and adipose, hepatic, brain and muscle tissues.

2.2.2 Bioactivity

Vitamin E is a powerful antioxidant, of which α-tocopherol is the most potent form. This is discussed more thoroughly in section 2.3.2. α-Tocopherol is the major chain-breaking antioxidant in the body, and protects against major degenerative diseases in which free radicals are implied. Examples are cancer, cardiovascular disease, and pollution damage. Vitamin E has also been suggested to protect against aging processes and free-radical mediated tissue damage during exercise.

In addition to its antioxidant activity, vitamin E has important regulatory responsibilities in prostaglandin synthesis, protein kinase

C activation, mitochondrial function and the metabolism of proteins and nucleic acids.

2.3 Antioxidants[28d]

Antioxidants have the ability to prevent the oxidation of other compounds. In a biological context, an antioxidant inhibits the oxidative degeneration of biological material by free radical reactive oxygen species (ROS). ROS are generated by singlet oxygen ($^1O_2$), a highly reactive, non-radical form of molecular oxygen formed by radiative exitation. As the relaxation of the singlet to the triplet state ($^1\Delta_g \rightarrow {}^3\Sigma_g^-$) is strictly forbidden by spin and parity, the $^1O_2$ species is relatively long-lived. $^1O_2$ in turn forms the highly toxic superoxide radical ($O_2^{\bullet -}$), subsequently forming the hydroxyl radical ($HO^\bullet$) and a wide variety of peroxyl and alkoxyl radicals ($ROO^\bullet$ and $RO^\bullet$).

In vivo, ROS are generated as a byproduct from the electron transport chain in mitochondrial respiration.[33a] If no measures are taken, ROS initiates chain radical reactions destroying cellular material like lipids, proteins and genetic material. To prevent this, the body relies on the presence of antioxidants to quench $^1O_2$ physically or scavenge radical species chemically. Antioxidants are assisted by enzymes such as superoxide dismutase If the generation of ROS exceeds the capacity of antioxidant protection, or if the ability of antioxidants to counteract ROS is compromised, the resulting physiological condition is called *oxidative stress*.

The generation and consequences of $^1O_2$ and ROS, and the preventive effect of antioxidants such as carotenoids and vitamin E, are illustrated in figure 2.3. The mechanism of action of carotenoids and vitamin E will be detailed in the following sections.

2.3.1 Antioxidative properties of carotenoids[28e]

As briefly mentioned in section 2.1.2, carotenoids are antioxidants. This property is explained in terms of the conjugated system common to all carotenoids. Carotenoids may act as antioxidants by several mechanisms. The major mode of action (shown in figure 2.3) is by

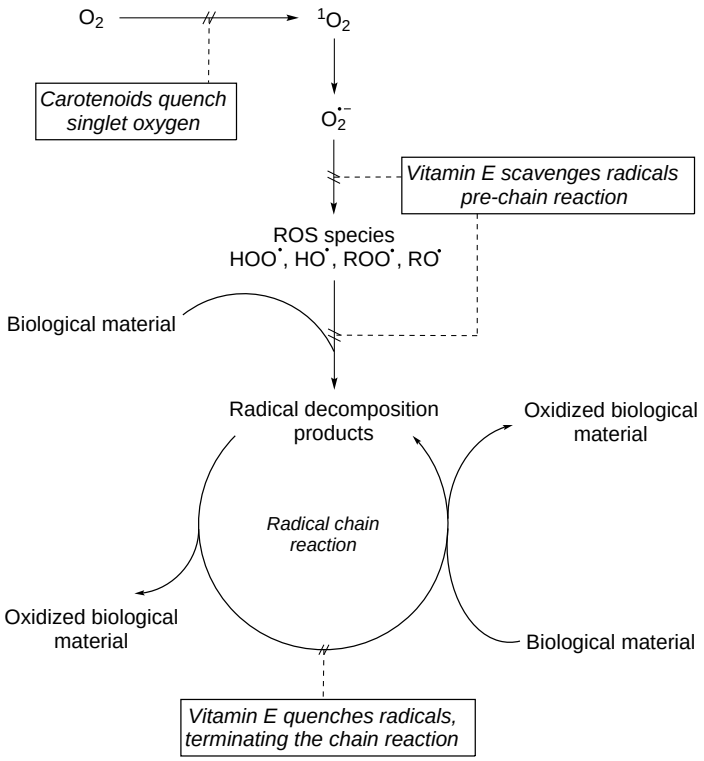

Figure 2.3: Generation of $^1O_2$ and ROS, and prevention of oxidative degeneration of biological material by carotenoid and vitamin E antioxidants.

physical quenching of $^1O_2$, as illustrated in equations 2.1 and 2.2. The high energy of $^1O_2$ is transferred to the carotenoid [Car], forming ground state $^3O_2$ and triplet carotenoid $^3[Car]^*$, which is relaxed to the ground state by dissipation of thermal energy. This process is expected to proceed through rotational and vibrational energy levels.[34]

$$^1O_2 + [Car] \rightarrow ^3O_2 + ^3[Car]^* \quad (2.1)$$

$$^3[Car]^* \rightarrow [Car] + \text{thermal energy} \quad (2.2)$$

The carotenoid is *not* decomposed in this process, so one carotenoid molecule may quench many $^1O_2$ before being metabolized. Chemical quenching, a minor antioxidant mechanism, destroys the carotenoid.[35]

Carotenoids are also radical scavengers and so may also exert an inhibitory antioxidative effect at all indicated steps in figure 2.3. This mechanism however contributes only minutely to the total antioxidant action of carotenoids. An example of the radical scavenging activity of β-carotene is shown in figure 2.4. The peroxide radical ROO$^\bullet$ forms a radical adduct with β-carotene. The radical is stabilized through extensive conjugation throughout the polyene system.

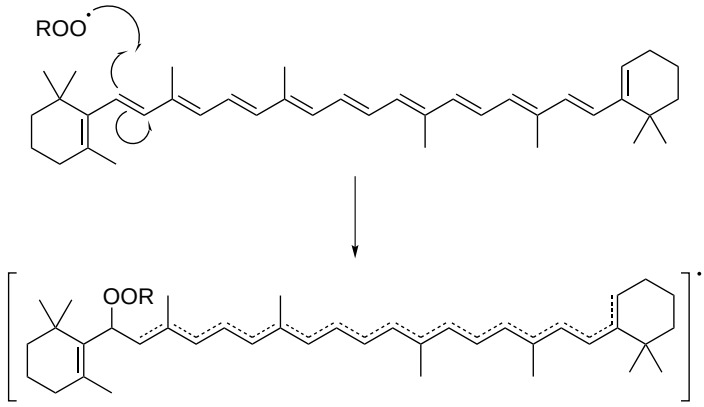

Figure 2.4: Mechanism for the radical scavenging activity of β-carotene.

2.3.2 Antioxidative properties of α-tocopherol[28c]

In section 2.2.2, vitamin E and in particular (*R*,*R*,*R*)-α-tocopherol was mentioned as a very potent radical scavenging antioxidant, and the most important lipid soluble antioxidant in the human body. It protects important unsaturated fatty acids in cell membranes.

The phenol group is instrumental to the activiy of α-tocopherol. Radical scavenging occurs via abstraction of the phenolic proton and formation of a resonance stabilized radical. The vitamin E radical may either form stable dimers, stable adducts with other radicals, or proceed through other radical reactions (figure 2.5).

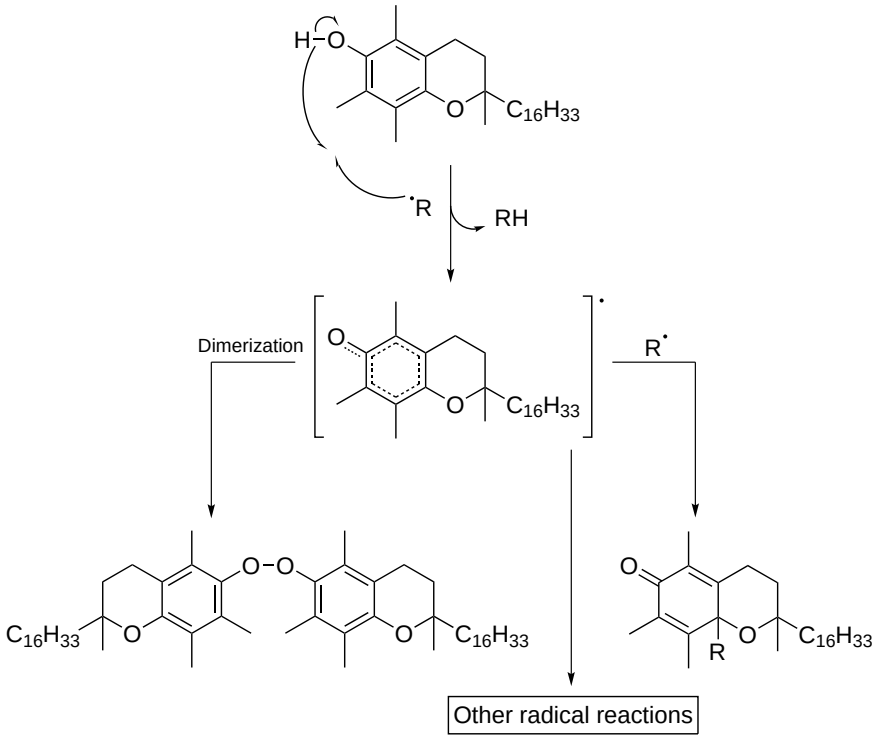

Figure 2.5: Mechanism for the radical scavenging activity of α-tocopherol and the fate of the resulting radical.

2.3.3 Synergism between antioxidants

Young *et al.*[36] have suggested that alterations in antioxidative properties may be observed if two antioxidants are in continguity. There are four potential outcomes of such an alteration of activity. If there is no unexpected alteration, antioxidant activities are *additive*, meaning the antioxidant activity of the system equals the sum of the individual activities of the constituent compounds. Alternatively one may observe a *synergistic* effect, where the total antioxidant activity equals *more* than the sum of the constituent compound activities. Finally, the outcome may be *antagonism*, in which the total activity is *less*

than the sum of the activity of the contributing compounds.

There are generally two possibilities for combining antioxidants. The first one is *physical* combination, i.e. mixtures of distinct compounds. The other method is *chemical* combination of two antioxidant moieties in the same molecule. This latter method has the additional advantage of allowing the uptake of several antioxidants through only one absorption and subsequent metabolic cleavage. Størseth made a survey of the effects of physical and chemical combinations of antioxidants in 2001.[2] This review forms the base of the following discussion of physical and chemical antioxidant combinations, with some additional newer references and updates.

Physical combination of antioxidants

As reported by Størseth,[2] there have been varying reports of synergism and antagonism in physical mixtures of antioxidants. Synergism is found in various binary and tertiary mixtures of assorted antioxidants like vitamin E (α-tocopherol), β-carotene, ascorbic acid (vitamin C), the flavonoid rutin, a selenaalkylglyceryl ether, and β-apo-8′-carotenoic acid esters.[7,8,11–13,37,38] However, there are also reports of an additive effect (α-tocopherol and rutin).[38]

The effects excerted between α-tocopherol and carotenoids are under particular controversy. Many studies[9,10,12,13,37] find there is a synergistic effect while others[5,6] find no effect or even antagonism.

Chemical combination of antioxidants

Chemically combining the key structural elements of different antioxidants (carotenoids, selenium, sulfur, α-tocopherol, Trolox (**7**), vitamin C) in one molecule has also been reported to increase antioxidant activity by synergism.[39,40] Other results include antagonism[41,42] and additive effects.[17,40] The activities of several combination antioxidants have not been measured.[16,43]

The novel trolox-carotenoid and BHT-carotenoid combinations (**18** and **19**, respectively) synthesized by Størseth[2,44] are shown in figure 2.6. **19** proved to be unstable and with no antioxidant properties,

while **18** was shown to have a concentration dependant antioxidant activity comparable to a mixture of α-tocopherol and β-carotene.[44]

Palozza *et al.*[3] reported in 2002 the synthesis of a partly unsaturated α-tocopherol antioxidant named FeAox-6 (figure 2.6). It was later shown to have an antioxidant activity greater than that of the tocotrienols.[14] The authors propose that the conjugated double bonds contribute to increased antioxidant activity by four mechanisms. *Reduced flexibility* leads to a more ordered distribution of FeAox-6 in a membrane bilayer. Enhancement of the *interaction of chromanyl ring with radicals* and possibility to *trap radicals in the chromanyl ring and polyene* also contribute. The final mechanism is suggested to be *increased efficiency of chromanyl regeneration.*

A novel class of combination antioxidants, carotenylflavonoids, were synthesized in 2007.[45] The class combines carotenoids with *flavonoids*, a class of natural compounds with a central tricyclic unsaturated system with inherent antioxidative properties. Compound **20** in figure 2.6 is an example of this class. Carotenylflavonoids show synergism in their antioxidant properties.

Atkinson *et al.*[4] synthesized a fully unsaturated α-tocopherol analogue α-T6 in 2010. Its structure is shown in figure 2.6. The antioxidant activity of α-T6 was not measured quantitatively, but it was shown by decay of fluorescence that the derivative is sensitive to peroxidative degradation, i.e. the polyene chain has antioxidant properties.

Assorted varieties of carotenoid retinoate esters were recently reported for the first time.[46] These compounds contain two or even three separate polyene chains. The group includes retinoate esters and diesters of *sec* allylic and non-allylic carotenols. A general structure of a carotenoid retinoate **21** is shown in figure 2.6. [Car] represents any carotenol moiety. The antioxidant activities of these compounds were not reported.

The synthesis of a series of novel phenolic antioxidants was recently described.[15] These antioxidants combine the chromanol moiety of vitamin E with catechol moieties to form very potent radical scavengers. An example is **22** in figure 2.6.

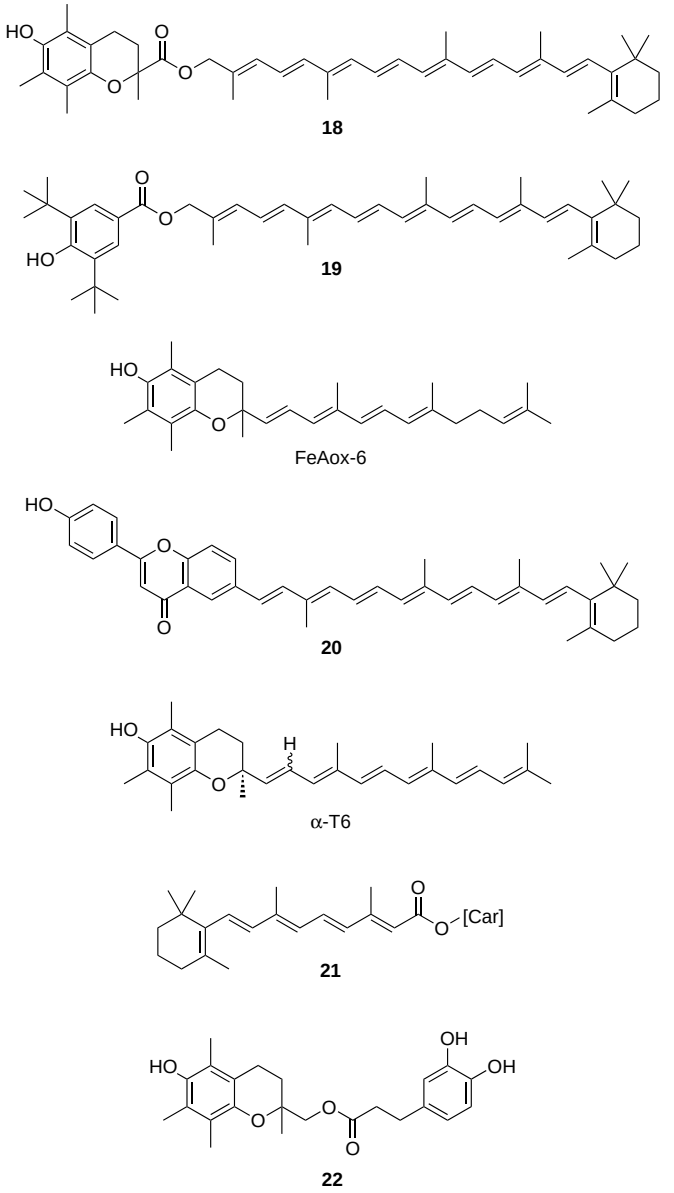

Figure 2.6: Structures of novel chemical combinations of antioxidants.

2.4 Transfection vectors in gene therapy[18,47,48]

Gene therapy aims to treat diseases at the genetic level by introduction of new genetic material into the cells. The introduced genetic material is typically DNA (to replace defective genes) or small interfering RNA (siRNA) designed to downregulate or silence overexpressed target genes. Because gene therapy does not simply relieve the symptoms, but rather alleviate the fundamental cause of disease, it has potential to cure serious illnesses previously considered difficult or impossible to treat. Examples of such diseases are *severe combined immunodeficiency disease (SCID)*[49] and *Duchenne muscular dystrophy*.[19,50]

Nucleic acid segments are quite polar and therefore unable to cross the lipid double layer constituting the cellular membrane. Additionally, nucleic acid strands have a net negative charge because of the phosphate groups in the strand backbone, as shown in figure 2.7. This means that passive diffusion of nucleic acids into cells would have to go against the voltage gradient of the transmembrane potential.[33b] Hence, the introduction of new genetic material requires facilitation. Currently, the most used methods rely on delivery by a *vector*, i.e. a transportation vehicle for the genetic material.

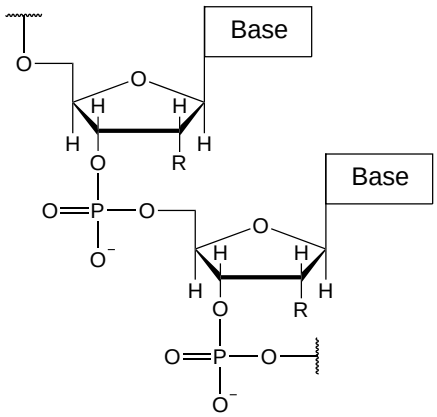

Figure 2.7: Chain phosphate linkers give RNA (R = OH) and DNA (R = H) net negative charge.

2.4.1 Classes of gene transfection vectors

Contrary to direct physical delivery techniques (e.g. microinjection and bioballistics), the use of vector delivery shows promise for clinical utilization in gene therapy. Gene carriers can be broadly classified as *viral* or *non-viral*.

Viral vectors have the advantage of supreme efficiency. The technique is based on insertion of the genetic material into the nucleic acid strands of a modified virus by bioengineering. The virus is then introduced into the body, transferring the therapeutic genetic material as well as its own into host cells as it spreads.[33c] Viral vectors may be based on adeno-viruses (AV), adeno-associated viruses (AAV) and retro-viruses.

Problems with viral vectors include their toxicity and immunogenicity and difficulty of upscaling.[51] Serious adverse effects in some patients has raised concerns about the safety of this class of transfection vectors.[52] This has increased the recent interest in non-viral vectors.

Non-viral delivery systems based on dendrimers, peptides and other biopolymers, and cationic lipids have been described. These carriers generally show lower toxicity and immunogenicity, and are easily produced in large scale. Non-viral vectors can carry more genetic material than viral vectors. However, their efficiency is low compared to viral vectors. In general, non-viral vectors are hydrophobic and cationic, and their function depends on the formation of lipophilic complexes — *lipoplexes*.

2.4.2 Nucleic acid delivery via lipoplexes

Cationic lipids coordinate to negatively charged nucleic acids in a self-assembly process driven by electrostatic attraction and hydrophobic interactions. The geometry of the lipoplex depends on among other factors the vector to nucleic acid ratio, and the presence of co-lipids. Pungente[18] hypothesized that structurally rigid lipids (e.g. based on carotenoids or steroids) are packed into more dense lipoplexes. Frequent geometries are lamellar and inverted hexagonal packing. The effect of packing geometry on transfection activity is under debate.

Lipoplexes are internalized by the target cells by endocytosis, forming an intracellular vesicle. Endosomal escape by the nucleic acids is instrumental to prevent lysis of the genetic material in a matured lysosome. It has been suggested that endosomal escape is assisted by cationic lipids by an invertion of the endosomal membrane.[53]

Cationic lipid derivatives of α-tocopherol were recently reported as a potential cationic lipid gene transfection vector.[20] This also suggests the use of rigid tocopherol analogues like **1** as gene transfection vectors. **1** is easily derivatized to a cationic lipid, allowing a structure-activity study to test the hypothesis of Pungente *et al.*[18]

2.5 Microwave technology in organic synthesis[54a]

The use of microwaves in replacement of conventional laboratory heating was first reported in 1986.[55,56] Over the previous decades, development of designated vessels and microwave reactors have greatly improved the safety and reproducibility of the technique. Today, the technology has established itself in both industrial and academic use.

The main advantage of microwave irradiation is a great reduction in reaction time. This is especially desirable from the viewpoint of a carotenoid chemist, as carotenoid reactions are plagued by long reaction times facilitating decomposition. Decrease in reaction time thus also may improve reaction yields. One other advantage may be improved purity of the crude product, as improved temperature control also controls side product formation. This would simplify subsequent purification steps. These advantages of course require detailed optimization of the reaction conditions. Only a few examples of microwave assisted syntheses with carotenoids have been reported.[57,58]

The microwave area of the electromagnetic spectrum ranges from wavelengths between 1 cm and 1 m. According to relation 2.3, longer wavelengths (λ) correspond to lower energy (E). c is the speed of light in vacuum and h is Planck's constant.

$$E = \frac{hc}{\lambda} \tag{2.3}$$

Microwave photons do not have sufficent energy to directly cause chemical reactions, in contrast to UV or visible photons in photochemistry. The efficiency of microwave irradiation to facilitate reactions is rather owed to *dielectric heating*. In short, dielectric heating is generation of heat by molecular friction and collisions caused by the effort of a molecular dipole to align with an oscillating electric field. An example is the electric field component of microwave electromagnetic radiation. Any ions present in the field will also begin to oscillate, generating additional thermal energy in the irradiated matrix. So, the presence of any polar or charged species in the reaction mixture will facilitate heating by microwave irradiation.

Compared to conventional thermal heating, microwave irratiation is much faster. External heating depends on heat transfer from the surroundings to the reaction mixture. This transfer of energy is often inefficient, and may cause temperature gradients and local overheating, causing decomposition of solutes. Microwave irradiation, on the other hand, causes the bulk reaction mixture itself to warm up internally. Internal heating may lead to reaction temperatures even higher than the solvent boiling point, thus decreasing the reaction time compared to thermal heating according to the Arrhenius equation (2.4):

$$k = Ae^{-E_a/RT} \tag{2.4}$$

where k is the rate constant of a chemical reaction with activation energy E_a at temperature T, A is the pre-exponential factor and R is the Universal gas constant. An inverted temperature gradient may also result from internal heating, and thus the design of the reaction vessel is crucial to maintaining a uniform heat distribution.

It is sometimes observed that the product distribution of a reaction differs whether the reaction mixture has been heated under conventional reflux or microwave conditions. The change may be in both chemo-, regio- and stereoselectivity. This has been rationalized through so-called *microwave effects* by some authors, but the existance and impact of such effects is under debate.[59–63] Suggested thermal microwave effects include superheating of solvents, avoidance of temperature gradients, and selective heating of solutes with a strong microwave absorption.

Non-thermal effects, more controversial and far less widely accepted than thermal effects, are defined by Kappe and Stadler[54b] as

> "accelerations of chemical transformations in a microwave field that cannot be rationalized in terms of either purely thermal/kinetic or specific microwave effects."

An example of such an effect is a change in the factors A and the entropy term of E_a in the Arrhenius equation, due to the alignment of dipoles in the electromagnetic field. It has also been suggested that the electromagnetic field stabilizes the development of charges in non-concerted reaction mechanisms, thus lowering the activation energy of the reaction.[59,60] Opponents of this view however argue that thermal agitation should override any statistically significant alignment of dipoles in the field.[61,62]

2.6 Reaction theory and mechanisms

2.6.1 Carbonyl reduction by hydride-donor reagents[64a]

Boron and aluminium hydride reagents are most commonly used for hydride reduction of carbonyl groups. The simplest ones are $NaBH_4$ and $LiAlH_4$, the latter being the strongest reducing agent. The reactivity of the hydride reagents can be fine-tuned by exchange of the counterion, and by derivatization to alkyl- or alkoxylithium or -borohydrides. Examples (figure 2.8) are diisobutylaluminium hydride (DiBAlH, **23**) and sodium *bis*-(2-methoxyethoxy)aluminium hydride (Red-Al®, **24**). It is also possible to introduce stereospecificity in the reducing agent through alkyl or alkoxy derivatization.

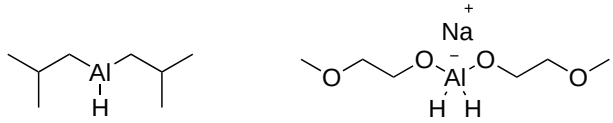

23 **24**

Figure 2.8: The structures of DiBAlH (**23**) and Red-Al® (**24**).

All hydrides in the reductant can be transferred to the substrate carbonyl group. The reaction mechanism involves coordination of the carbonyl group to a metal cation, thereby activating it for nucleophilic attack of a hydride. The resulting aluminium alkoxides are hydrolyzed to the corresponding alcohols and $Al(OH)_3$ at the end of the reaction time.

Highly oxidized carbonyls like acids and esters, are first reduced to aldehydes, and then further to alcohols. Aldehydes are more reactive to reduction than acids and esters, so it is challenging to stop the reduction at the aldehyde. Acids initially consumes one additional equivalent of hydride, generating one equivalent H_2 gas.

The general reaction mechanism for reduction of an acid by a lithium aluminium hydride reagent is shown in figure 2.9. R can be any alkyl or alkoxy group, and R′ can be any alkyl or aryl group.

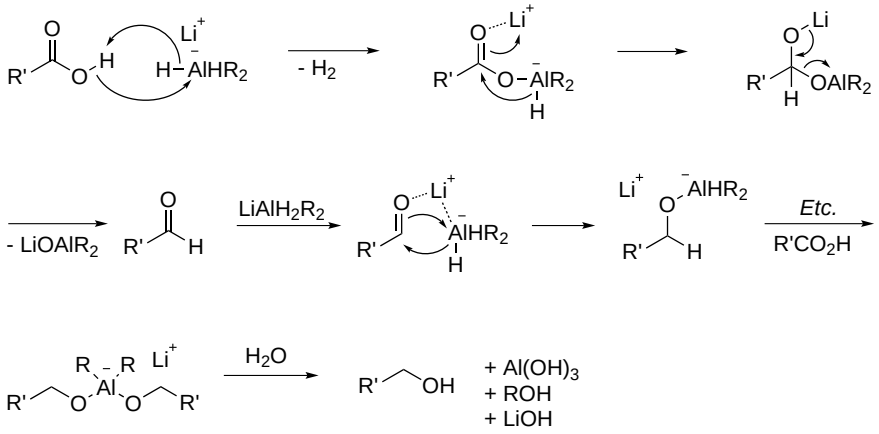

Figure 2.9: Reaction mechanism for reduction of an acid by a lithium aluminium hydride reagent.

2.6.2 The Swern oxidation

Oxidation of alcohols to aldehydes by electrophile activated DMSO was first reported in 1965.[65] Swern later reported that oxalyl chloride ($(COCl)_2$) was the most efficient activator of DMSO.[21] Other

ways of activating sulfoxides or using activated sulfinimides have been reported later,[66] but the Swern oxidation is still the most popular method for DMSO based oxidations, due to the low cost and relatively low toxicity of the required reagents.

The Swern oxidation mechanism is given in figure 2.10.[2164,b,67] R may be any alkyl or aryl group. The initial activation of DMSO is facilitated by the significantly dipolar character of the S–O bond, and driven by the liberation of CO and CO_2 by decomposition of oxalyl chloride. After the addition of the alcohol to the sulfoxonium species, addition of base generates an unstable sulfur ylide. This ylide decomposes to eliminate the corresponding aldehyde. Base is also required to quench the generated hydrochloric acid.

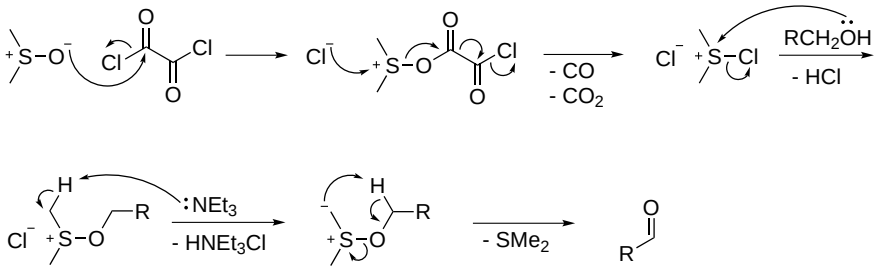

Figure 2.10: The mechanism of the Swern oxidation.

The Swern oxidation is very sensitive to temperature changes. The standard conditions suggested are at −78 °C. Maintaining a low temperature is very important to minimize side reactions. Examples of a common side reaction is the formation of mixed thioacetals by rearrangement of the sulfur ylide (figure 2.11).[67]

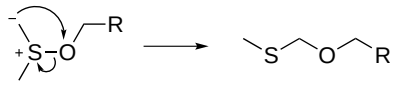

Figure 2.11: A common side reaction to the Swern oxidation, forming thioacetal byproducts.

2.6.3 The Dess-Martin oxidation

Oxidation of primary and secondary alcohols to their corresponding carbonyl compounds by a pentavalent iodine compound **25** is a very mild oxidation method. It was first reported by Dess and Martin in 1983,[68] and so the reagent is called *Dess-Martin periodinane*.

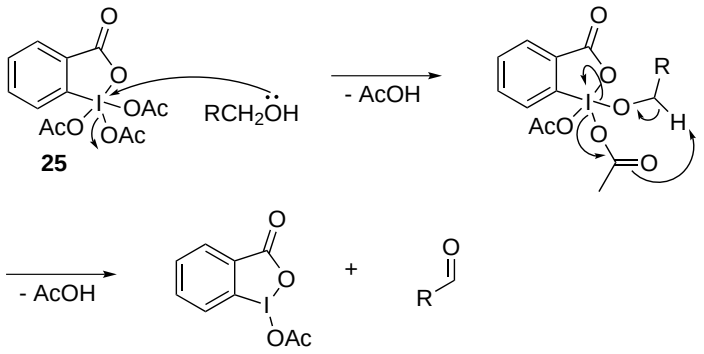

Figure 2.12: The mechanism of the Dess-Martin oxidation.

The mechanism of the Dess-Martin oxidation is shown in figure 2.12.[64b] R can be any alkyl or aryl group. The reaction proceeds by exchange of acetate with the alcohol, followed by decomposition of the resulting alkoxyperiodinane, liberating the aldehyde and acetic acid. Periodinane is reduced to acetoxyiodinane in the process. Workup of base-sensitive compounds can be performed with sodium thiosulfate to reduce the resulting acetoxyiodinane to sodium 2-iodobenzoate.[21]

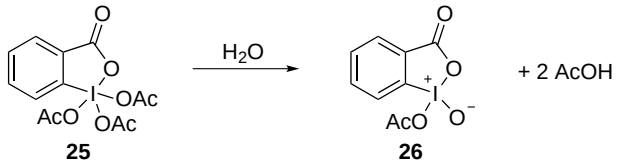

Figure 2.13: Hydrolysis of **25** generates the more active reagent **26**.

It has been shown that the Dess-Martin oxidation is greatly accelerated by the addition of water.[69] It is believed that water hydrolyzes

25 *in situ* to the more effective reagent **26** (figure 2.13). For this reason, the Dess-Martin oxidation is most frequently performed in water saturated solvents, or with the addition of H_2O.

2.6.4 The Wittig reaction[64c]

The classical *Wittig reaction* is a very useful method for creating C=C bonds. It involves the conversion of carbonyl compounds to olefines by the reaction of a phosphorous stabilized carbanion (a *phosphonium ylide*). The Wittig reaction is of tremendous importance in carotenoid chemistry, as it efficiently allows the formation of C=C bonds prominent in the carotenoid structure.[70]

The general mechanism of the Wittig reaction with an aldehyde is shown in figure 2.14. R and R′ are alkyl or aryl groups, and X is a halogen. B is a general base. Under strongly basic conditions, a phosphonium salt is deprotonated generating the phosphonium ylide. The ylide then reacts with the carbonyl compound to produce a cyclic *oxaphosphetane* intermediate. The mechanism for the formation of this intermediate is open to question. It may be formed by direct cycloaddition between the ylide and the carbonyl,[71] or it may be formed via a dipolar *betaine* intermediate from nucleophilic addition to the carbonyl group.[72] The oxaphosphetane subsequently decomposes into phosphine oxide and the desired alkene. The driving force is the formation of the very thermodynamically stable P=O bond.

The Wittig reaction may also be performed using an epoxide to mediate the reaction.[73] This procedure is very mild, as no base is required. The formation of the ylide by 1,2-epoxybutane is shown in figure 2.15.

The stereoselectivity of the Wittig reaction[74]

The stereochemical outcome of the Wittig reaction is thought to be dependant on steric effects in the formation of the oxaphosphetane intermediate (figure 2.14). *Stabilized ylides* contain electron withdrawing groups that contribute to stabilizing the carbanion. Stabilization decreases the reactivity (increases the stability) of the ylide, and so the transition state for oxaphosphetane formation will be late and

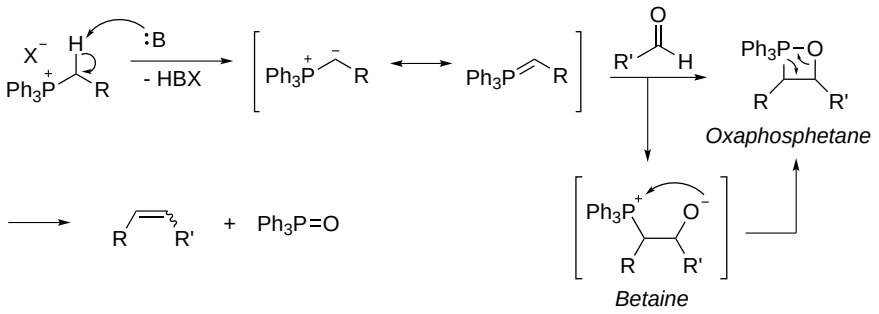

Figure 2.14: The general mechanism for the Wittig reaction with an aldehyde.

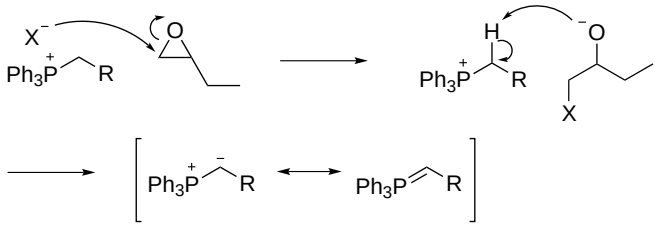

Figure 2.15: Epoxide mediated ylide formation.

product-like according Hammond's postulate.[75] Accordingly, the energy of the transition state is governed by steric strain in the rigid, cyclic transition state. As illustrated in figure 2.16, this results in formation of the *trans* transition state **A** to minimize steric 1,2-interaction between the substituents of the aldehyde and ylide.

Correspondingly, *non-stabilized ylides* are more reactive due to lack of carbanion stabilization. Again according to Hammond's postulate,[75] non-stabilized ylides proceed through an earlier, more flexible transition state. The transition state adopts a twisted conformation to minimize 1,2- and 1,3-interactions (between the aldehyde substituent and the ylide and phosphorous substituents, respectively), see figure 2.16. The favoured late transition state **D** leads to the formation of *cis* product.

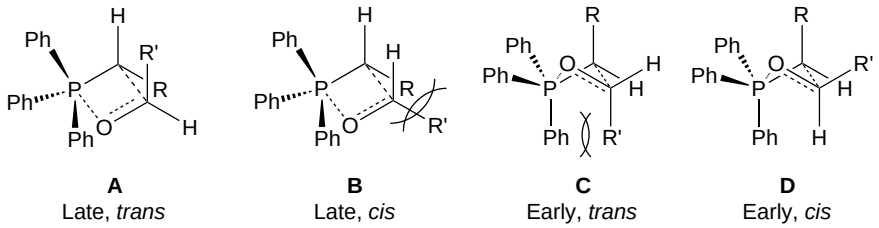

Figure 2.16: Kinetic (transition state) control of stereoselectivity in the Wittig reaction. For late transition states, **A** is more stable. For early transition states, **D** is more stable.

2.6.5 Hydrolysis of acetals[76a]

The hydrolysis of acetals is rapid and driven by a favourable equilibrium, liberating the alcohol(s) used for acetal formation. The hydrolysis usually exhibits specific acid catalysis. A general mechanism for the acid catalysed hydrolysis of an acetal is shown in figure 2.17. R may be H or any alkyl or aryl group. R′ is normally an alkyl group. The R′ groups may also be connected to form five or six member ringed cyclic acetals (i.e. from a diol). Initially, the acetal is hydrolyzed to the corresponding hemiacetal. The hemiacetal is rapidly hydrolyzed to the carbonyl via an intramolecular proton shift. The catalytic acid is regenerated in the final deprotonation.

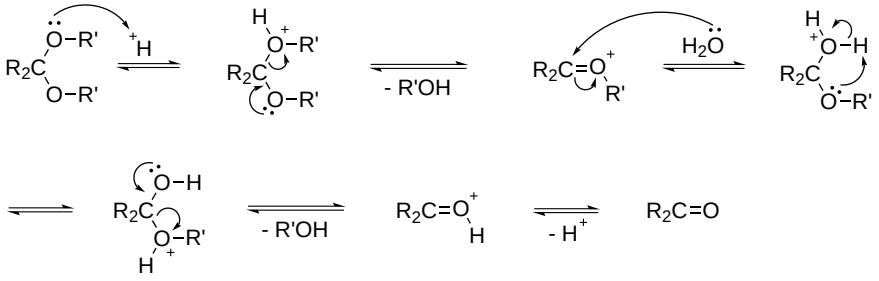

Figure 2.17: General mechanism for acid catalyzed hydrolysis of an acetal.

2.6.6 Benzoyl protection and deprotection[64d,77a]

Protection of alcohols by acylation is an efficient and well-explored transformation. The mechanism is shown in figure 2.18, where X is a halide and R may be any alkyl or aryl group. The benzoyl group is imposed on the alcohol by nucleophilic addition-elimination with a benzoyl halide. The reaction is catalyzed by pyridine as shown or (even more efficiently) by 4-(dimethylamino)pyridine (DMAP).[78] Pyridine is a stronger nucleophile than the alcohol, but the rate of alcohol addition to the acyl pyridinium ion is far greater than the rate of addition to the acyl halide. The presence of base is also required to quench liberated hydrogen halide acid.

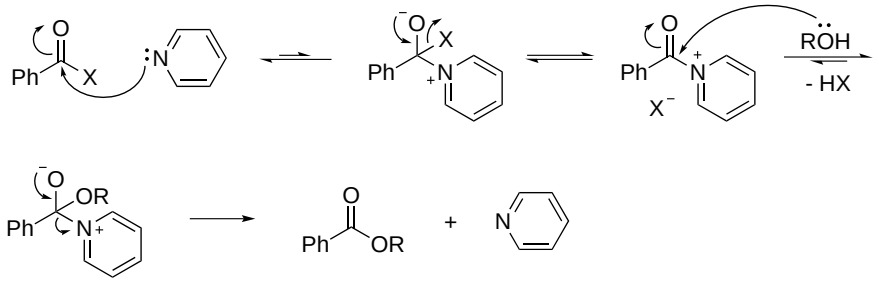

Figure 2.18: Mechanism for benzoylation of a general alcohol with pyridine catalysis.

Cleavage of benzoyl ethers is often performed by hydrolysis under basic conditions. A mild deprotection method of protected carotenoids with DiBAlH has been reported to leave the polyene chain intact.[26] The mechanism of this deprotection step goes via an addition of hydride to the benzoyl carbonyl, and subsequent elimination of the alcohol to form benzaldehyde as a byproduct. This is in analogy to the mechanism for hydride-donor reductions in section 2.6.1.

2.6.7 Silyl protection and deprotection[64d,77b]

Introduction of silyl ethers as protective groups for alcohols proceeds by nucleophilic attack by the alcohol at a substituted silyl halide, lib-

erating hydrochloric acid. The reaction is catalyzed by tertiary amines like imidazol, in a manner analogous to acylations in the previous section. The amine is also required to quench liberated acid. A general mechanism for the formation of silyl ethers is shown in figure 2.19. R and R′ may be any alkyl or aryl group, X is a halogen.

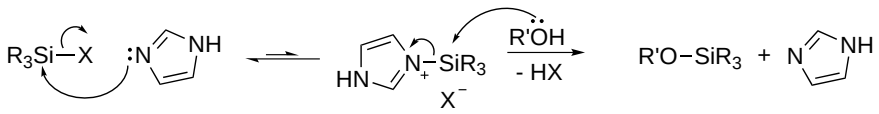

Figure 2.19: Mechanism for silylation of a general alcohol with imidazol catalysis.

Deprotection of silyl ethers is commonly facilitated by tetrabutylammonium fluoride. The driving force is the formation of the thermodynamically stable Si–F bond. The mechanism proceeds by fluoride ion displacement of the alcohol by a nucleophilic attack at Si. However, the fluoride ion is a very strong base, particularly under anhydrous conditions, and may decompose sensitive moieties like carotenoid polyene chains. An alternative deprotection method with DiBAlH has been reported.[79]

2.6.8 Benzyl protection and deprotection[64d,77c]

The classical Williamson reaction between an alcohol and a benzyl halide, forming a benzyl ether, is a convenient way of protecting alcohol functionalities. The general mechanism is shown in figure 2.20. R may be any alkyl or aryl group, X is a halogen, and B is a base. By using a weak base, e.g. K_2CO_3, selectivity for phenols over alkyl alcohols may be achieved. This is owed to the greater acidity of phenolic protons.

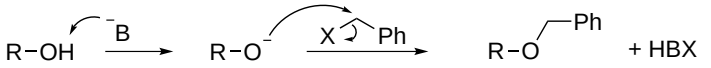

Figure 2.20: Mechanism for the Williamson synthesis of benzyl ethers.

The cleavage of benzyl ethers is most often performed by reductive hydrogenolysis. When this is not an option, as with unsaturated carotenoids, alternatives include dissolving-metal reductions or treatment with Lewis acids like BBr_3. It is however not certain that carotenoid substrates will survive under such conditions.

Chapter 3

Results and Discussion

3.1 Synthesis of 2-hydroxymethyl-2,5,7,8-tetramethylchroman-6-ol (8)

The chromanol alcohol **8** was synthesized by reduction of Trolox (**7**) with Red-Al® ($NaAlH_2(OCH_2CH_2OCH_3)_2$, **24**) according to the procedure previously employed by Schiefer,[80] see figure 3.1, table 3.1. The experimental description is given in 6.2. The reaction mechanism is outlined in section 2.6.1.

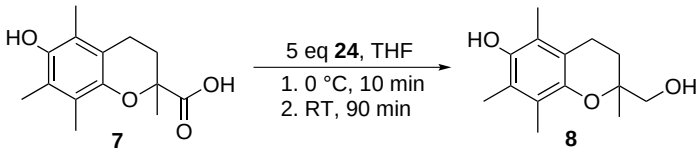

Figure 3.1: Synthesis of **8**.

The reaction proceeds readily under dry conditions and N_2 atmosphere. Upon quenching with aqueous HCl, hydrogen gas is liberated by excess reduction agent in an exothermic reaction according

Table 3.1: Yields and conditions for the synthesis of **8**.

Attempt	Scale (g **7**)	Reaction conditions	Yield (%)
1	1.500	Conc. **7** = 60 mg/mL Red-Al added over 10 min	66
2	3.108	Conc. **7** = 60 mg/mL Red-Al added over 10 min	85
3	5.000	Conc. **7** = 60 mg/mL Red-Al added over 15 min	21
4	5.353	Conc. **7** = 37 mg/mL Red-Al added over 20 min	95

to equation 3.1. The alkoxyhydride aluminate is converted to sparingly soluble $Al(OH)_3$, which is dissolved and removed during acidic workup with aqueous HCl (equation 3.2).[81]

$$\begin{aligned} &Na(MeOEtO)_2AlH_2 + HCl + 3H_2O \rightarrow \\ &Al(OH)_3(s) + 2H_2(g) + 2ROH + NaCl \end{aligned} \tag{3.1}$$

$$Al(OH)_3(s) + 3HCl \rightarrow AlCl_3(aq) + 3H_2O \tag{3.2}$$

In most attempts the reaction gives high yields of **8**. In attempt 4 (table 3.1), crude product purity was assessed by TLC and ^{1}H NMR (appendix A, figure A.2) and found to be high enough to make purification unnecessary.

Attempt 3 however did afford low yields, and the crude product was discoloured by a reddish brown contaminant. In this case, the product was purified by recrystallization from petroleum ether. The poor results from attempt 3 were caused by the accidental use of an old bottle of Red-Al® reagent. The reagent is sensitive to degradation by atmospheric moisture (equation 3.1), forming precipitation of white $Al(OH)_3$ over time even when stored under septum in containers sealed by the manufacturer. Decomposition also leads to an increase in viscosity of the already viscous reagent toluene solution.

The highest yields are observed in attempt 4. This may be an additional effect of performing the reaction at lower concentrations of **7** (larger volume of THF) in an attempt to counteract solubility problems. Red-Al® solidifies at 4 °C, creating problems towards the end of its addition on an ice/water cooling bath. Upon removal of the cooling bath and consequent liquefaction of the reaction mixture, sudden bursts of hydrogen bubbles and inhomogeneous distribution of solid material in the reaction mixture were observed. Dilution in combination with slower addition of Red-Al® (table 3.1) and high speed stirring helped alleviate the problem. Very careful stepwise removal of the cooling bath is recommended to prevent the reaction from becoming too vigorous.

3.2 Synthesis of 6-hydroxy-2,5,7,8-tetramethylchroman-2-carbaldehyde (9)

Initially, the synthesis of **9** by the Swern oxidation (figure 1.4) faced severe problems, as discussed in the following section 3.2.1. Alternative strategies for the transformation were attempted, including protection and deprotection. These efforts are summarized in figure 3.2, and discussed more thoroughly in sections 3.2.2–3.2.4. Oxidation of **8C** by $CrO_3 \cdot 2\,C_5H_5N$ (Collins reagent) has been reported,[82] but was not considered due to the health hazards associated with chromium(VI).

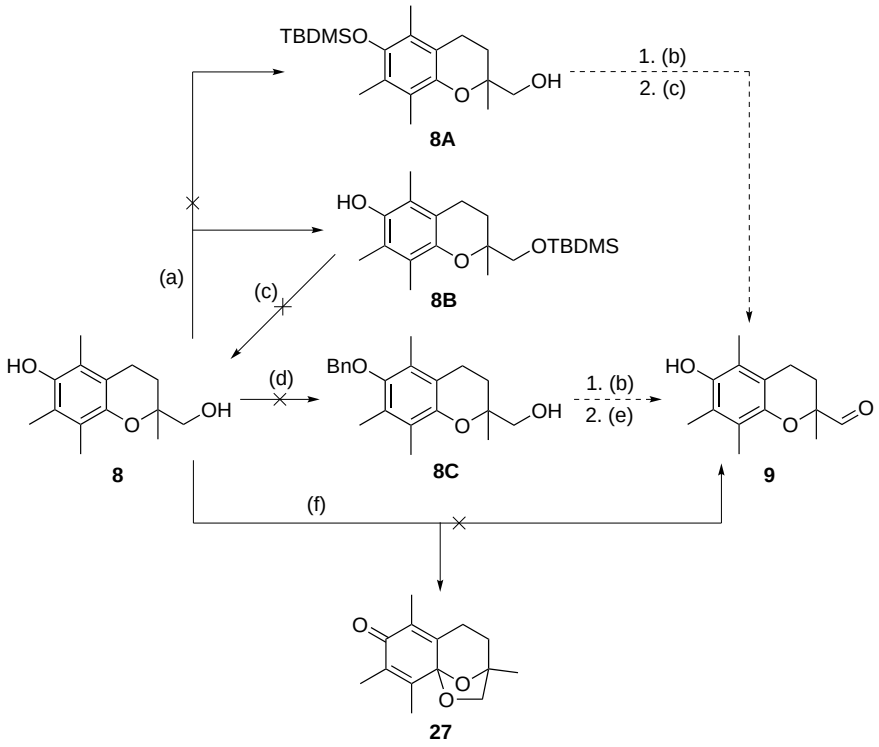

Figure 3.2: Alternative strategies to **9**. (a) 1. TBDMS-Cl, imidazol, DMF. 2. HCl, MeOH.[83,84] (b) DMSO, $(COCl)_2$, NEt_3, CH_2Cl_2, −78 °C.[21] (c) TBAF, THF.[85] (d) BnCl, 18-crown-6, **30**, K_2CO_3, acetone.[86] (e) BBr_3, CH_2Cl_2.[77d] (f) Dess-Martin periodinane, H_2O, CH_2Cl_2.[68,69]

3.2.1 The Swern oxidation

The chromanol aldehyde **9** was synthesized from (**8**) by means of the Swern oxidation (figure 3.3). Experimental details are found in section 6.4.2. The mechanism for this reaction is given in figure 2.10 and discussed in section 2.6.2. Yields and conditions of various attempts are shown in table 3.2.

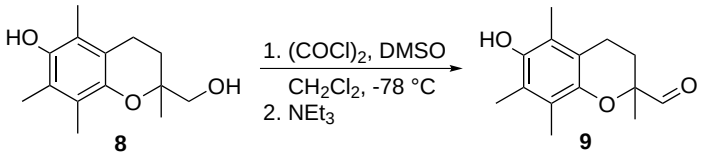

Figure 3.3: Synthesis of **9**.

The Swern oxidation of chromanol alcohol **8** to **9** has been reported previously with a yield of 24%,[80] and with unreported yield.[87] It is apparent from table 3.2 that the oxidation is troublesome. Early attempts according to the procedure of Schiefer afforded a yellow oil, whereas **9** is reported to be crystalline and white.[80] ^{1}H NMR evaluation showed the product formed in the first attempt was a complex mixture of products, containing a considerable amount of DMSO.

The reaction was repeated (attempt 2) under more carefully controlled conditions under septum (and N_2 atmosphere, as in attempt 1), with addition of reagents by syringe. The intention was to minimize the apparatus and the possibility for leakage and exposure to atmospheric oxygen. Oxalyl chloride ($(COCl)_2$) is sensitive to decomposition by hydrolysis, as are several of the intermediates in the reaction mechanism (figure 2.10). However, these efforts did not result in any improvement.

In the following attempts the amount of oxidizing reagents was increased to the point of decomposition of the reaction mixture. The ratio of oxalyl chloride to DMSO was additionally increased, but no advancement was made. One large-scale attempt (attempt 6) aimed to produce a sufficient amount of **9** for characterization, but the complexity of the product mixture made purification a daunting task.

As discussed in section 2.6.2, the Swern oxidation is sensitive to

Table 3.2: Yields and conditions for the synthesis of **9**.

Attempt	**Scale (mg 8)**	**Reaction conditions**	**Yield (%)**
1	200	1.1 eq $(COCl)_2$, 2.4 eq DMSO, 5 eq NEt_3, CO_2/acetone	0
2	100	As in attempt 1, with septum and add. by syringe	0
3	201	5 eq $(COCl)_2$, 5 eq DMSO, 10 eq NEt_3, CO_2/acetone	5[a]
4	206	10 eq $(COCl)_2$, 2.5 eq DMSO, 15 eq NEt_3, CO_2/acetone	–[b]
5	100	5 eq $(COCl)_2$, 1 eq DMSO, 10 eq NEt_3, CO_2/acetone	20[c]
6	1005	1.5 eq $(COCl)_2$, 3 eq DMSO, 5 eq NEt_3, CO_2/acetone	–[d]
7	500	1.1 eq $(COCl)_2$, 2.4 eq DMSO, 5 eq NEt_3, CO_2/Et_2O	28
8	1000	1.2 eq $(COCl)_2$, 2.4 eq DMSO, 5 eq NEt_3, CO_2/Et_2O	65
9	2500	As in attempt 8	51

[a] Purified by TLC
[b] Decomposed rapidly
[c] Crude
[d] Complex mixture

temperature conditions. Elevation of the temperature leads to the formation of mixed thioethers in preference to the desired aldehyde.[67] Based on this, attempts were made at lower temperature. Exchange of the CO_2/dry ice cooling bath with CO_2/diethyl ether (Et_2O) resulted in formation of the desired aldehyde **9** in satisfying yields and good purity. The crude product was in some attempts still a yellow oil, but formed white crystals after purification.

9 was purified by flash chromatography on silica or TLC. Schiefer[80] also suggests recrystallization from hexane/acetone as a suitable method for purification. Initially, purification was performed with tedious acetone/hexane gradient elution and did not give good separation. A change of eluent to ethyl acetate in CH_2Cl_2 (2%) gave good separation, and eluted **9** first from the column.

3.2.2 Silyl ether protection and deprotection

The difficulties of synthesizing **9** discussed in section 3.2.1 might be due to the reactivity of the phenolic group of **8** and consequent formation of byproducts. Therefore, pre-oxidation protection of the phenol was attempted.

Silylation involved protection of the phenol with TBDMS-Cl by imidazol catalysis (figure 3.4). The mechanism for silylation of alcohols is given in figure 2.19 (section 2.6.7) and the experimental description in section 6.3.1.

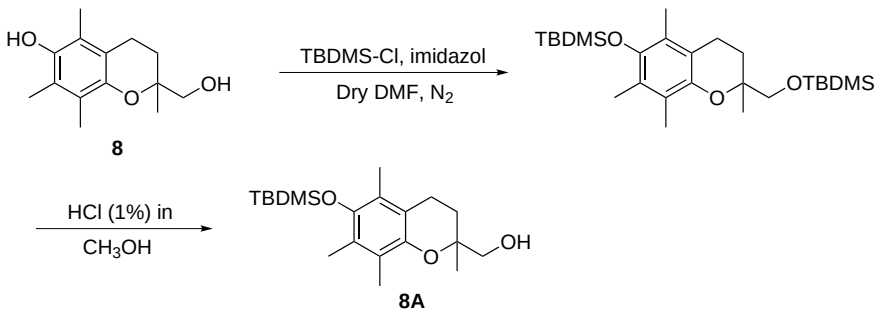

Figure 3.4: Synthesis of **8A**.

The transformation is a two-step reaction, and was intended to be

performed without purification of the intermediate disilylated chromanol alcohol. This is the reason for the twofold excess of silylation agent. The second step is based on the selective acidic hydrolysis of primary silyl enol ethers, as described by Davies *et al.*[84] Under these conditions, aromatic silyl ethers are quite stable.

The reaction between **8** and TBDMS-Cl with imidazole proceeded smoothly in dry DMF overnight. A small sample of the crude product was purified by TLC for evaluation by ^{1}H NMR (appendix B, figure B.1). The analysis showed only the primary hydroxy group had reacted with TBDMS-Cl to form **8B** (structure in figure 3.2).

Preferential silylation of the primary hydroxy group may be explained by the sterical situation of the phenolic group. The steric bulk of *tert*-butyldimethylsilyl group is too large for the hindered nucleophile to approach the silicon atom. Extensive silylation of the primary hydroxy group is not surprising, as the nucleophilicity of primary alcohols is larger than for phenols, owing to the delocalization of phenoxy electrons in the aromatic system.[76b]

Deprotection by TBAF

As protection of the primary alcohol is of no interest, an attempt was made to recover the chromanol **8** from **8B**. This was endeavoured by treatment of **8B** with *tert*-butylammonium fluoride, as shown in figure 3.5. The mechanism is discussed in section 2.6.7.

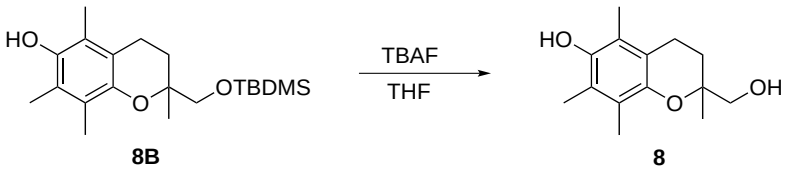

Figure 3.5: Deprotection of **8B**.

This method was used by Atkinson *et al.*[4] in their final step to the unsaturated α-tocopherol analogue α-T6 (yield 38%, see section 1.1). The polyene chain of α-T6 was reported to be intact. No **8** was formed, due to the extensive decomposition of the reactants. Reaction time (2 h by Atkinson *et al.*, 4 h in the current attempt) may be one

explanation of the decomposition. The fluoride ion is a strong base, particularly in organic solvents. This may contribute to side reactions and decomposition.[77e]

3.2.3 Benzyl ether protection and deprotection

Benzylation is another method to protect the phenol group in **8** as exemplified by Acuña *et al.*[86] (figure 3.6). The mechanism is shown in figure 2.20, section 2.6.8. The experimental description is given in section 6.3.3.

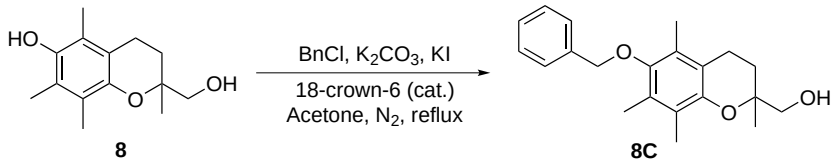

Figure 3.6: Synthesis of **8C**.

The reaction progress was monitored by TLC, until decomposition after 96 h without any formation of **8C**.

The reaction is mediated by a weak base in order to make it selective for the more acidic phenolic group, as achieved for **8** earlier by Cohen *et al.* (97% yield).[82] Addition of KI and 18-crown-6 catalyzes the reaction. In polar aprotic solvents like acetone, K^+ is selectively solvated, increasing the distance to the anion. This *naked anion effect* is enhanced by the addition of 18-crown-6, forming complexes with the cation (illustrated in figure 3.7).

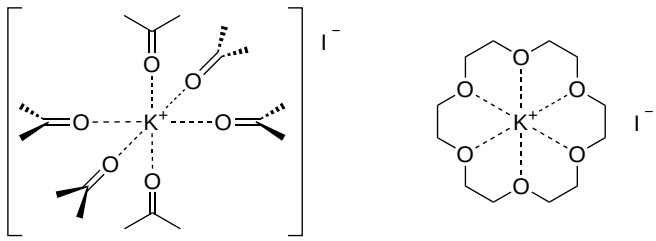

Figure 3.7: Selective solvation and complexation of K^+ by 18-crown-6 in acetone.

One consequence of the naked anion effect is improved solubility of the inorganic salt in organic solvents. More importantly, the nucleophilicity of the anion I^- is increased, causing displacement of chloride and *in situ* generation of benzyl iodide. Iodide, being a better leaving group than chloride, thus increases the rate of attack by the alcohol and consequent product formation.[64e,76c] The mechanism of this catalysis is shown in figure 3.8.

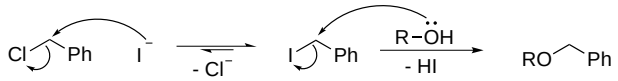

Figure 3.8: Mechanism for catalysis of the formation of **8C** by KI.

Subsequent deprotection of the phenol was to be performed with a Lewis acid like BBr_3,[77d] although the substrate *might* not be stable to this treatment.

3.2.4 The Dess-Martin oxidation

The Dess-Martin oxidation with periodinane was an alternative attempt to oxidize **8** to **9**. The general mechanism is shown in figure 2.12 (section 2.6.3), and the experimental procedure is given in section 6.4.1. Product **9** was not formed (figure 3.9).

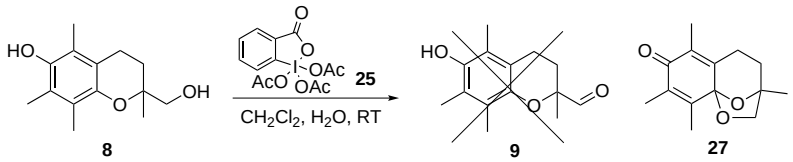

Figure 3.9: Attempted Dess-Martin oxidation of **8**. **27** was formed in favour of expected **9**.

The reaction proceeds smoothly in aqueous CH_2Cl_2 and gives pure **27** as the only product in good yields. The reaction was performed twice to determine whether the conditions affected the chemoselectivity. These attempts are summarized in table 3.3. No attempts were made in which the periodinane **25** was hydrolyzed to **26** (figure 2.13) before addition of **8**.

Table 3.3: Yields and conditions for the synthesis of **27**.

Attempt	Scale (mg 8)	Reaction conditions	Yield (%)
1	100	2.5 eq **27**, 2.5 eq H_2O in dry CH_2Cl_2, 4.5 h. NaOH workup	52
2	100	1.5 eq **27**, H_2O sat. CH_2Cl_2, 1 h 40 min. $Na_2S_2O_3$ workup	71

^{1}H NMR (appendix C, figure C.2) clearly showed that the aldehyde **9** had not been formed by the absence of the aldehydic proton signal around δ 9.5 ppm. Further NMR experiments and characterization by MS and IR elucidated **27** (section 5.3 and appendix C).

The *p*-hydroquinone-like chroman system of **8** was oxidized to a *p*-quinone-like tocophorone by the Dess-Martin periodinane **25** (figure 3.9). This transformation occurs in preference to the oxidation of the primary hydroxy group. The precise origin of this chemoselectivity is not clear. The same transformation has been achieved with cerium(IV) sulphate.[82] Similar oxidation products of tocopherols have been reported,[32b,88,89] including the oxidation of α-tocopherol to "α-tocopheroxide" (**28**). **28** may be regarded as an acetal of the corresponding *p*-tocophorone (**29**, see figure 3.10). The oxidation is performed by $FeCl_3$, tetrachloro-*o*-quinone or *N*-bromosuccinimide in the presence of alcohols. **27** may similarly be regarded an intramolecular acetal of a *p*-tocopherone.

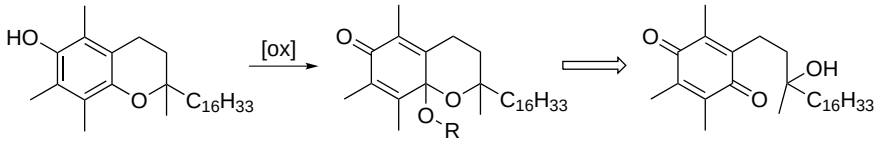

Figure 3.10: Oxidation of α-tocopherol to "α-tocopheroxide". Reported oxidizing agents are $FeCl_3$, tetrachloro-*o*-quinone or *N*-bromosuccinimide.

A tentative mechanism for the oxidation of **8** to **27** is shown in figure 3.11. It must be emphasized that this mechanism is deduced

solely on the base of chemical rationale. Mechanistic studies have not been performed. One objection to the proposed mechanism is the steric stituation of the phenolic group, expected to preclude addition of this group to the periodinane reagent.

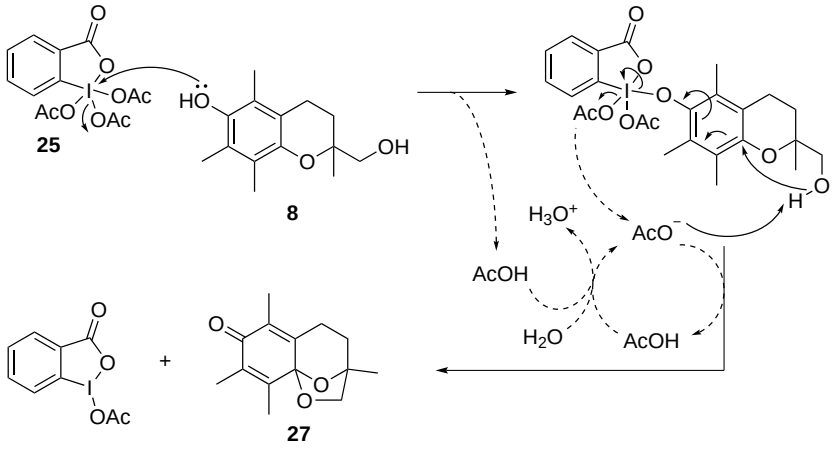

Figure 3.11: Tentative mechanism for the formation of **27** from **8**.

3.3 Synthesis of 5-(6-hydroxy-2,5,7,8-tetramethylchroman-2-yl)-2-methylpenta-2,4-dienal (11)

In a Wittig reaction, phosphonium salt **10** was reacted with **9** to form **11** according to the two procedures in figure 3.12. A general mechanism for the reaction is shown in figures 2.14 and 2.15. Subsequent hydrolysis of the resulting acetal afforded **11** (mechanism in figure 2.17). The experimental procedures are given in section 6.5. Table 3.4 gives an overview of the conditions and yields of various attempts.

Some initial attempts to run the reaction with crude **9** from failed Swern oxidation attempts resulted in complex product mixtures. As purification would be a daunting endeavour, the crude products were not purified. Later TLC co-chromatography with a pure sample of **11** showed that reaction 2 afforded a small amount of product.

Table 3.4: Yields and conditions for the synthesis of **11**.

Attempt	Scale (mg 9)	Reaction conditions	Yield (%)
1	20[a]	10 eq **10**, MeOK (10 eq), MeOH, CH_2Cl_2, MW (80 W, 20 min)	–[b]
2	100[c]	10 eq **10**, MeOK (10 eq), MeOH, CH_2Cl_2, reflux (21 h)	–[d]
3	55	10 eq **10**, MeOK (10 eq), MeOH, CH_2Cl_2, MW (80 W, 20 min)	–[e]
4	20	5 eq **10**, MeOK (5 eq), MeOH, CH_2Cl_2, reflux (114 h)	–[e]
5	20	5 eq **10**, 1,2-epoxybutane, EtOH, MW (320 W, 1 h 10 min)	–[e]
6	20	5 eq **10**, 1,2-epoxybutane, EtOH, reflux (72 h)	–[e]
7	100	5 eq **10**, MeONa (5 eq), MeOH, CH_2Cl_2, reflux (20 h)	33
8	50	2.6 eq **10**, MeONa (6.1 eq), MeOH, CH_2Cl_2, MW (80 W, 20 min)	–[e]
9	389	5 eq **10**, MeONa (5 eq), MeOH, THF, reflux (22 h)	26
10	504	5 eq **10**, MeOK (5 eq), MeOH, CH_2Cl_2, MW (90 W, 26 min)	19

[a] Crude, from early attempt of Swern oxidation
[b] Not purified due to complexity of product mixture
[c] Impure, from early attempt at Swern oxidation
[d] Very low. Used for qualitative TLC assessment of methods
[e] Used for qualitative TLC assessment of methods

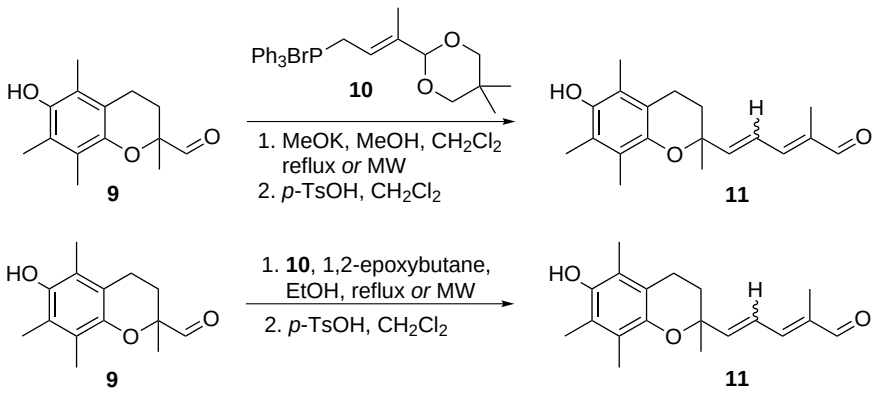

Figure 3.12: Synthesis of **11**.

Each method was optimized in small scale (table 3.4, attempts 3–6). Conditions for the microwave reactions were chosen in collaboration with Ph.D. candidate Muhammad Zeeshan, who had experience in microwave Wittig reactions.[90] The crude products were compared by TLC co-chromatography. After analysis, the combined crude products were purified by flash column chromatography, as described below, to afford a common batch of **11**.

The mild method mediated by 1,2-epoxybutane proved to be inefficient, as the reaction mixture still contained a substantial amount of starting material. This may be due to the steric hindrance imposed on aldehyde **9** by the quaternary α-position. As product to byproduct ratios seemed similar to the base mediated method, the epoxide mediated method was rejected for this step. However, it might be interesting to consider this method for the subsequent second elongation in future work.

A base driven reaction under microwave conditions was selected for further development. This decision was based on the full conversion of starting material **9** in these attempts, and the shortening of reaction time from ca. 20 h to 20–25 min compared to refluxing. Some variations of base and solvent were examined in late attempts, but admittedly not investigated systematically enough to make any conclusions as to their affect on the reaction outcome.

The hydrolysis of the intermediate acetal formed in most cases proceeded rapidly. **11** was even found to be present in the crude intermediate pre-hydrolysis (minor hydrolysis of the acetal under basic conditions). In a few cases, the reaction was very sluggish or did not proceed. In the case of attempt 3, even refluxing the crude intermediate with *p*-toluenesulfonic acid for 20 h did not completely hydrolyze the product. A milder method with citric acid in methanol (30%) and refluxing for 26 h proved to be successful (section 6.5.5).

Chromatographic workup of crude **11** proved to be a demanding task. Gradient elution is required due to the small differences in polarity between the starting material and product. In eluent systems based on ethyl acetate in hexane, the product spot showed two compounds of almost identical polarity. Detailed development of a tertiary eluent system ((2 : 1 CH_2Cl_2 : ethyl acetate)/hexane) with gradient elution afforded separation. ^{1}H NMR analysis showed they were *cis*/*trans* isomers, the *cis* isomer being the most nonpolar fraction. The analysis is detailed in section 5.5. NMR spectra are given in appendix E.

Cis/*trans* isomers were separated and the *cis* : *trans* ratio was found to be 72 : 28 for attempt 9, and 37 : 63 for attempt 10. As the ylide from **10** is stabilized by delocalization, formation of the *trans* isomer is expected to be favoured (see the discussion of Wittig reaction stereoselectivity in section 2.6.4). The stereochemical preference, although modest, is reversed in the two attempts without any apparent reason.

3.4 Synthesis of 9-(6-hydroxy-2,5,7,8-tetramethylchroman-2-yl)-2,6-dimethylnona-2,4,6,8-tetraenal (12)

Compound **12** has been synthesized from **11** by a microwave Wittig reaction with phosphonium salt **10** and following hydrolysis of the intermediate acetal with *p*-toluenesulfonic acid (figure 3.13). Mechanisms are given in figures 2.14 and 2.17. The experimental description is given in section 6.6. Table 3.5 shows conditions and yields for the different attempts.

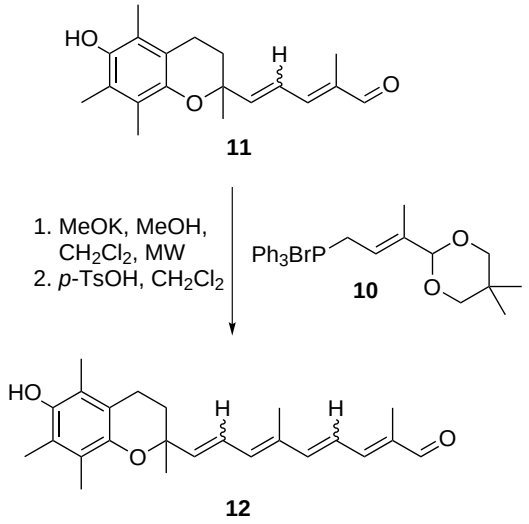

Figure 3.13: Synthesis of **12**.

The yields of the second elongation step are low since there was not enough time to optimize the reaction conditions. The crude products were purified by ethyl acetate/cyclohexane gradient elution, but this system did not give good separation and the NMR spectra (appendix F) indicated the presence of impurities. Time concerns precluded optimization of the eluent system.

The complexity of the spectra may be attributed to the presence of various *cis*/*trans* isomers. The reaction was performed with mixtures of (*Z*)-**11** and (*E*)-**11**. The intention was to isomerize the double bonds to the more thermodynamically favourable *trans* geometry once the target compound **1** had been produced. This may be achieved by treatment of a solution of **1** with I_2 in light, as shown in figure 3.14.[91,92]

Solutions of **12** appear orange compared to the yellow solutions of **11**. λ_{max} increases from 275 nm to 350 nm. The colour of **12** in solution was found to be pH dependant. During workup, a sudden change from orange to deep, intense red was observed when the organic phase was washed with $NaHCO_3$ solution. The colour returned to orange when the organic phase was washed with H_2O.

Table 3.5: Yields and conditions for the synthesis of **12**.

Attempt	Scale (mg 11)	Reaction conditions	Yield (%)
1	14	5 eq **10**, MeONa (5 eq), MeOH, THF, MW (80 W, 20 min)	–[a]
2	52	3 eq **10**, MeONa (3.5 eq), MeOH, CH_2Cl_2, MW (80 W, 25 min)	14[b]
3	125	3 eq **10**, MeOK (3 eq), MeOH, CH_2Cl_2, MW (80 W, 25 min)	7[b]

[a]Purification by TLC and identification of **12** by MS
[b]Not pure

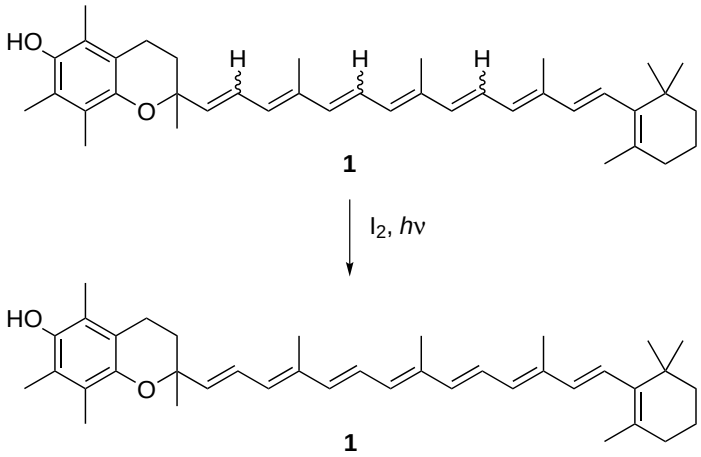

Figure 3.14: Photoinduced isomerization of **1** by I_2.

3.5 Protection of 9

The Wittig synthesis of **12** had not afforded good yields. Consequently, an attempt was made to protect the phenyl group of chromanol aldehyde **9** before retrying the Wittig reactions. Unfortunately, the efforts to protect the phenol did not give any useful result as further discussed in the following sections.

3.5.1 Synthesis of 2-formyl-2,5,7,8-tetramethylchroman-6-yl benzoate (9A)

Protection of **9** by benzoylation to **9A** was achieved by the method shown in figure 3.15. The experimental description is given in section 6.7.1. Table 3.6 shows the yields achieved under different conditions.

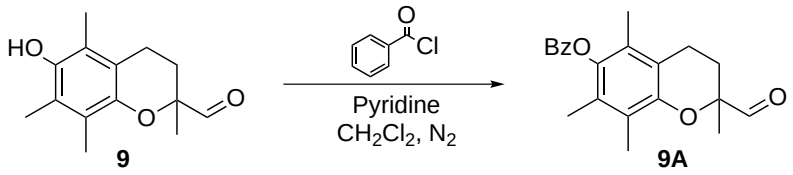

Figure 3.15: Synthesis of **9A**.

Table 3.6: Yields and conditions for the synthesis of **9A**.

Attempt	Scale (mg 9)	Reaction conditions	Yield (%)
1	145	1.1 eq BzCl, CH_2Cl_2, pyridine, 0 °C, then RT	–[a]
2	114	1.5 eq BzCl, pyridine, RT	87[b]

[a] Not isolated or purified
[b] Crude

TLC analysis of the reaction mixture from attempt 1 showed no apparent product formation, even after 22 h of stirring. DMAP was added to increase the reaction rate. It acts as a better catalyst of the reaction due to additional resonance stabilization of the intermediate acyl pyridinium ion.[78] However, even after 90 h of stirring, no product was visible by TLC. The sensitive benzoyl chloride might have been hydrolyzed to benzoic acid. *N*,*N*′-Dicyclohexylcarbodiimide (DCC) was then used to catalyse the esterification of possible benzoic acid with phenol **9** (Steglich esterification, figure 3.16).[64f,93] The attempt was aborted after 114 h of total reaction time with no product formation (TLC evidence).

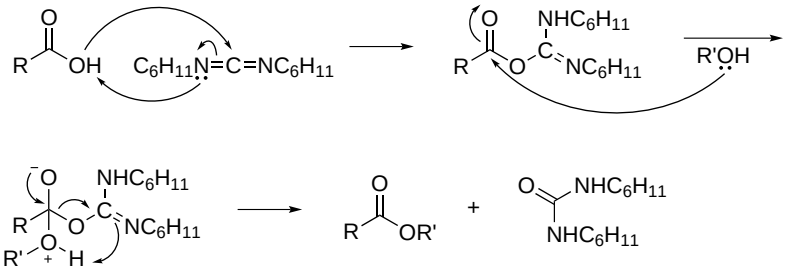

Figure 3.16: A general mechanism for the Steglich esterification.

The reaction was repeated with fresh benzoyl chloride. Now, the reaction proceeded smoothly and was finished in 15 min. Upon addition of benzoyl chloride, the reaction mixture became opaque. This was assumed to be due to formation of pyridinium salt. However, it turned out that the product itself was precipitated. Furthermore, the product proved to be insoluble in all common laboratory solvents. Its identity could only be confirmed by MS analysis, run with the solid sample. The insolubility of the product precludes purification, and further Wittig elongation.

During the workup, one curious effect was noticed. Although the crude product was insoluble, it was readily dispersed in liquids. When washing the CH_2Cl_2 solution with H_2O, the solid material distributed over both phases. Upon acidification with HCl, the solid material only dispersed in the organic phase. Washing with aqueous $NaHCO_3$ resulted in the product being dispersed solely in the aqueous phase.

3.5.2 Attempted synthesis of 6-(*tert*-butyldimethylsilyloxy)-2,5,7,8-tetramethylchroman-2-carbaldehyde (9B)

Following the synthesis of **9A**, another protection method by silylation of the phenolic group was attempted (figure 3.17). The experimental procedure is given in section 6.7.2.

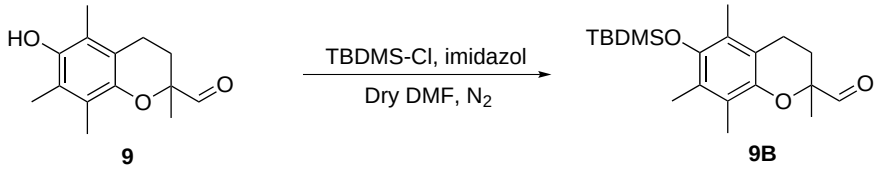

9 **9B**

Figure 3.17: Synthesis of **9B**.

This is the protection method employed by Atkinson *et al.*[4] in their synthesis of α-tocopherol analogue α-T6, as discussed in section 1.1. Their procedure was followed exactly, but product formation was not apparent by TLC after 5 h. For practical reasons, the reaction mixture was left overnight. At the following morning the reaction had decomposed. Due to lack of time, the protection reaction could not be repeated.

3.6 Future work

The obvious continuation of this work is the synthesis of target molecule **1** as outlined in figure 1.4. Before the final Wittig elongation step with phosphonium salt **13**, optimization of reaction conditions for the synthesis of **12** should be performed to increase yields. Purification methods for this step also require optimization. As mentioned in section 3.3, the epoxide mediated Wittig reaction may be appropriate for the synthesis of **12**. The reason for this is the reduced steric demand in the α position of the aldehyde in **11** compared to **9**.

A systematic investigation of the effect of solvent or choice of base in the Wittig synthesis of **11** may also lead to increased yields for this step. This may also give further insight into what parameters cause a shift in *cis*/*trans* stereoselectivity for the Wittig reaction.

The synthesis may be extended to more homologues in this novel chromanol carotenoid class. Variations in polyene chain length and cyclic end groups may be beneficial for structure—activity relationship studies of antioxidant activity and gene transfection vector efficiency. A suggestion for an analogue library based on β-carotene, zeaxanthin and astaxanthin is given in figure 3.18.

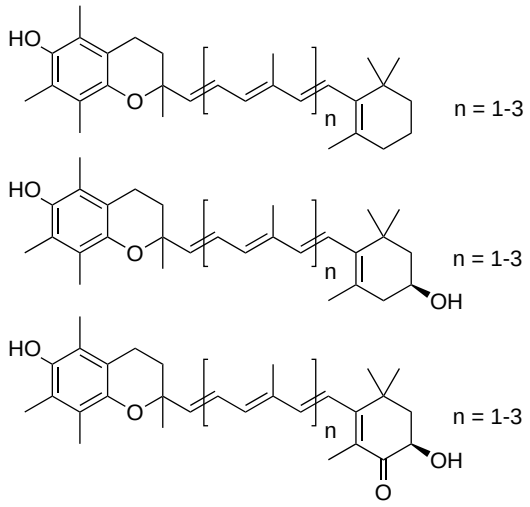

Figure 3.18: A suggested analogue library for future structure-activity relationship studies.

The Dess-Martin oxidation (section 3.2.4) seemed to be a suitable method of oxidixing **8** to **9**. Unexpectedly **27** was formed, with chemoselective oxidation of the *p*-hydroquinone-like chromanol system in preference to the primary alcohol. Further mechanistic studies of this step could provide insight into the nature of the oxidation method, and the reactivity of other chromanols. For the purpose of synthetic utilization in the synthesis of **1**, the Dess-Martin oxidation might as well be worth a revisit. The transformation may be attempted in a procedure employing hydrolysis of the reagent **25** to **26** (see section 2.6.3) prior to addition of **8**, or even under anhydrous conditions.

Chapter 4

Conclusion

The precursor **12** of target molecule **1** has been synthesized by a Wittig reaction with microwave irradiation.

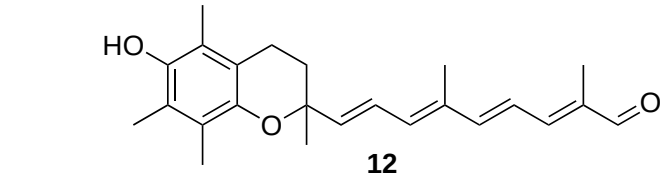

12

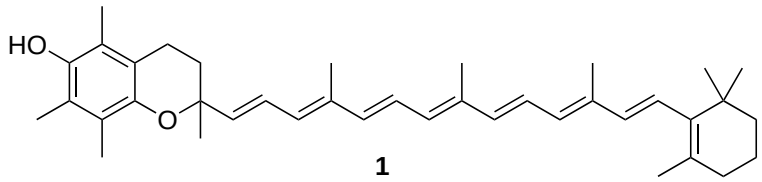

1

The total yield is 3%, which is low. The reaction conditions and purification method for the final step in the synthesis of **12** require optimization.

11, the precursor to **12**, has been synthesized by a Wittig reaction with reflux and microwave irratiation. **11** was separated into its *cis* and *trans* isomers by flash column chromatography. The *cis* : *trans* ratio was found to be varying.

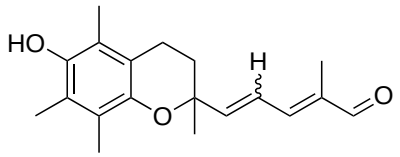

11

Attempts were made to protect the intermediate **8** by silylation to **8A** and benzylation to **8C**. Only **8B** was formed. Similarly, efforts were made to protect the intermediate **9** by benzoylation to **9A** and silylation to **9B**. Only **9A** was formed, but found to be insoluble in all common laboratory solvents.

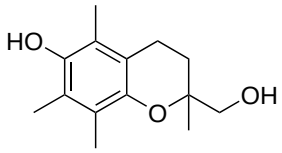

8

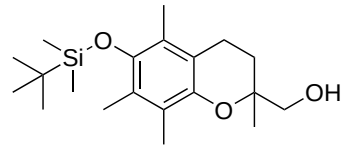

8A

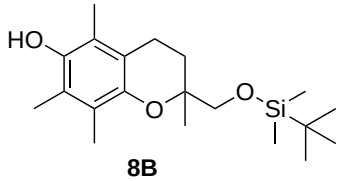

8B

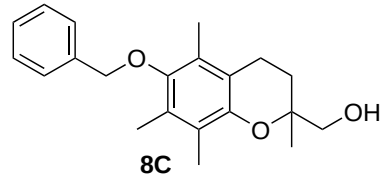

8C

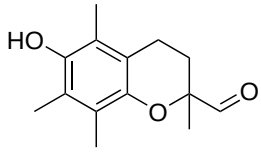

9

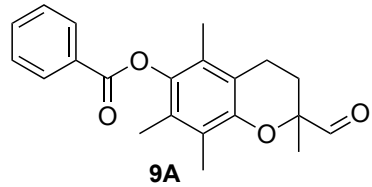

9A

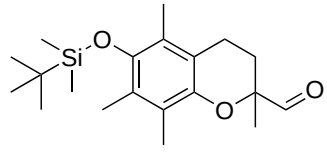

9B

Intermediate **9** was formed from **8** by the Swern oxidation. The Dess-Martin oxidation was also attempted, but led to the formation of an unexpected quinone-like derivative **27**.

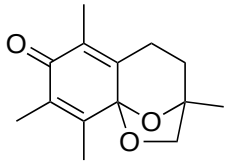

27

Chapter 5

Spectroscopy

5.1 2-Hydroxymethyl-2,5,7,8-tetramethylchroman-6-ol (8)

The IR spectrum of **8** (appendix A, figure A.1) shows characteristic O–H stretching at 3280 cm^{-1}. The absence of a strong C=O stretching signal in the 1700–1750 cm^{-1} region is a clear indication that the precursor acid **7** has been fully reduced (see section 3.1).

5.1.1 NMR spectroscopy

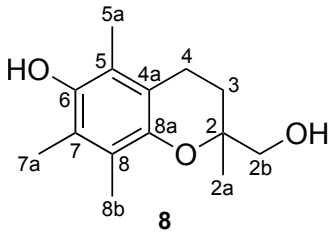

8

Figure 5.1: Structure and numbering of atoms in **8**.

The assignment of ^{1}H NMR shifts (δ H), multiplicity (M) and ^{13}C NMR shifts (δ C) for **8** is shown in table 5.1. Coupling constants (J) are not included as all ^{1}H signals are either singlets or multiplets. The numbering of the atoms is shown in figure 5.1. ^{1}H and ^{13}C shifts are assigned in accordance with ^{1}H (figure A.2), ^{13}C (figure A.3), HSQC

(figure A.4), HMBC (figure A.5–A.6) and COSY (figure A.7) NMR spectra (appendix A).

Table 5.1: Assigned shifts for **8**.

Carbon no.	**δ H (ppm)**	**M**	**δ C (ppm)**
C-2	–	–	75.20
C-2a	1.22	s	20.51
C-2b	3.69–3.55	m	69.51
C-2b–O**H**	2.05–1.90	s[a]	–
C-3	2.05–1.90	m[a]	28.00
	1.77–1.69	m	
C-4	2.74–2.59	m	20.38
C-4a	–	–	117.5
C-5	–	–	118.9
C-5a	2.12	s	11.42
C-6	–	–	145.2
C-6–O**H**	4.29	s	–
C-7	–	–	121.5
C-7a	2.17	s	12.31
C-8	–	–	122.7
C-8a	–	–	145.0
C-8b	2.11	s	11.97

[a]Overlapping with other signals

5.1.2 MS fragmentation

MS ionization by electron impact (EI) may cause fragmentation of the molecule. Such fragments contain important information about the molecular structure. The LRMS spectrum by EI ionization of **8** (appendix A, figure A.8) is summarized in table 5.2. The fragments are named in accordance with figure 5.2.

Table 5.2: Main MS fragments of **8**.

m/z	**Rel. intensity (%)**	**Fragment**	**Name**
236	94	$[M]^+$	–
218	5	$[M-H_2O]^+$	A
205	90	$[M-CH_3O]^+$	B
203	62		–
166	55	$[M-C_4H_6O]^+$	–
165	100	$[M-C_4H_7O]^+$	C
164	38	$[M-C_4H_8O]^+$	D
121	11	$[M-C_6H_{11}O_2]^+$	–

Figure 5.2 shows possible radical ion fragments of **8**. These fragments contribute to confirming the identity of compound **8**. The fragments may be formed either by direct fragmentation of the molecular ion or by subsequent fragmentation of a fragment. Fragmentation may also be preceded by migrations and rearrangements.

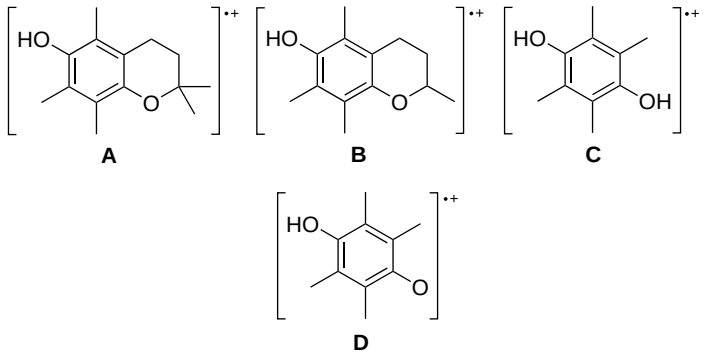

Figure 5.2: Possible radical ion fragments of **8**.

5.2 2-(*tert*-Butyldimethylsilyloxymethyl)-2,5,7,8-tetramethylchroman-6-ol (8B)

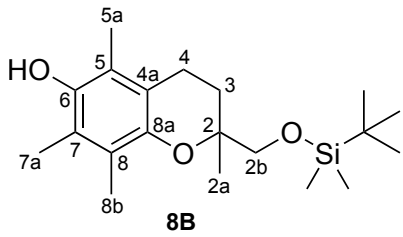

Figure 5.3: Structure and numbering of atoms in **8B**.

The assignment of ^{1}H NMR shifts (δ H), multiplicity (M), coupling constants (J) and ^{13}C NMR shifts (δ C) for **8B** is shown in table 5.3. The numbering of the atoms is shown in figure 5.3. ^{1}H and ^{13}C shifts are assigned in analogy to **8**. ^{1}H (figure B.1) and ^{13}C (figure B.2) NMR spectra are shown in appendix B.

Table 5.3: Assigned shifts for **8B**.

Carbon no.	**δ H (ppm)**	**M**	***J* (Hz)**	**δ C (ppm)**
C-2	–	–	–	75.31
C-2a	1.24	s	–	18.37
C-2b	3.64–3.58	d	9.76	68.57
	3.54–3.48	d	9.76	
C-3	2.02–1.91	m	–	28.32
	1.80–1.71	m	–	
C-4	2.65–2.57	t	6.84	20.54
C-4a	–	–	–	117.7
C-5	–	–	–	118.6
C-5a	2.12	s	–	11.44
C-6	–	–	–	145.7
C-6–O**H**	4.19	s	–	–
C-7	–	–	–	121.2
C-7a	2.16	s	–	12.35

Table 5.3 (*cont.*)

Carbon no.	δ H (ppm)	M	*J* (Hz)	δ C (ppm)
C-8	–	–	–	122.6
C-8a	–	–	–	144.8
C-8b	2.11	s	–	11.97
-Si-C($\mathbf{C}H_3$)$_3$	0.91	s	–	25.99
-Si-CH_3	0.07	s	–	−5.25
	0.04	s	–	−5.32
-Si-$\mathbf{C}(CH_3)_3$	–	–	–	22.18

5.3 3,6,8,9-Tetramethyl-2,4,5-trihydro-3,9a-epoxybenzooxepin-7-one (27)

The IR spectrum of compound **27** (figure C.1, appendix C) shows a strong C=O stretching signal at 1629 cm^{-1}. This wavenumber is too low to originate from an aldehyde, but is consistent with a conjugated, cyclic ketone or quinone. The absence of an O–H stretching signal around 3200–3500 cm^{-1} is also in accordance with the proposed structure of **27**.

5.3.1 NMR spectroscopy

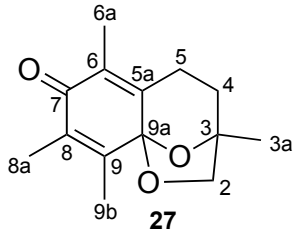

27

Figure 5.4: Structure and numbering of atoms in **27**.

The absence of an aldehydic signal in the δ 9–10 ppm region of the ^{1}H NMR spectrum of **27** (figure C.2) is an indication that the

expected aldehyde (**9**) was not formed in the Dess-Martin oxidation of **8** (see section 3.2.4).

The assignment of ^{1}H NMR shifts (δ H), multiplicity (M), coupling constants (J) and ^{13}C NMR shifts (δ C) for **27** is shown in table 5.4. The numbering of the atoms is shown in figure 5.4. ^{1}H and ^{13}C shifts are assigned in accordance with ^{1}H (figure C.2), ^{13}C (figure C.3), DEPT135 (figure C.4), HSQC (figure C.5), HMBC (figure C.6–C.7) and COSY (figure C.8) NMR spectra (appendix C).

Table 5.4: Assigned shifts for **27**.

Carbon no.	**δ H (ppm)**	**M**	***J* (Hz)**	**δ C (ppm)**
C-2	4.18–4.14	d	6.88	74.68
	3.65–6.61	d	6.88	
C-3	–	–	–	80.93
C-3a	1.42	s	–	22.15
C-4	1.96–1.82	m[a]	–	35.83
C-5	2.74–2.53	m	–	22.70
C-5a	–	–	–	147.5
C-6	–	–	–	126.8
C-6a	1.79	s	–	10.41
C-7	–	–	–	185.3
C-8	–	–	–	134.5
C-8a	1.86	s[a]	–	11.67
C-9	–	–	–	145.4
C-9a	–	–	–	100.1
C-9b	1.90	s[a]	–	12.91

[a] Overlapping with other signals

5.3.2 MS fragmentation

The LRMS spectrum by EI ionization of **27** (appendix C, figure C.9) is summarized in table 5.5. The naming of the fragments is in accordance with figure 5.5.

Table 5.5: Main MS fragments of **27**.

m/z	Rel. intensity (%)	Fragment	Name
234	88	$[M]^+$	–
216	12	$[M-H_2O]^+$	E
206	29	$[M-CO]^+$	F
204	96	$[M-CH_2O]^+$	G
189	100	$[M-C_2H_5O]^+$	H
177	21	$[M-C_3H_5O]^+$	–
161	46	$[M-C_3H_5O_2]^+$	I
148	17	$[M-C_4H_6O_2]^+$	–
136	15		–
105	10		–
91	19	$[M-C_7H_{11}O_3]^+$	–

Figure 5.5 shows possible radical ion fragments of **27**. These fragments contribute to confirming the identity of compound **27**. The fragments may be formed either by direct fragmentation of the molecular ion or by subsequent fragmentation of a fragment. Fragmentation may also be preceded by migrations and rearrangements.

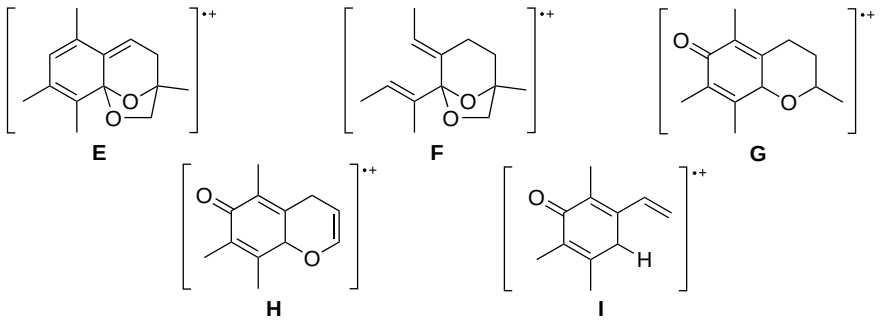

Figure 5.5: Possible radical ion fragments of **27**.

5.4 6-Hydroxy-2,5,7,8-tetramethylchroman-2-carbaldehyde (9)

The IR spectrum of **9** (figure D.1) exhibits characteristic O–H stretching at 3535 cm^{-1} *and* a strong C=O stretching signal at 1732 cm^{-1}. This is in agreement with the expected oxidation of **8** to **9** by the Swern oxidation (see section 3.2.1).

5.4.1 NMR spectroscopy

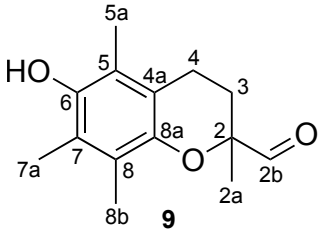

Figure 5.6: Structure and numbering of atoms in **9**.

The assignment of ^{1}H NMR shifts (δ H), multiplicity (M) and ^{13}C NMR shifts (δ C) for **9** is shown in table 5.6. Coupling constants (J) are not included as all ^{1}H signals are either singlets or multiplets. The numbering of the atoms is shown in figure 5.6. ^{1}H and ^{13}C shifts are assigned in accordance with ^{1}H (figure D.2), ^{13}C (figure D.3), HSQC (figure D.4) , HMBC (figure D.5–D.6) and COSY (figure D.7) NMR spectra (appendix D).

Table 5.6: Assigned shifts for **9**.

Carbon no.	δ H (ppm)	M	δ C (ppm)
C-2	–	–	80.41
C-2a	1.38	s	21.66
C-2b	9.61	s	204.7
C-3	2.31–2.22	m	28.05
	1.86–1.76	m	
C-4	2.67–2.48	m	20.51

Table 5.6 (*cont.*)

Carbon no.	δ H (ppm)	M	δ C (ppm)
C-4a	–	–	117.6
C-5	–	–	118.8
C-5a	2.06	s	11.34
C-6	–	–	145.7
C-6–O**H**	4.30	s	–
C-7	–	–	121.7
C-7a	2.17	s	12.32
C-8	–	–	122.9
C-8a	–	–	145.3
C-8b	2.20	s	12.00

5.4.2 MS fragmentation

The main fragments of **9** from LRMS by EI ionization (appendix D, figure D.8) are shown in table 5.7. The naming of the fragments is in accordance with figure 5.7.

Table 5.7: Main MS fragments of **9**.

m/z	Rel. intensity (%)	Fragment	Name
234	31	$[M]^+$	–
205	100	$[M-CHO]^+$	B
190	22	$[M-C_2H_4O]^+$	J
149	13	$[M-C_4H_5O]^+$	–
91	11	$[M-C_7H_{11}O_3]^+$	–
70	19	$[M-C_{10}H_{12}O_2]^+$	–

Figure 5.7 shows possible radical ion fragments of **9**. The loss of CHO (fragment **B**) is typical to aldehydes. The fragment at m/z 91 is most likely the tropylium ion. These fragments contribute to confirming the identity of compound **9**. The fragments may be formed either by direct fragmentation of the molecular ion or by subsequent fragmentation of a fragment. Fragmentation may also be preceded by migrations and rearrangements. Fragment **B** (m/z 205) is also seen in the LRMS spectrum of **8**, cf. figure 5.2.

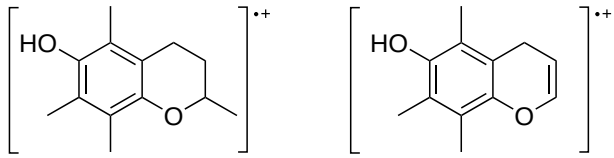

B **J**

Figure 5.7: Possible radical ion fragments of **9**.

5.5 5-(6-Hydroxy-2,5,7,8-tetramethylchroman-2-yl)-2-methylpenta-2,4-dienal (4*Z*-11)

The IR spectra (appendix E, figure E.1) of the *cis* and *trans* isomers of **11** are identical. The spectrum shows characteristic O–H and C=O stretching at 3450 and 1667 cm^{-1}, respectively. A strong signal owing to conjugated C=C stretching is also seen at 1630 cm^{-1}.

Both isomers of **11** are coloured. In solution, they are both light yellow, while as a neat liquid they are dark orange to red in colour. The *trans* isomer appears darker in colour than the *cis* isomer. Even so, both isomers have a UV/Vis λ_{max} of 275 nm (figure E.2). The theoretically calculated λ_{max} value according to Woodward's rules for conjugated carbonyls is 268 nm.

5.5.1 NMR spectroscopy

(4*Z*)-isomer

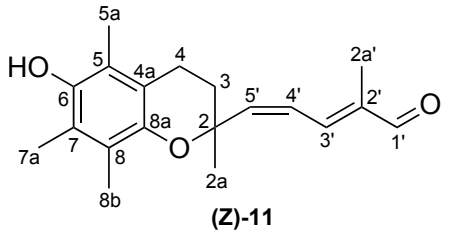

(Z)-11

Figure 5.8: Structure and numbering of atoms in (4*Z*)-**11**.

The assignment of ^{1}H NMR shifts (δ H), multiplicity (M), coupling constants (J) and ^{13}C NMR shifts (δ C) for (4*Z*)-**11** is shown in table 5.8. The numbering of the atoms is shown in figure 5.8. ^{1}H and ^{13}C shifts are assigned in accordance with ^{1}H (figure E.3), ^{13}C (figure E.4), HSQC (figure E.5–E.6), HMBC (figure E.7–E.8) and COSY (figure E.9) NMR spectra (appendix E).

The *cis* isomer of **11** is distinguishable from the *trans* isomer by comparison of the ^{3}J(H,H) coupling constants. The C-4′ and C-5′ protons exhibit a coupling of 11.80 Hz in the *cis* isomer and 15.12 Hz in the *trans* isomer (cf. table 5.9). These coupling values are typical for *cis* and *trans* isomers, respectively.[94]

Table 5.8: Assigned shifts for (4*Z*)-**11**.

Carbon no.	**δ H (ppm)**	**M**	***J* (Hz)**	**δ C (ppm)**
C-2	–	–	–	76.77
C-2a	1.56	s	–	27.79
C-3	2.15–2.01	m[a]	–	33.91
	1.90–1.79	m[a]	–	
C-4	2.74–2.55	m	–	21.35
C-4a	–	–	–	117.7
C-5	–	–	–	119.1
C-5a	2.10	s[a]	–	11.66
C-6	–	–	–	145.5
C-6–O**H**	4.32	s	–	–
C-7	–	–	–	121.8
C-7a	2.15	s[a]	–	12.57
C-8	–	–	–	122.4
C-8a	–	–	–	145.2
C-8b	2.20	s[a]	–	12.62
C-1′	9.45	s	–	195.7
C-2′	–	–	–	139.1
C-2a′	1.77	s[a]	–	9.13
C-3′	7.82–7.77	d	11.96	144.4
C-4′	6.49–6.38	ft[b]	11.96	124.8
			11.80	
C-5′	5.91–5.82	d	11.80	143.6

[a] Overlapping with other signals
[b] False triplet, should be interpreted as doublet of doublets

(4*E*)-isomer

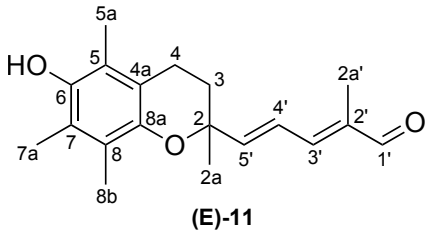

(E)-11

Figure 5.9: Structure and numbering of atoms in (4*E*)-**11**.

The assignment of ^{1}H NMR shifts (δ H), multiplicity (M), coupling constants (J) and ^{13}C NMR shifts (δ C) for (4*E*)-**11** is shown in table 5.9. The numbering of the atoms is shown in figure 5.9. ^{1}H and ^{13}C shifts are assigned in accordance with ^{1}H (figure E.10), ^{13}C (figure E.11), HSQC (figure E.12–E.13), HMBC (figure E.14–E.15) and COSY (figure E.16) NMR spectra (appendix E).

As mentioned in the previous subsection, the *trans* isomer of **11** is identified by the ^{3}J(H,H) coupling constant of 15.12 Hz.[94]

Table 5.9: Assigned shifts for (4*E*)-**11**.

Carbon no.	**δ H (ppm)**	**M**	***J* (Hz)**	**δ C (ppm)**
C-2	–	–	–	75.45
C-2a	1.45	s	–	27.00
C-3	2.05–1.84	m[a]	–	32.47
C-4	2.71–2.43	m	–	21.26
C-4a	–	–	–	117.5
C-5	–	–	–	119.0
C-5a	2.09	s[a]	–	11.62
C-6	–	–	–	145.4[a]
C-6–O**H**	4.50	s	–	–
C-7	–	–	–	121.7
C-7a	2.17	s[a]	–	12.55
C-8	–	–	–	122.5
C-8a	–	–	–	145.4[a]
C-8b	2.20	s[a]	–	12.11
C-1′	9.39	s	–	195.4
C-2′	–	–	–	137.8
C-2a′	1.75	s	–	9.73
C-3′	6.83–6.76	d	11.28	148.5
C-4′	6.67–6.58	dd	15.12 11.28	124.1
C-5′	6.28–6.20	d	15.12	147.8

[a]Overlapping with other signals

5.5.2 MS fragmentation

The main fragments of **11** from LRMS by EI ionization (appendix E, figure E.17) are shown in table 5.10. The fragmentation pattern is identical for both isomers of **11**. The naming of the fragments is in

accordance with figure 5.2.

Table 5.10: Main MS fragments of **11**.

m/z	Rel. intensity (%)	Fragment	Name
300	61	$[M]^+$	–
205	27	$[M-C_6H_7O]^+$	B
203	43	$[M-C_6H_9O]^+$	–
165	100	$[M-C_9H_{11}O]^+$	C
164	67	$[M-C_9H_{12}O]^+$	D
136	33		–
121	24	$[M-C_{11}H_{15}O_2]^+$	–
91	20	$[M-C_{12}H_{17}O_3]^+$	–
77	11	$[M-C_{13}H_{19}O_3]^+$	–

Fragments **B**, **C** and **D** are also seen in the LRMS spectrum of **8**, cf. figure 5.2. Fragment **B** is also seen in the LRMS spectrum of **9**. The presence of tropylium (m/z 91) and $C_6H_5^+$ (m/z 77) is also notable. These fragments contribute to confirming the identity of compound **11**. The fragments may be formed either by direct fragmentation of the molecular ion or by subsequent fragmentation of a fragment. Fragmentation may also be preceded by migrations and rearrangements.

5.6 9-(6-Hydroxy-2,5,7,8-tetramethyl-chroman-2-yl)-2,6-dimethylnona-2,4,6,8-tetra-enal (12)

The IR spectrum of **12** (appendix F, figure F.1) shows a characteristic O–H stretching signal at 3437 cm^{-1} and a C=O stretching signal at 1668 cm^{-1}. A C=C stretching signal at 1579 cm^{-1} is also present. Also notable is the presence of several weaker signals around 1600–

1730 cm^{-1}, some partly overlapping with the two larger signals. These may be due to C=O and C=C stretching in minor isomers of **12**.

The UV/Vis spectrum of **12** is shown in figure F.2. The λ_{max} of **12** is 350 nm, compared to 275 nm for the precursor **11**. This bathochromic shift is a clear indication that the lenght of the polyene chain has been increased. The theoretically calculated λ_{max} value according to Woodward's rules for conjugated carbonyls is 346 nm.

5.6.1 NMR spectroscopy

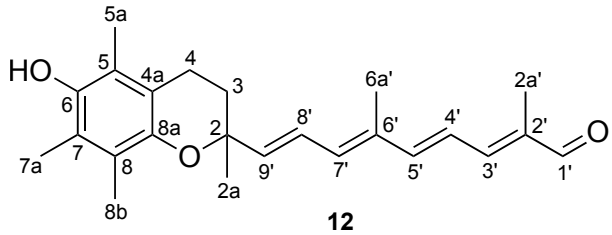

12

Figure 5.10: Structure and numbering of atoms in **12**.

The assignment of ^{1}H NMR shifts (δ H), multiplicity (M), coupling constants (J) and ^{13}C NMR shifts (δ C) for **12** is shown in table 5.11. The numbering of the atoms is shown in figure 5.10. ^{1}H and ^{13}C shifts are assigned in accordance with ^{1}H (figure F.3), ^{13}C (figure F.4), HSQC (figure F.5–F.6), HMBC (figure F.7–F.8) and COSY (figure F.9) NMR spectra (appendix F).

Impurities in the spectra can be distinguished from the signals belonging to **12** by HSQC correlations. Some of the additional peaks may be due to isomers of **12**. All ^{1}H NMR signals < 1.35 ppm are caused by impurities. Out of all the candidates for the ^{13}C shift of C-2, the signal with no protons attached is assigned (see figure F.5, appendix F). Due to overlapping of ^{1}H signals in the δ 6.70–6.50 ppm region, the stereochemistry of the C-4′=C-5′ bond cannot be determined.

Table 5.11: Assigned shifts for **12**.

Carbon no.	**δ H (ppm)**	**M**	***J* (Hz)**	**δ C (ppm)**
C-2	–	–	–	75.19
C-2a	1.44	s	–	27.01
C-3	2.09–1.91	m[a]	–	32.41
C-4	2.72–2.46	m	–	21.04
C-4a	–	–	–	117.4
C-5	–	–	–	118.5
C-5a	2.09	s[a]	–	11.31
C-6	–	–	–	144.9
C-6–O**H**	4.23	s	–	–
C-7	–	–	–	121.1
C-7a	2.18	s[a]	–	12.24
C-8	–	–	–	122.3
C-8a	–	–	–	145.3
C-8b	2.21	s[a]	–	11.85
C-1′	9.44	s	–	194.7
C-2′	–	–	–	136.9
C-2a′	1.88	s[a]	–	9.62
C-3′	6.94–6.87	d	9.44	149.2
C-4′	6.71–6.61	m[a]	–	122.7
C-5′	6.71–6.61	m[a]	–	146.0
C-6′	–	–	–	134.6
C-6a′	1.87	s[a]	–	12.56
C-7′	6.28–6.22	d	11.32	136.0
C-8′	6.60–6.50	dd	15.12 11.32	124.8
C-9′	5.97–5.90	d	15.12	141.6

[a]Overlapping with other signals

5.6.2 MS fragmentation

The main fragments of **12** from LRMS by EI ionization (appendix F, figure F.10) are shown in table 5.12. The naming of the fragments is in accordance with figure 5.2.

Table 5.12: Main MS fragments of **12**.

m/z	**Rel. intensity (%)**	**Fragment**	**Name**
366	81	$[M]^+$	–
229	15	$[M-C_9H_{13}O]^+$	–
205	21	$[M-C_{11}H_{13}O]^+$	B
203	25	$[M-C_{11}H_{15}O]^+$	–
165	100	$[M-C_{14}H_{17}O]^+$	C
121	16	$[M-C_{16}H_{21}O_2]^+$	–
105	16	$[M-C_{16}H_{21}O_3]^+$	–
91	23	$[M-C_{17}H_{23}O_3]^+$	–

Fragments **B** and **C** are also seen in the LRMS spectrum of **8** and **11**, cf. figure 5.2. Fragment **B** is additionally seen in the LRMS spectrum of **9**. As for **11**, the tropylium ion appears in the spectrum at m/z 91. These fragments contribute to confirming the identity of compound **12**. The fragments may be formed either by direct fragmentation of the molecular ion or by subsequent fragmentation of a fragment. Fragmentation may also be preceded by migrations and rearrangements.

Table 5.13: Main MS fragments of **9A**.

m/z	Rel. intensity (%)	Fragment	Name
338	8	$[M]^+$	–
309	16	$[M-CHO]^+$	K
234	19	$[M-C_7H_4O]^+$	–
205	53	$[M-C_8H_5O_2]^+$	B
161	10	$[M-C_{10}H_9O_3]^+$	–
136	12		–
105	100	$[M-C_{14}H_{17}O_3]^+$	L
77	48	$[M-C_{15}H_{17}O_4]^+$	–

5.7 2-Formyl-2,5,7,8-tetramethylchroman-6-yl benzoate (9A)

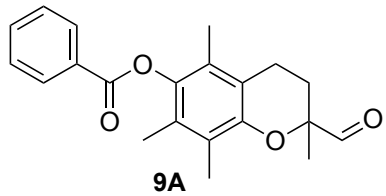

9A

Figure 5.11: Structure of **9A**.

Because no suitable solvent was found for **9A** (figure 5.11) , NMR analysis could not be performed. The identitification of **9A** therefore depends on MS spectrometry. The LRMS spectrum by EI ionization of **9A** (appendix G, figure G.1) is summarized in table 5.13. The naming of the fragments is in accordance with figures 5.2 and 5.12.

Figure 5.12 shows the proposed structure of some of the fragments. The loss of CHO (fragments **B** and **K**) is typical to aldehydes. Fragment **B** is also seen in the LRMS spectra of **8** and **9**, cf. figure 5.2. The $C_6H_5^+$ ion appears in the spectrum at m/z 77. These fragments contribute to confirming the identity of compound **9A**. The fragments

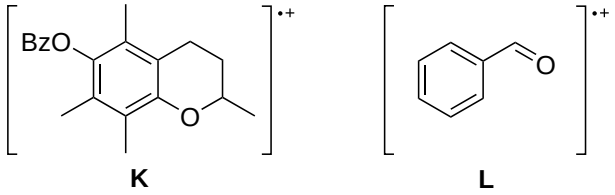

Figure 5.12: Possible radical ion fragments of **9A**.

may be formed either by direct fragmentation of the molecular ion or by subsequent fragmentation of a fragment. Fragmentation may also be preceded by migrations and rearrangements.

Chapter 6

Experimental

6.1 General methods

6.1.1 Chemicals and solvents

Solvents and chemicals were supplied by Sigma-Aldrich, Merck, VWR, Fluka Chemica and Fisher Scientific. The Wittig salts **10** and **13** were generously donated by BASF.

Drying of solvents and reagents

Dry CH_2Cl_2, THF and DMF were obtained from a MBraun MB SPS-800 Solvent Purification System and kept on activated molecular sieves (4 Å) under N_2 in pre-dried glassware. Other solvents and reagents were dried with activated molecular sieves (4 Å).[95]

6.1.2 Chromatographic techniques

TLC was used for analytical monitoring of reaction progress (silica 60 on Al sheets, F_{254}, 0.2 mm, Merck) and in some instances for preparative purification of samples (silica 60 on glass plates, F_{254}, 2.0 mm, Merck). Compounds with no UV absorption were developed with phosphomolybdic acid (in ethanol, 20 wt%) and heat.

Flash column chromatography was performed on silica gel (60 Å, 230–400 mesh, Sigma-Aldrich Fluka). The eluent systems are specified

for each compound.

6.1.3 Spectroscopic analyses

NMR spectroscopy

All samples were dissolved in $CDCl_3$ containing tetramethylsilane (TMS, 0.05% V/V) as internal reference. ^1H and ^{13}C NMR spectra were recorded on a Bruker Advance DPX 400 MHz spectrometer equipped with autosampler. The spectroscopic data was analyzed with Bruker TopSpin 3.1. Shifts were assigned according to the following NMR experiments:

1D-NMR: ^1H, ^{13}C
2D-NMR: HSQC, HMBC, COSY

In the elucidation of the structure of compound **27**, information from the 1D-NMR experiment DEPT135 was also used. Shifts are assigned in chapter 5. ^1H signal splitting patterns are abbreviated s (singlet), d (doublet), dd (doublet of doublets), ft (false triplet) and m (multiplet). All spectra are found in appendixes A to F.

Mass spectrometry

Accurate mass determination was performed on a MAT95XL ThermoFinnigan (EI ionization mode) and Agilent G1969 TOF MS (ESI ionization mode) instruments. For ESI analyses, samples were injected into the instrument using an Agilent 1100 series HPLC instrument. A direct injection analysis without any chromatography was performed for the EI analyses.

UV/Vis spectroscopy

UV/Vis spectra were recorded on a Hitachi U-1900 J30-0003 single beam spectrophotometer. Samples were dissolved in CH_2Cl_2 and contained in a quartz cell.

IR spectroscopy

All IR spectroscopy analyses were performed on neat samples on a Thermo Nicolet 20SXF FT-IR single beam spectrophotometer with a Smart Endurance reflection cell. Only the most characteristic IR signals are reported, with signal intensities specified as *s* (strong), *m* (medium) or *br* (broad).

6.2 Synthesis of 2-hydroxymethyl-2,5,7,8-tetramethylchroman-6-ol (8)

A solution of **7** (5.353 g, 21.4 mmol) in dry THF (145 mL) was placed in a pre-dried two-neck flask under N_2 and cooled to 0° C. Under stirring, a solution of $NaAlH_2(OCH_2CH_2OCH_3)_2$ in toluene (65% w/w, 32.5 mL, 108 mmol, 5.0 eq) was added dropwise over 20 min. The solution was carefully warmed to room temperature and stirred for 1.5 h. The reaction mixture was carefully poured over a mixture of HCl (6 M, 50 mL) and ice (50 mL). The aqueous phase was separated from the organic phase and extracted with diethyl ether (3×50 mL). The combined organic phases were washed with HCl (2 M, 3×50 mL) and a solution of $NaHCO_3$ (sat., 3×50 mL) before drying over $MgSO_4$. The solvent was removed and the product was obtained as white crystals with no further purification necessary.[80]

Yield: 4.779 g, 20.22 mmol, 95%.

R_f: 0.65 (silica, hexane : acetone 6 : 4).

^{1}H-NMR ($CDCl_3$, 400 MHz): δ 4.29 (s, 1H, C-6–O**H**), 3.69–3.55 (m, 2H, C-2b), 2.74–2.59 (m, 2H, C-4), 2.17 (s, 3H, C-7a), 2.12 (s, 3H, C-5a), 2.11 (s, 3H, C-8b), 2.05–1.90 (m, 2H, C-3 + C-2b–O**H**), 1.77–1.69 (m, 1H, C-3), 1.22 (s, 3H, C-2a). **^{13}C-NMR ($CDCl_3$ 100 MHz):** δ 145.2 (C-6), 145.0 (C-8a), 122.7 (C-8), 121.5 (C-7), 118.9 (C-5), 117.5 (C-4a), 75.20 (C-2), 69.51 (C-2b), 28.00 (C-3), 20.51 (C-2a), 20.38 (C-4), 12.31 (C-7a), 11.97 (C-8b), 11.42 (C-5a). **LRMS (EI, 70 eV):** [*m*/*z* (%)] 236 (94) $[M]^+$, 218 (5) $[M-H_2O]^+$, 205 (90) $[M-CH_3O]^+$, 165 (100) $[M-C_4H_7O]^+$, 164 (38) $[M-C_4H_8O]^+$. **HRMS (EI, 70 eV):** *m*/*z* calcd. for $C_{14}H_{20}O_3$ $[M]^+$ 236.1412, found 236.1415. **IR (solid):** cm^{-1}

3280*br* (O–H stretch), 1048*s* (C–O stretch).

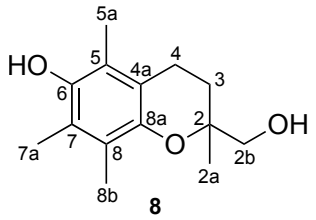

8

6.3 Attempted protection of 8

6.3.1 Attempted synthesis of (6-(*tert*-butyldimethylsilyloxy)-2,5,7,8-tetramethylchroman-2-yl)methanol (8A)

A solution of TBDMS-Cl (1 M in THF, 1.1 mL, 1.1 mmol, 2.3 eq) and imidazole (93 mg, 1.37 mmol, 3.2 eq) were dissolved in dry DMF (0.5 mL) under N_2 atmosphere. A solution of **8** (102 mg, 0.43 mmol) was added under stirring. The reaction mixture was stirred while the reaction progress was monitored by TLC. After 19 h all starting material had been converted to a single product. The solvent was removed, the residue dissolved in diethyl ether (5 mL) and washed with HCl (1 M, 10 mL), aqueous $NaHCO_3$ (sat., 10 mL) and water (2×10 mL) and dried over $MgSO_4$. After removal of the solvent, a sample of the residue was purified by TCL (silica, 20% ethyl acetate in hexane) for spectroscopic assessment. The product was isolated as pale beige crystals.[83] Spectroscopic data indicate that only the primary hydroxy group was silylated (compound **8B**). An attempt was made to recover compound **8** directly from the crude product. See section 6.3.2.

R_f: 0.76 (silica, hexane : ethyl acetate 8 : 2)
^{1}H-NMR ($CDCl_3$, 400 MHz): δ 4.19 (s, 1H, C-6–O**H**), 3.64–3.58 (d, 1H, $J = 9.76$ Hz, C-2b), 3.54–3.48 (d, 1H, $J = 9.76$ Hz, C2-b), 2.65–2.57 (t, 2H, $J = 6.84$, C-4), 2.16 (s, 3H, C-7a), 2.12 (s, 3H, C-5a), 2.11 (s, 3H, C-8b), 2.02–1.91 (m, 1H, C-3), 1.80–1.71 (m, 1H, C-3), 1.24 (s, 3H, C-2a), 0.91 (s, 9H, -Si-C-(C**H$_3$**)$_3$), 0.07 (s, 3H, -Si-C**H$_3$**), 0.04 (s, 3H, -Si-C**H$_3$**). **^{13}C-NMR ($CDCl_3$ 100 MHz):** δ 145.7 (C-6), 144.8 (C-8a), 122.6 (C-8), 121.2 (C-7), 118.6

(C-5), 117.7 (C-4a), 75.31 (C-2), 68.57 (C-2b), 28.32 (C-3), 25.99 (-Si-C-($\mathbf{C}H_3)_3$), 22.18 (-Si-$\mathbf{C}$-$(CH_3)_3$), 20.54 (C-4), 18.37 (C-2a), 12.35 (C-7a), 11.97 (C-8b), 11.44 (C-5a), −5.25 (-Si-$\mathbf{C}H_3$), −5.32 (-Si-$\mathbf{C}H_3$). **HRMS (ESI, 70 eV):** m/z calcd. for $C_{20}H_{35}O_3Si$ $[M + H]^+$ 351.2350, found 351.2344.

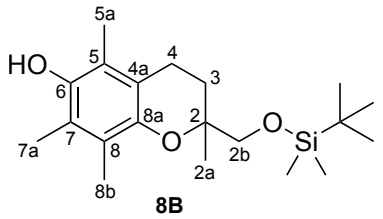

8B

6.3.2 Attempted recovery of 8 from 8B

The crude product (assuming 0.43 mmol) from the attempted synthesis of **8A** (see section 6.3.1) was dissolved in THF (3 mL) and cooled to 0 °C. A solution of TBAF (1.0 M in THF, 0.63 mL, 0.63 mmol, 1.5 eq) was added dropwise under stirring. The reaction mixture was stirred for 90 min at 0 °C, then warmed to room temperature and stirred for 4 h. TLC monitoring showed the reaction mixture had decomposed.[85]

6.3.3 Attempted synthesis of (6-benzyloxy-2,5,7,8-tetramethylchroman-2-yl)methanol (8C)

Benzyl chloride (80 µL, 0.63 mmol, 1.5 eq) was added to a solution of **8** (100 mg, 0.42 mmol) in dry acetone (7 mL). K_2CO_3 (319 mg, 2.31 mmol, 5.5 eq), 18-crown-6 (1 mg, 1 mol%) and KI (trace) was added to the reaction mixture. The mixture was refluxed under N_2 with TLC monitoring of the reaction progress. After 96 h the reaction mixture had decomposed without any apparent product formation.[86]

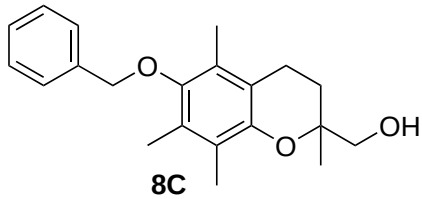

8C

6.4 Synthesis of 6-hydroxy-2,5,7,8-tetramethylchroman-2-carbaldehyde (9)

6.4.1 Attempted synthesis by the Dess-Martin oxidation

Method 1

Dess-Martin periodinane **25** (445 mg, 1.05 mmol, 2.5 eq) was added to a solution of **8** (100 mg, 0.423 mmol) in dry CH_2Cl_2 (5 mL) under stirring. A solution of H_2O (19 µL, 1.05 mmol, 2.5 eq) in CH_2Cl_2 (3 mL) was added dropwise to the reaction mixture, followed by stirring under N_2 for 4 h 30 min. The reaction mixture was diluted with diethyl ether (10 mL) and the solvent was removed. The residue was dissolved in diethyl ether (15 mL) and washed with aqueous NaOH (1 M, 20 mL), water (3 × 20 mL) and brine (20 mL) and dried over Na_2SO_4. The solvent was removed and the product was obtained as pale yellow crystals without further purification necessary.[68,69] Spectroscopic data show that another product (**27**) than the desired one was obtained.

Yield: 51 mg, 0.22 mmol, 52%
R_f: 0.61 (silica, hexane : ethyl acetate 8 : 2)
^{1}H-NMR ($CDCl_3$, 400 MHz): δ 4.18–4.14 (d, 1H, J = 6.88 Hz, C-2), 3.65–3.61 (d, 1H, J = 6.88 Hz, C-2), 2.74–2.53 (m, 2H, C-5), 1.96–1.82 (2 × s + m, 8H, C-9b, C-8a, C-4), 1.79 (s, 3H, C-6a), 1.42 (s, 3H, C-3a). **^{13}C-NMR ($CDCl_3$ 100 MHz):** δ 185.3 (C-7), 147.5 (C-5a), 145.4 (C-9), 134.5 (C-8), 126.8 (C-6), 100.1 (C-9a), 80.93 (C-3), 74.68 (C-2), 35.83 (C-4), 22.70 (C-5), 22.15 (C-3a), 12.91 (C-9b), 11.67 (C-8a), 10.41 (C-6a). **LRMS (EI, 70 eV):** [m/z (%)] 234 (88) $[M]^+$, 216 (12) $[M-H_2O]^+$, 206 (29) $[M-CO]^+$, 204 (96) $[M-CH_2O]^+$, 189 (100) $[M-C_2H_5O]^+$, 161 (46) $[M-C_3H_5O_2]^+$. **HRMS (ESI, 70 eV):** m/z calcd. for $C_{14}H_{19}O_3$ $[M+H]^+$ 235.1329, found 235.1324. **IR (solid):** cm^{-1} 1629s (C=O stretch), 941s (C–O stretch).

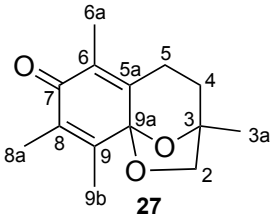

27

Method 2

Dess-Martin periodinane **25** (270 mg, 0.637 mmol, 1.5 eq) was added to a solution of **8** (100 mg, 0.423 mmol) in water saturated CH_2Cl_2 (5 mL) under stirring. The solution was stirred vigorously under N_2 for 1 h 40 min while reaction progress was monitored by TLC. When the reaction was complete, the reaction mixture was diluted with diethyl ether (10 mL) and the solvent was removed. The residue was dissolved in diethyl ether (15 mL) and treated with a 1:1 mixture (in total 15 mL) of aqueous $Na_2S_2O_3$ (10%) and aqueous $NaHCO_3$ (sat.). The organic phase was washed with H_2O (10 mL) and brine (10 mL). The combined aqueous washings were extracted with diethyl ether (2×20 mL). The combined organic phases were washed with H_2O (2×20 mL) and brine (20 mL) and dried over Na_2SO_4. The solvent was removed and the product was obtained as pale yellow crystals without further purification necessary.[68,69] Spectroscopic data show that another product (**27**) than the desired one was obtained.

Yield: 71 mg, 0.30 mmol, 71%

Spectroscopic data were identical to the product from method 1.

6.4.2 Synthesis by the Swern oxidation

A solution of oxalyl chloride (0.45 mL, 5.3 mmol, 1.25 eq) in dry CH_2Cl_2 (30 mL) was cooled and maintained under −75 °C on a dry ice/diethyl ether cooling bath under N_2 flow. Under stirring, a solution of dry DMSO (0.75 mL, 10.6 mmol, 2.51 eq) in dry CH_2Cl_2 (20 mL) was added carefully over 15 min. After stirring for 15 min, a solution of **8** (1000 mg, 4.23 mmol) in dry CH_2Cl_2 (40 mL) was added over 10 min. The reaction mixture was stirred for 45 min. Triethylamine (3.0 mL, 21.5 mmol, 5.08 eq) in dry CH_2Cl_2 (8 mL) was added

over 5 min with careful monitoring of the temperature. The reaction mixture was stirred for 5 min, before warming to room temperature. H_2O (50 mL) was added to the reaction mixture. The phases were separated and the aqueous layer was extracted with CH_2Cl_2 (3×50 mL). The combined organic phases were washed with HCl (1%, 3×50 mL), water (3×50 mL), Na_2CO_3 (5%, 3×50 mL) and brine (5×50 mL) and dried over $MgSO_4$. The solvent was evaporated *in vacuo* and the crude product was purified by flash column chromatography (silica, 2% ethyl acetate in CH_2Cl_2). The product was obtained as white crystals.[21,80]

Yield: 645 mg, 2.75 mmol, 65%

R_f: 0.55 (silica, hexane : ethyl acetate 8 : 2)

^{1}H-NMR ($CDCl_3$, 400 MHz): δ 9.61 (s, 1H, C-2b), 4.30 (s, 1H, C-6–O**H**), 2.67–2.48 (m, 2H, C-4), 2.31–2.22 (m, 1H, C-3), 2.20 (s, 3H, C-8b), 2.17 (s, 3H, C-7a), 2.06 (s, 3H, C-5a), 1.86–1.76 (m, 1H, C-3), 1.38 (s, 3H, C-2a). **^{13}C-NMR ($CDCl_3$ 100 MHz):** δ 204.7 (C-2b), 145.7 (C-6), 145.3 (C-8a), 122.9 (C-8), 121.7 (C-7), 118.8 (C-5), 117.6 (C-4a), 80.41 (C-2), 28.05 (C-3), 21.66 (C-2a), 20.51 (C-4), 12.32 (C-7a), 12.00 (C-8b), 11.34 (C-5a). **LRMS (EI, 70 eV):** [m/z (%)] 234 (31) $[M]^+$, 205 (100) $[M-CHO]^+$, 190 (22) $[M-C_2H_4O]^+$. **HRMS (EI, 70 eV):** m/z calcd. for $C_{14}H_{18}O_3$ $[M]^+$ 236.1250, found 234.1247. **IR (solid):** cm^{-1} 3535*br* (O–H stretch), 1732*s* (C=O stretch), 1085*s* (C–O stretch).

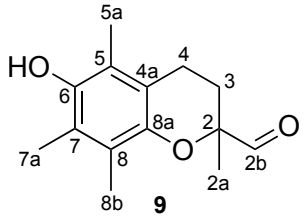

9

6.5 Synthesis of 5-(6-hydroxy-2,5,7,8-tetramethylchroman-2-yl)-2-methylpenta-2,4-dienal (11)

6.5.1 Method 1: Epoxide mediation under microwave conditions

A solution of **9** (20 mg, 0.085 mmol) in absolute ethanol (2 mL) was added slowly by syringe to a suspension of **10** (220 mg, 0.431 mmol, 5.1 eq) in 1,2-epoxybutane (5 mL) in a pre-dried glass vial at 0 ° C under stirring. The cooling bath was removed and the reaction mixture was stirred for 30 min at room temperature. After equipping the vial with a screwcap, the reaction mixture was irradiated by MW radiation (320 W) for in total 1 h 10 min, with regular intermediate monitoring of reaction progress by TLC. Due to beginning decomposition the reaction was stopped, even though starting material was still present in the reaction mixture. H_2O (5 mL) was carefully added and the mixture was stirred for 10 min. The solvent was removed and the residue was dissolved in CH_2Cl_2 (10 mL) and washed with H_2O (3×10 mL). After drying over $MgSO_4$ the solvent was removed. The residue was dissolved in dry CH_2Cl_2 (10 mL), a few crystals of *p*-TsOH was added and the mixture was stirred under N_2 for 30 min until TLC monitoring showed the reaction was complete. The reaction mixture was transferred to a separatory funnel and washed with a solution of $NaHCO_3$ (5%, 3×10 mL), H_2O (3×10 mL) and brine (10 mL). After drying over $MgSO_4$ the solvent was removed. A sample of the crude product was saved for TLC evaluation and comparison with other methods.

6.5.2 Method 2: Epoxide mediation under reflux

A solution of **9** (20 mg, 0.085 mmol) in absolute ethanol (1.5 mL) was added slowly by syringe under N_2 to a suspension of **10** (230 mg, 0.451 mmol, 5.3 eq) in 1,2-epoxybutane (5 mL) at 0 ° C under stirring. The cooling bath was removed and the reaction mixture was stirred for 30 min at room temperature. The reaction mixture was refluxed while reaction progress was monitored by TLC. After 72 h the reaction

was stopped due to beginning decomposition, even though starting material was still present in the reaction mixture. H_2O (5 mL) was carefully added and the mixture was stirred for 10 min. The solvent was removed and the residue was dissolved in CH_2Cl_2 (10 mL) and washed with H_2O (3×10 mL). After drying over $MgSO_4$ the solvent was removed. The residue was dissolved in dry CH_2Cl_2 (10 mL), a few crystals of *p*-TsOH was added and the mixture was stirred under N_2 for 30 min until TLC monitoring showed the reaction was complete. The reaction mixture was transferred to a separatory funnel and washed with a solution of $NaHCO_3$ (5%, 3×10 mL), H_2O (3×10 mL) and brine (10 mL). After drying over $MgSO_4$ the solvent was removed. A sample of the crude product was saved for TLC evaluation and comparison with other methods.

6.5.3 Method 3: Base mediation under microwave conditions

To a solution of **10** (3.285 g, 6.424 mmol, 3.0 eq) in dry methanol (15 mL), CH_3OK (25% in methanol, 1.9 mL, 6.4 mmol, 3.0 eq) in dry methanol (3 mL) was added dropwise at 0 ° C under stirring. The solution was stirred on ice cooling for 15 min before a solution of **9** (504 mg, 2.15 mmol) in dry CH_2Cl_2 (5 mL) was added slowly. The reaction mixture was warmed to room temperature and stirred for 15 min, before being submitted to irradiation by MW radiation (90 W) for 26 min. The reaction was quenched with H_2O (5 mL) and the mixture was concentrated *in vacuo*. CH_2Cl_2 (30 mL) was added, the mixture was washed with H_2O (5×30 mL) and dried over $MgSO_4$. The solvent was removed and the residue dissolved in dry CH_2Cl_2 (15 mL). *p*-TsOH (215 mg, 1.13 mmol, 0.53 eq) was added and the reaction mixture stirred under N_2 for 45 min until TLC monitoring showed the reaction was complete. The mixture was transferred to a separatory funnel and washed with a solution of $NaHCO_3$ (5%, 3×50 mL) and H_2O (3×50 mL). The organic phase was dried over $MgSO_4$ and the solvent was removed. The crude product was dissolved in CH_2Cl_2 and filtered through silica before purification by flash column chromatography (silica, (2 : 1 CH_2Cl_2 : ethyl acetate)/hexane gradient).

Yield: 125 mg, 0.416 mmol, 19% (37 : 63 *cis* : *trans*)
R_f: 0.53 (*cis*), 0.46 (*trans*) (silica, hexane : ethyl acetate 7 : 3)
Spectroscopic data were identical to the products from method 4.

6.5.4 Method 4: Base mediation under reflux

To a solution of **10** (4.375 g, 8.555 mmol, 5.15 eq) in dry methanol (25 mL), CH_3ONa (25% in methanol, 2.0 mL, 8.7 mmol, 5.2 eq) in dry methanol (4 mL) was added dropwise at 0 ° C under stirring and N_2. The solution was stirred on ice cooling for 20 min before a solution of **9** (389 mg, 1.66 mmol) in dry THF (4 mL) was added slowly. The reaction mixture was warmed to room temperature and stirred for 30 min, before being refluxed for 22 h. The reaction was quenched with H_2O (5 mL) and the mixture was concentrated *in vacuo*. CH_2Cl_2 (40 mL) was added, the mixture was washed with H_2O (3×30 mL) and dried over $MgSO_4$. The solvent was removed and the residue dissolved in dry CH_2Cl_2 (25 mL). One spatula measure *p*-TsOH was added and the reaction mixture stirred under N_2 for 60 min until TLC monitoring showed the reaction was complete. The mixture was transferred to a separatory funnel and washed with a solution of $NaHCO_3$ (5%, 3×50 mL) and H_2O (3×50 mL). The organic phase was dried over $MgSO_4$ and the solvent was removed. The crude product was purified by flash column chromatography (silica, (2 : 1 CH_2Cl_2 : ethyl acetate)/hexane gradient).

Yield: 131 mg, 0.44 mmol, 26% (72 : 28 *cis* : *trans*)
R_f: 0.53 (*cis*), 0.46 (*trans*) (silica, hexane : ethyl acetate 7 : 3)
***cis*-Isomer: ^{1}H-NMR ($CDCl_3$, 400 MHz):** δ 9.45 (s, 1H, C-1′), 7.82–7.72 (d, 1H, J = 11.96 Hz, C-3′), 6.49–6.38 (dd, 1H, J = 11.96, 11.80, C-4′), 5.91–5.82 (d, 1H, J = 11.80, C-5′), 4.32 (s, 1H, C-6–O**H**), 2.74–2.55 (m, 2H, C-4), 2.20 (s, 3H, C-8b), 2.15 (s, 3H, C-7a), 2.10 (s, 3H, C-5a), 2.15–2.01 (m, 1H, C-3), 1.90–1.79 (m, 1H, C-3), 1.77 (s, 3H, C-2a′), 1.56 (s, 3H, C-2a). **^{13}C-NMR ($CDCl_3$ 100 MHz):** δ 195.7 (C-1′), 145.5 (C-6), 145.2 (C-8a), 144.4 (C-3′), 143.6 (C-5′), 139.1 (C-2′), 124.8 (C-4′), 122.4 (C-8), 121.8 (C-7), 119.1 (C-5), 117.7 (C-4a), 76.77 (C-2), 33.91 (C-3), 27.79 (C-2a), 21.35 (C-4), 12.62 (C-8b), 12.57 (C-7a), 11.66 (C-5a), 9.13 (C-2a′). **LRMS (EI, 70 eV):** [**m/z** (%)] 300 (61)

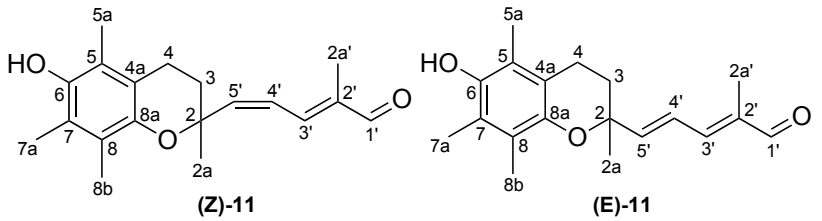

$[M]^+$, 205 (27) $[M-C_6H_7O]^+$, 165 (100) $[M-C_9H_{11}O]^+$, 164 (67) $[M-C_9H_{12}O]^+$. **HRMS (ESI, 70 eV):** m/z calcd. for $C_{19}H_{25}O_3$ $[M+H]^+$ 301.1798, found 301.1797. **IR (neat):** cm^{-1} 3450*br* (O–H stretch), 1667*s* (C=O stretch), 1630*s* (C=C stretch), 1084*s* (C–O stretch). **UV/Vis (CH_2Cl_2)**: λ_{max} 275 nm.
***trans*-Isomer: ^{1}H-NMR ($CDCl_3$, 400 MHz):** δ 9.39 (s, 1H, C-1′), 6.83–6.76 (d, 1H, J = 11.28 Hz, C-3′), 6.67–6.58 (dd, 1H, J = 15.12, 11.28, C-4′), 6.28–6.20 (d, 1H, J = 15.12, C-5′), 4.50 (s, 1H, C-6–O**H**), 2.71–2.43 (m, 2H, C-4), 2.20 (s, 3H, C-8b), 2.17 (s, 3H, C-7a), 2.09 (s, 3H, C-5a), 2.05–1.84 (m, 2H, C-3), 1.75 (s, 3H, C-2a′), 1.45 (s, 3H, C-2a). **^{13}C-NMR ($CDCl_3$ 100 MHz):** δ 195.4 (C-1′), 148.5 (C-3′), 147.8 (C-5′), 145.4 (C-6), 145.4 (C-8a), 137.8 (C-2′), 124.1 (C-4′), 122.5 (C-8), 121.7 (C-7), 119.0 (C-5), 117.5 (C-4a), 75.45 (C-2), 32.47 (C-3), 27.00 (C-2a), 21.26 (C-4), 12.55 (C-7a), 12.11 (C-8b), 11.62 (C-5a), 9.73 (C-2a′). **UV/Vis (CH_2Cl_2)**: λ_{max} 275 nm.

6.5.5 Alternative method of hydrolyzing the acetal precursor to 11

The crude intermediate after MW irradiation and washing with H_2O according to method 3 (section 6.5.3) was dissolved in a solution of citric acid in dry methanol (30%) and refluxed for 26 h until TLC monitoring showed the reaction was complete. Workup of the product was performed according to method 3 (section 6.5.3).

6.6 Synthesis of 9-(6-hydroxy-2,5,7,8-tetramethylchroman-2-yl)-2,6-dimethylnona-2,4,6,8-tetraenal (12)

In a pre-dried glass vial with septum and N_2 flow, a solution of **10** (639 mg, 1.25 mmol, 3.0 eq) in dry methanol (1 mL) was cooled to −10 ° C. A solution of CH_3OK (25% in methanol, 365 µL, 1.24 mmol, 3.0 eq) in dry methanol (1 mL) was added dropwise over 10 min. The mixture was stirred at −10 ° C for 20 min before **11** (125 mg, 0.416 mmol) in dry CH_2Cl_2 (1.5 mL) was added over 10 min. The reaction mixture was stirred for 5 min, then warmed to room temperature and stirred for an additional 30 min. After equipping the vial with a screwcap, the reaction mixture was irradiated by MW radiation (80 W) for 25 min. H_2O (1 mL) was added and the mixture was stirred for 10 min. The solvent was removed and the residue was dissolved in CH_2Cl_2 (10 mL) and washed with H_2O (3×25 mL). After drying over $MgSO_4$ the solvent was removed. The residue was dissolved in dry CH_2Cl_2 (10 mL), *p*-TsOH (150 mg, 0.794 mmol, 1.9 eq) was added and the mixture was stirred under N_2 for 30 min. The reaction mixture was transferred to a separatory funnel and washed with a solution of $NaHCO_3$ (5%, 3×25 mL), H_2O (3×25 mL) and brine (25 mL). After drying over $MgSO_4$ the solvent was removed. The crude product was purified by flash column chromatography (silica, ethyl acetate/cyclohexane gradient).

Yield: 11 mg, 0.030 mmol, 7%

R_f: 0.62 (silica, hexane : ethyl acetate 7 : 3)

^{1}H-NMR ($CDCl_3$, 400 MHz): δ 9.44 (s, 1H, C-1′), 6.94–6.87 (d, 1H, $J = 9.44$ Hz, C-3′), 6.71–6.61 (m, 2H, C-4′ + C-5′), 6.60–6.50 (dd, 1H, $J = 15.12, 11.32$ Hz, C-8′), 6.28–6.22 (d, 1H, $J = 11.32$ Hz, C-7′), 5.97–5.90 (d, 1H, $J = 15.12$, C-9′), 4.23 (s, 1H, C-6–O**H**), 2.72–2.46 (m, 2H, C-4), 2.21 (s, 3H, C-8b), 2.18 (s, 3H, C-7a), 2.09 (s, 3H, C-5a), 2.09–1.91 (m, 2H, C-3), 1.88 (s, 3H, C-2a′), 1.87 (s, 3H, C-6a′), 1.44 (s, 3H, C-2a). **^{13}C-NMR ($CDCl_3$ 100 MHz):** δ 194.7 (C-1′), 149.2 (C-3′), 146.0 (C-5′), 145.3 (C-8a), 144.9 (C-6), 141.6 (C-9′), 136.9 (C-2′), 136.0 (C-7′), 134.6 (C-6′), 124.8 (C-8′), 122.7 (C-4′), 122.3 (C-8), 121.1 (C-7),

118.5 (C-5), 117.4 (C-4a), 75.19 (C-2), 32.41 (C-3), 27.01 (C-2a), 21.04 (C-4), 12.24 (C-7a), 11.85 (C-8b), 11.31 (C-5a), 12.56 (C-6a′), 9.62 (C-2a′). **LRMS (EI, 70 eV):** [m/z (%)] 366 (81) $[M]^+$, 205 (21) $[M-C_{11}H_{13}O]^+$, 165 (100) $[M-C_{14}H_{17}O]^+$. **HRMS (EI, 70 eV):** m/z calcd. for $C_{24}H_{30}O_3$ $[M]^+$ 366.2189, found 366.2186. **IR (neat):** cm^{-1} 3437*br* (O–H stretch), 1668*s* (C=O stretch), 1579*s* (C=C stretch), 1191*s* (C–O stretch). **UV/Vis (CH_2Cl_2):** λ_{max} 350 nm.

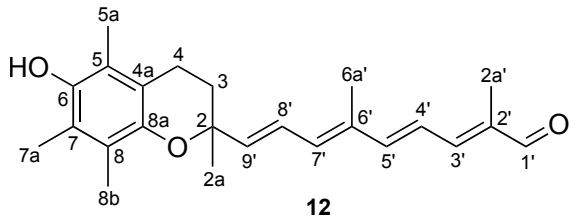

12

6.7 Attempted protection of 9

6.7.1 Synthesis of 2-formyl-2,5,7,8-tetramethylchroman-6-yl benzoate (9A)

Method 1

9 (145 mg, 0.619 mmol) was dissolved in dry CH_2Cl_2 (2 mL) under N_2 atmosphere. A solution of dry pyridine (60 µL, 0.74 mmol, 1.2 eq) in dry CH_2Cl_2 (1 mL) was added slowly under stirring on ice cooling. After stirring for 30 min on ice cooling, a solution of benzoyl chloride (90 µL, 0.77 mmol, 1.2 eq) in dry CH_2Cl_2 (1 mL) was added slowly. After stirring for 10 min, the reaction mixture was allowed to warm to room temperature and stirred for 22 h.[25] TLC monitoring showed no reaction had taken place. DMAP (78 mg, 1 eq) was added[78] and the reaction mixture was stirred for an additional 68 h. As TLC monitoring still indicated no product was formed, DCC (143 mg, 0.693 mmol, 1.1 eq) in dry CH_2Cl_2 (1 mL) was added to the reaction mixture.[93] After an additional 24 h of stirring, H_2O (10 mL) was added and the reaction mixture stirred for 30 min. The phases were separated and the organic phase washed with HCl (1%, 3×25 mL), H_2O (3×25 mL),

a solution of $NaHCO_3$ (sat., 3×25 mL) and brine (3×25 mL). The organic phase was dried over $MgSO_4$ and the solvent was removed. The white crystals formed were insoluble in all common laboratory solvents.

Method 2

9 (114 mg, 0.487 mmol) was dissolved in dry pyridine (2 mL) under N_2 atmosphere. Under stirring, benzoyl chloride (100 µL, 0.86 mmol, 1.77 eq) was added dropwise. The reaction mixture was stirred for 15 min until TLC monitoring showed no starting material remained. The reaction mixture was diluted with CH_2Cl_2 (100 mL) and the resulting suspension was washed with a solution of $NaHCO_3$ (sat., 3×100 mL), HCl (2 M, 4×50 mL) and brine (3×100 mL). The organic phase was dried over $MgSO_4$. After removal of the solvent, no residue was formed. The combined aqueous phases were acidified to suspend the solid material in the organic phase, and extracted with CH_2Cl_2 (3×50 mL). The combined organic phases were washed with brine (1×50 mL) and the solvent was removed. The crude product (pale yellow crystals) was very poorly soluble in all common laboratory solvents. A small sample of the crude product was found by MS to contain the desired product (**9A**).

Yield: 143 mg, 0.423 mmol, 87% (crude)
HRMS (ESI, 70 eV): m/z calcd. for $C_{21}H_{22}O_4$ $[M]^+$ 338.1513, found 338.1512.

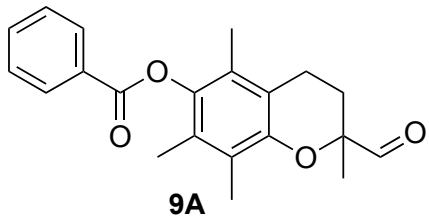

9A

6.7.2 Attempted synthesis of 6-(*tert*-butyldimethylsilyloxy)-2,5,7,8-tetramethylchroman-2-carbaldehyde (9B)

A solution of **9** (100 mg, 0.427 mmol), TBDMS-Cl (1 M in THF, 0.64 mL, 0.64 mmol, 1.5 eq) and imidazole (116 mg, 1.71 mmol, 4 eq) in dry DMF (4 mL) was stirred at 90 °C for 5 h under N_2 atmosphere. As TLC analysis showed no product had been formed, the reaction mixture was refluxed overnight. The following morning, the reaction had decomposed with no apparent product formation.[96]

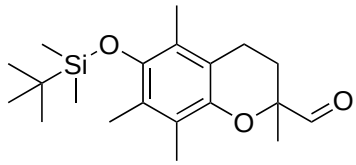

9B

References

1. Mohr, P. J.; Taylor, B. N.; Newell, D. B. *Rev. Mod. Phys.* **2008**, *80*, 633–730.

2. Størseth, T. R.; Master thesis; Norges teknisk-naturvitenskapelige universitet; Trondheim; **2001**.

3. Palozza, P.; Piccioni, E.; Avanzi, L.; Vertuani, S.; Calviello, G.; Manfredini, S. *Free Radical Bio. Med.* **2002**, *33*, 1724–1735.

4. Wang, Y.; Panagabko, C.; Atkinson, J. *Bioorgan. Med. Chem.* **2010**, *18*, 777–786.

5. Biacs, P. A.; Daood, H. G. *Biochem. Soc. Trans.* **2000**, *28*, 839–845.

6. Castro, I. A.; Moraes Barros, S. B.; Lanfer Marquez, U. M.; Motizuki, M.; Higashi Sawada, T. C. *Food Research Int.* **2005**, *38*, 861–866.

7. Yanishlieva, N. V.; Marinova, E. M.; G., R. V.; Partali, V.; Sliwka, H.-R. *J. Am. Oil Chem. Soc.* **2001**, *78*, 641–644.

8. Truscott, T. G. *Bibl. Nutr. Dieta* **2001**, *55*, 68–79.

9. Wrona, M.; Korytowski, W.; Rózanowska, M.; Sarna, T.; Truscott, T. G. *Free Radical Bio. Med.* **2003**, *35*, 1319–1329.

10. Shixian, Q.; Dai, Y.; Kakuda, Y.; Shi, J.; Mittal, G.; Yeung, D.; Jiang, Y. *Food Rev. Int.* **2005**, *21*, 295–311.

11. Chen, J.; Shi, J.; Macnaughton, L.; Kakuda, Y.; Xue, S. J.; Ma, Y.; Zhang, M.; Jiang, Y. *J. Food Biochem.* **2009**, *33*, 232–245.

12. Zanfini, A.; Corbini, G.; La Rosa, C.; Dreassi, E. *LWT—Food Sci. Technol.* **2010**, *43*, 67–72.

13. Kotíková, Z.; Lachman, J.; Hejtmánková, A.; Hejtmánková, K. *LTW—Food Sci. Technol.* **2011**, *44*, 1703–1710.

14. Palozza, P.; Verdecchia, S.; Avanzi, L.; Vertuani, S.; Serini, S.; Iannone, A.; Manfredini, S. *Mol. Cell. Biochem.* **2006**, *287*, 21–32.

15. Catel, Y.; Aladedunye, F.; Przybylski, R. *J. Am. Oil Chem. Soc.* **2012**, *89*, 55–66.

16. Larsen, E.; Abendroth, J.; Partali, V.; Schulz, B.; Sliwka, H.-R.; Quartey, E. G. K. *Chem. Eur. J.* **1998**, *4*, 113–117.

17. Naalsund, T.; Malterud, K. E.; Partali, V.; Sliwka, H.-R. *Chem. Phys. Lipids* **2001**, *112*, 59–65.

18. Pungente, M. D.; Jubeli, E.; Øpstad, C. L.; Al-Kawaz, M.; Barakat, N.; Ibrahim, T.; Khalique, N. A.; Raju, L.; Jones, R.; Leopold, P. L.; Sliwka, H.-R.; Partali, V. *Molecules* **2012**, *17*, 3484–3500.

19. Popplewell, L. J.; Abu-Dayya, A.; Khanna, T.; Flintermann, F.; Khalique, A.; Rayu, L.; Øpstad, C. L.; Sliwka, H.-R.; Partali, V.; Dickson, G.; Pungente, M. D. *Molecules* **2012**, *17*, 1139–1148.

20. Kedika, B.; Patri, S. V. *J. Med. Chem.* **2011**, *54*, 548–561.

21. Mancuso, A. J.; Huang, S.-L.; Swern, D. *J. Org. Chem.* **1978**, *43*, 2480–2482.

22. Øpstad, C. L.; Sliwka, H.-R.; Partali, V. *Eur. J. Org. Chem.* **2010**, *1*, 435–469.

23. Hengartner, U.; Bernhard, K.; Meyer, K.; Englert, G.; Glinz, E. *Helv. Chim. Acta* **1992**, *75*, 1848–1865.

24. Englert, G.; Noack, K.; Broger, E. A.; Glinz, E.; Vecchi, M.; Zell, R. *Helv. Chim. Acta* **1991**, *74*, 969–982.

25. Schmidt, M.; Ph.D. thesis; Heinrich—Heine—Universität; Düsseldorff; **2001**.

26. Kock, S. C.; Ph.D. thesis; Heinrich—Heine—Universität; Düsseldorff; **2007**.

27. Isler, O.; Gutmann, H.; Solms, U. *Carotenoids*; Birkhäuser: Basel, **1971**; pp 12–60.

28. Cadenas, E.; Packer, L. *Handbook of Antioxidants*, 2nd ed.; Marcel Dekker: New York, **2002**; pp (a) 189–221; (b) 201–202; (c) 75–108; (d) 1–45; (e) 223–233.

29. Rock, C. L.; Robert, A. J.; Phyllis, E. B. *J. Am. Diet. Assoc.* **1996**, *96*, 693–702.

30. Lakshman, M. R. *J. Nutr.* **2004**, *134*, 241–245.

31. Combs, G. F. *The Vitamins: Fundamental Aspects in Nutrition and Health*, 3rd ed.; Elsevier: Amsterdam, **2008**; pp 95–141.

32. Ellis, G. P. *Chromans and Tocopherols*; Wiley: New York, **1981**; pp (a) 96–97; (b) 87–89.

33. Nelson, D. L.; Lehninger, A. L.; Cox, M. M. *Principles of Biochemistry*, 5th ed.; Freeman: New York, **2008**; pp (a) 715–721; (b) 390; (c) 333–334.

34. Yanishlieva, N. V.; Aitzetmüller, K.; Raneva, V. G. *Lipid/Fett* **1998**, *100*, 444–462.

35. Krinsky, N. I. *Pure Appl. Chem.* **1979**, *54*, 649–660.

36. Young, A. M.; Gregoriadis, G. *Photochem. photobiol.* **1996**, *63*, 344–352.

37. Heinonen, M.; Haila, K.; Lampi, A. M.; Piironen, V. *J. Am. Oil Chem. Soc.* **1997**, *74*, 1047–1052.

38. Négre-Salvayre, A.; Affany, A.; Hariton, C.; Salvayre, R. *Pharmacology* **1991**, *42*, 262–272.

39. Suetsugu, K.; Ogata, K.; Yoshida, K.; Uehara, K.; Tomita, K.; *Patent US 5306713 A: Highly active antioxidant comprising tocopheryl ascorbyl phosphate*; **1994**.

40. Morizaki, K.; Ozaki, S. *Bull. Chem. Soc. Jpn.* **1996**, *69*, 725–734.

41. Morizaki, K.; Ozaki, S. *Chem. Pharm. Bull.* **1996**, *44*, 1647–1655.

42. Yamano, Y.; Masayoshi, I. *Heterocycles* **1998**, *47*, 289–299.

43. Houte, H.; Partali, V.; Sliwka, H.-R.; Quartey, E. G. K. *Chem. Phys. Lipids* **2000**, *105*, 105–113.

44. Karagiannidou, E.; Størseth, T. R.; Sliwka, H.-R.; Partali, V.; Malterud, K. E.; Tsimidou, M. *Eur. J. Lipid Sci. Tech.* **2003**, *105*, 419–426.

45. Beutner, S.; Frixel, S.; Ernst, H.; Hoffmann, T.; Hernandez-Blanco, I.; Hundsdoerfer, C.; Kiesendahl, N.; Kock, S.; Martin, H.-D.; Mayer, B.; Noack, P.; Perez-Galvez, A.; Kock, G.; Scherrers, R.; Schrader, W.; Sell, S.; Stahl, W. *Arkivoc* **2007**, *8*, 279–295.

46. Hertzberg, S.; Lutnæs, B. F.; Liaaen-Jensen, S. *Natural Product Research* **2011**, *25*, 511–525.

47. Miller, A. D. *Angew. Chem. Int. Ed.* **1998**, *37*, 1768–1785.

48. Tarahovsky, Y. S. *Biochemistry* **2009**, *74*, 1293–1304.

49. Cavazzana-Calvo, M.; Hacein-Bey, S.; de Saint Basile, G.; Gross, F.; Yvon, E.; Nusbaum, P.; Selz, F.; Hue, C.; Certain, S.; Casanova, J.-L.; Bousso, P.; Le Deist, F.; Fischer, A. *Science* **2000**, *288*, 669–672.

50. Fairclough, R. J.; Bareja, A.; Davies, K. E. *Exp. Physiol.* **2011**, *96*, 1101–1113.

51. Verma, I. M.; Somia, N. *Nature* **1997**, *389*, 239–242.

52. Kaiser, J. *Science* **2007**, *317*, 580.

53. Niculescu-Duvaz, D.; Heyes, J. *Curr. Med. Chem.* **2003**, *10*, 1233–1261.

54. Kappe, C. O.; Stadler, A. *Microwaves in Organic and Medicinal Chemistry*, 1st ed.; Wiley: Weinheim, **2005**; pp (a) 9–27, 91–95, 219–222; (b) 24.

55. Gedye, R.; Smith, F.; Westaway, K.; Ali, H.; Baldisera, L.; Laberge, L.; Rousell, J. *Tetrahedron Lett.* **1986**, *27*, 279–282.

56. Giguere, R. J.; Bray, T. L.; Duncan, S. M.; Majetich, G. *Tetrahedron Lett.* **1986**, *27*, 4945–4958.

57. Ruzié, C.; Krayer, M.; Lindsey, J. S. *Org. Lett.* **2009**, *11*, 1761–1764.

58. Gauger, K. A.; Lindsey, J. S.; Master thesis; North Carolina State University; Raleigh; **2009**. `http://www.lib.ncsu.edu/resolver/1840.16/6303`.

59. Perreux, L.; Loupy, A. *Tetrahedron* **2001**, *57*, 9199–9223.

60. de la Hoz, A.; Díaz-Ortiz, A.; Moreno, A. *Chem. Soc. Rev.* **2005**, *34*, 164–178.

61. Kuhnert, N. *Angew. Chem. Int. Ed.* **2002**, *41*, 1863–1866.

62. Strauss, C. R. *Angew. Chem. Int. Ed.* **2002**, *41*, 3589–3590.

63. Berlan, J. *Radiat. Phys. Chem.* **1995**, *45*, 581–589.

64. Carey, F. A.; Sundberg, R. J. *Advanced Organic Chemistry, Part B: Reactions and Synthesis*, 5th ed.; Springer: New York, **2007**; pp (a) 396–403; (b) 1070–1073; (c) 157–164; (d) 258–267; (e) 224–225; (f) 247.

65. Pfitzner, K. E.; Moffatt, J. G. *J. Am. Chem. Soc.* **1965**, *87*, 5661–5670.

66. Matsuo, J.; Iida, D.; Tatani, K.; Mukaiyama, T. *Bull. Chem. Soc. Jpn.* **2002**, *75*, 223–234.

67. Tidwell, T. T. *Synthesis* **1990**, *10*, 857–870.

68. Dess, D. B.; Martin, J. C. *J. Org. Chem.* **1983**, *48*, 4155–4156.

69. Meyer, S. D.; Schreiber, S. L. *J. Org. Chem.* **1994**, *59*, 7549–7552.

70. Ernst, H. *Pure Appl. Chem.* **2002**, *74*, 2213–2226.

71. Vedejs, E.; Snoble, K. A. J. *J. Am. Chem. Soc.* **1973**, *95*, 5778–5780.

72. Neumann, R. A.; Berger, S. *Eur. J. Org. Chem.* **1998**, *6*, 1085–1087.

73. Buddrus, J. *Angew. Chem. Int. Ed.* **1968**, *7*, 536–537.

74. Vedejs, E.; Fleck, T. J. *J. Am. Chem. Soc.* **1989**, *111*, 5861–5871.

75. Hammond, G. S. *J. Am. Chem. Soc.* **1955**, *77*, 334–338.

76. Carey, F. A.; Sundberg, R. J. *Advanced Organic Chemistry, Part A: Structure and Mechanisms*, 5th ed.; Springer: New York, **2007**; pp (a) 641; (b) 407–411; (c) 411–415.

77. Greene, T. W.; Wuts, P. G. M. *Greene's Protective Groups in Organic Synthesis*, 4th ed.; Wiley: Hoboken, **2007**; pp (a) 414–416; (b) 407–409; (c) 396–402; (d) 400; (e) 197–198.

78. Steglich, W.; Hoefle, G. *Angew. Chem. Int. Ed.* **1969**, *8*, 981.

79. Tichkowsky, I.; Lett, R. *Tetrahedron Lett.* **2002**, *43*, 3997–4001.

80. Schiefer, F. *Research report: Synthesis of a novel antioxidant combining tocopherol and carotenoid*; Norwegian University of Science and Technology, **2009**.

81. Rayner-Canham, G.; Overton, T. *Descriptive Inorganic Chemistry*, 4th ed.; Freeman: New York, **2006**; pp 293–294.

82. Cohen, N.; Lopresti, R. J.; Saucy, G. *J. Am. Chem. Soc.* **1979**, *101*, 6710–6716.

83. Mourino, A.; Lewicka-Piekut, S.; Norman, A. W.; Okamura, W. H. *J. Org. Chem.* **1980**, *45*, 4015–4020.

84. Davies, J. S.; Higginbotham, C. L.; Tremeer, E. J.; Brown, C.; Treadgold, R. *J. Chem. Soc. Perkin Trans. 1* **1992**, *1*, 3043–3048.

85. Paquette, L. A.; Doherty, A. M.; Rayner, C. M. *J. Am. Chem. Soc.* **1992**, *114*, 3910–3926.

86. Acuña, U.; Amat-Guerri, F.; Morcillo, P.; Liras, M.; Rodríguez, B. *Org. Lett.* **2009**, *11*, 3020–3023.

87. Koufaki, M.; Kiziridi, C.; Alexi, X.; Alexis, M. N. *Bioorgan. Med. Chem.* **2009**, *17*, 6432–6441.

88. Boyer, P. D. *J. Am. Chem. Soc.* **1951**, *73*, 733–740.

89. Martius, C.; Eilingsfeld, H. *Biochem. Z.* **1957**, *328*, 507–508.

90. Zeeshan, M. U.; Ph.D. thesis; Norwegian University of Science and Technology (Unpublished); Trondheim; **2012**.

91. Zechmeister, L.; Tuzson, P. *Ber. Dtsch. Chem. Ges. B* **1939**, *72B*, 1340–1346.

92. Molnár, P.; Szabolcs, J. *J. Chem. Soc. Perkin Trans. 2* **1993**, *2*, 261–266.

93. Neises, B.; Steglich, W. *Angew. Chem.* **1978**, *90*, 556–557.

94. Friebolin, H. *Basic One- and Two-Dimensional NMR Spectroscopy*, 4th ed.; Wiley: Weinheim, **2004**; p 94.

95. Armarego, W. L. F.; Chai, C. L. L. *Purification of Laboratory Chemicals*, 6th ed.; Butterworth-Heinemann/Elsevier: Oxford, **2009**; pp 90, 133, 159, 425.

96. Lei, H.; Atkinson, J. *J. Org. Chem.* **2000**, *65*, 2560–2567.

Appendixes

A Spectroscopic data of 8

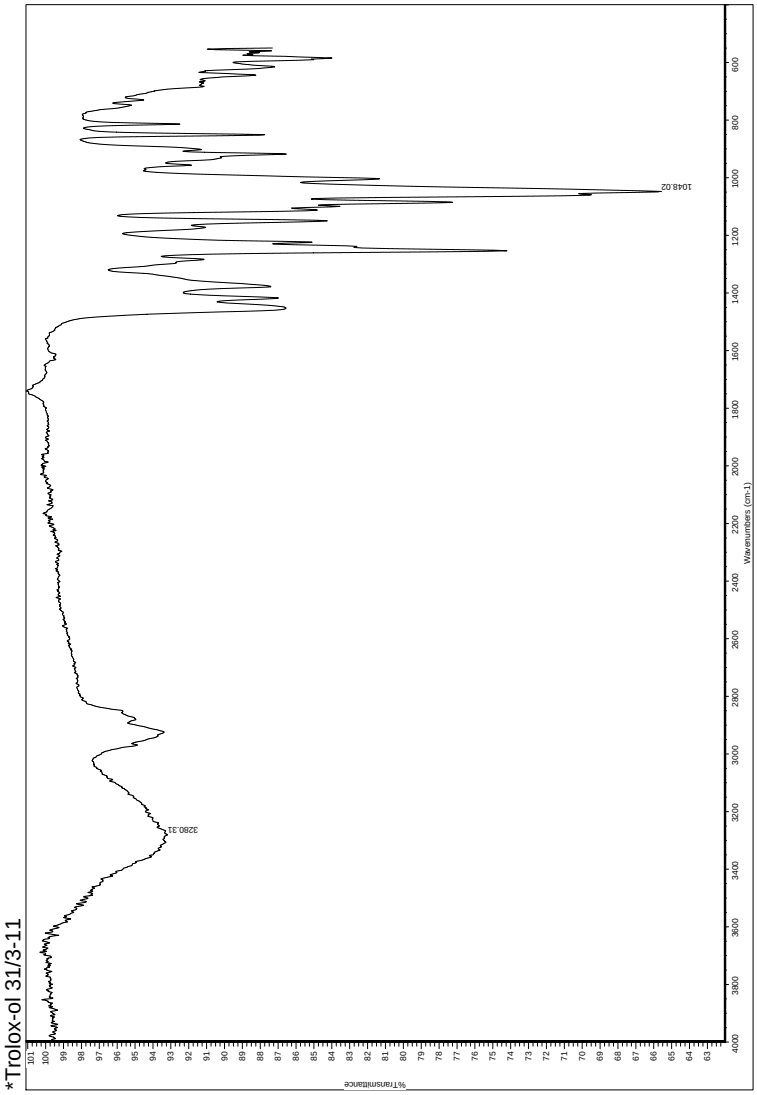

Figure A.1: IR spectrum of **8**.

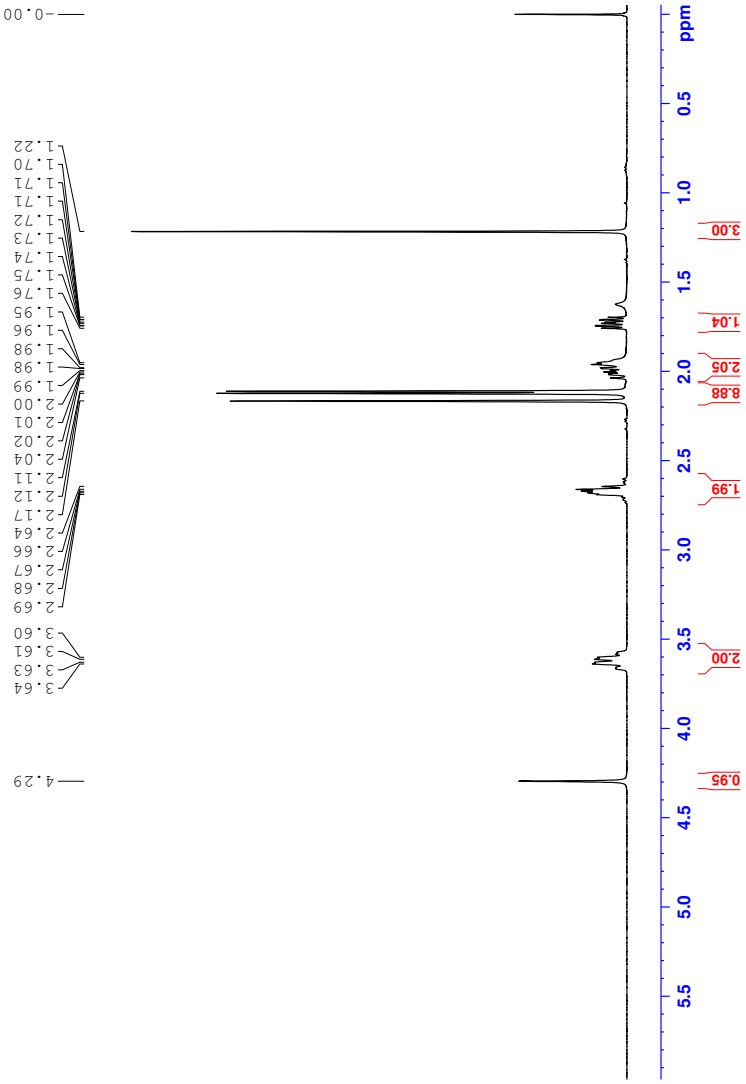

Figure A.2: ^{1}H NMR spectrum of **8**.

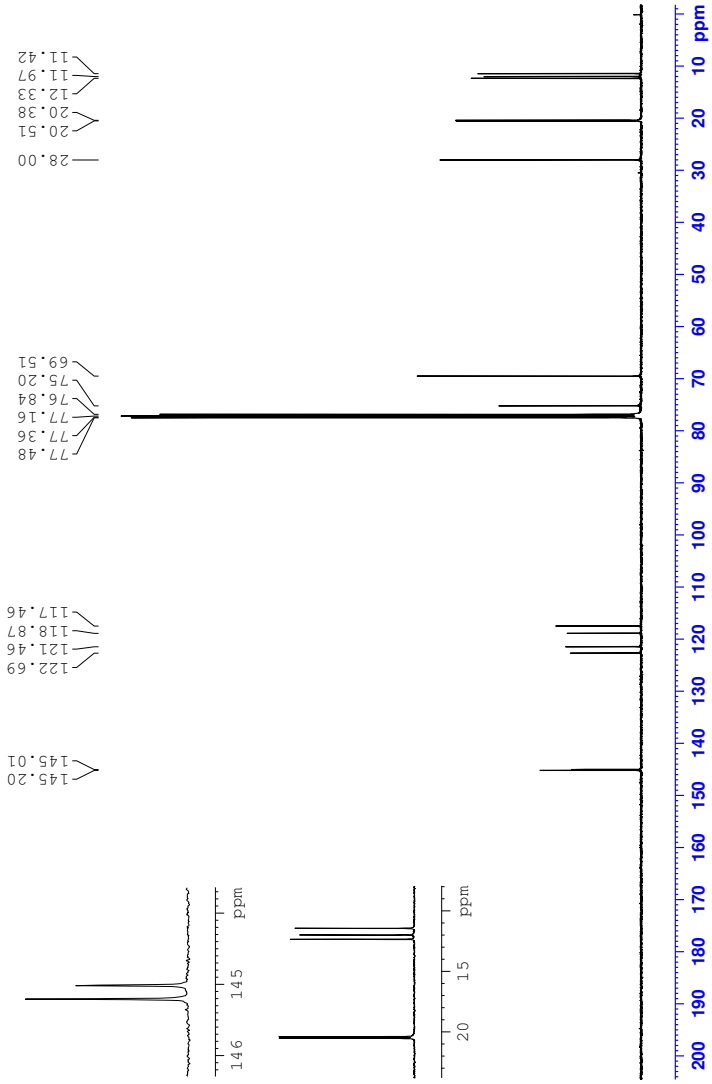

Figure A.3: ^{13}C NMR spectrum of **8**.

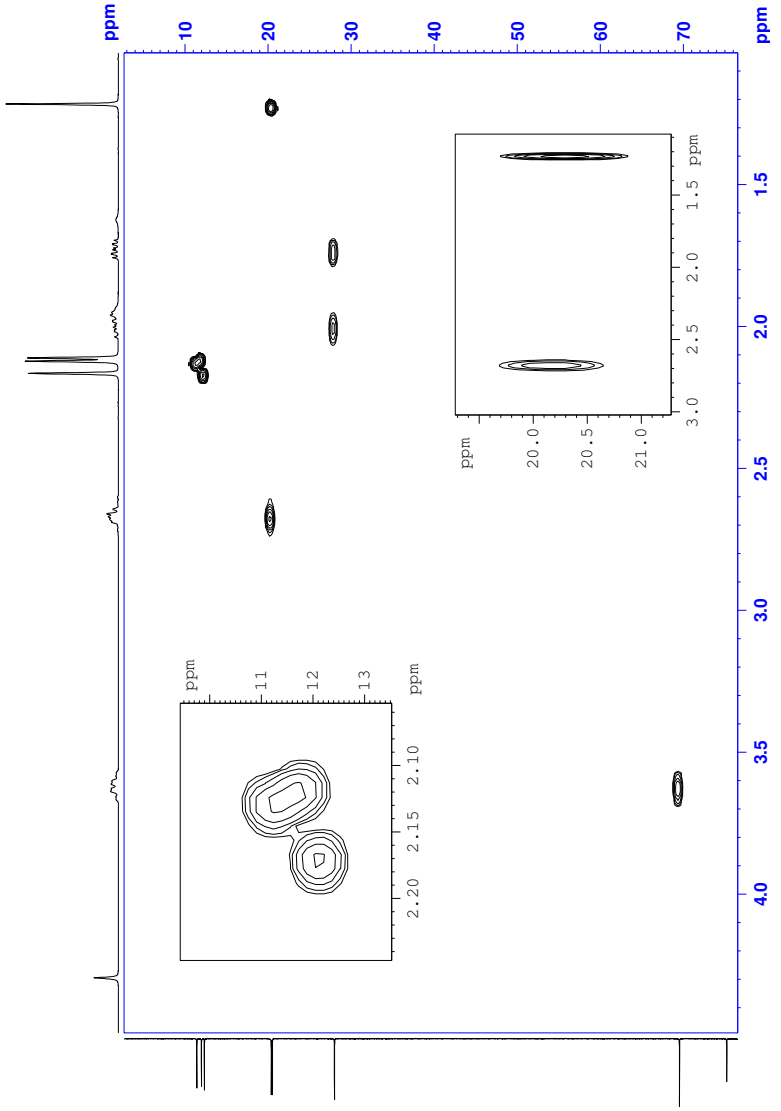

Figure A.4: HSQC NMR spectrum of **8**.

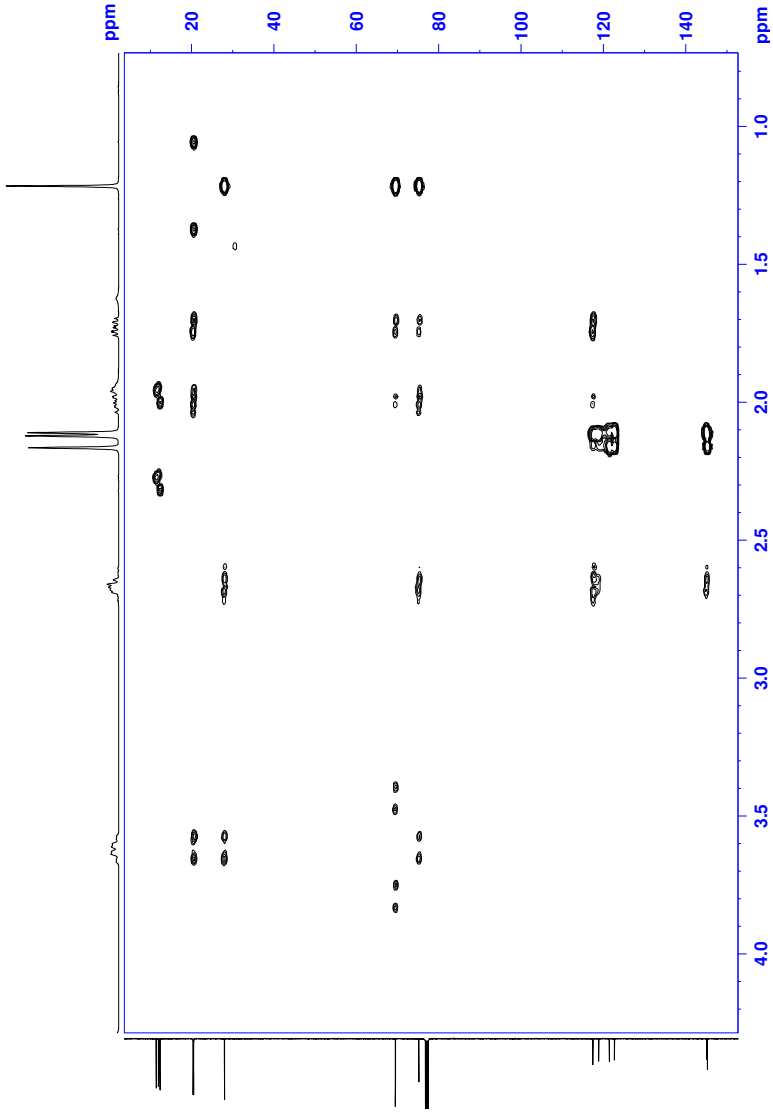

Figure A.5: HMBC NMR spectrum of **8**.

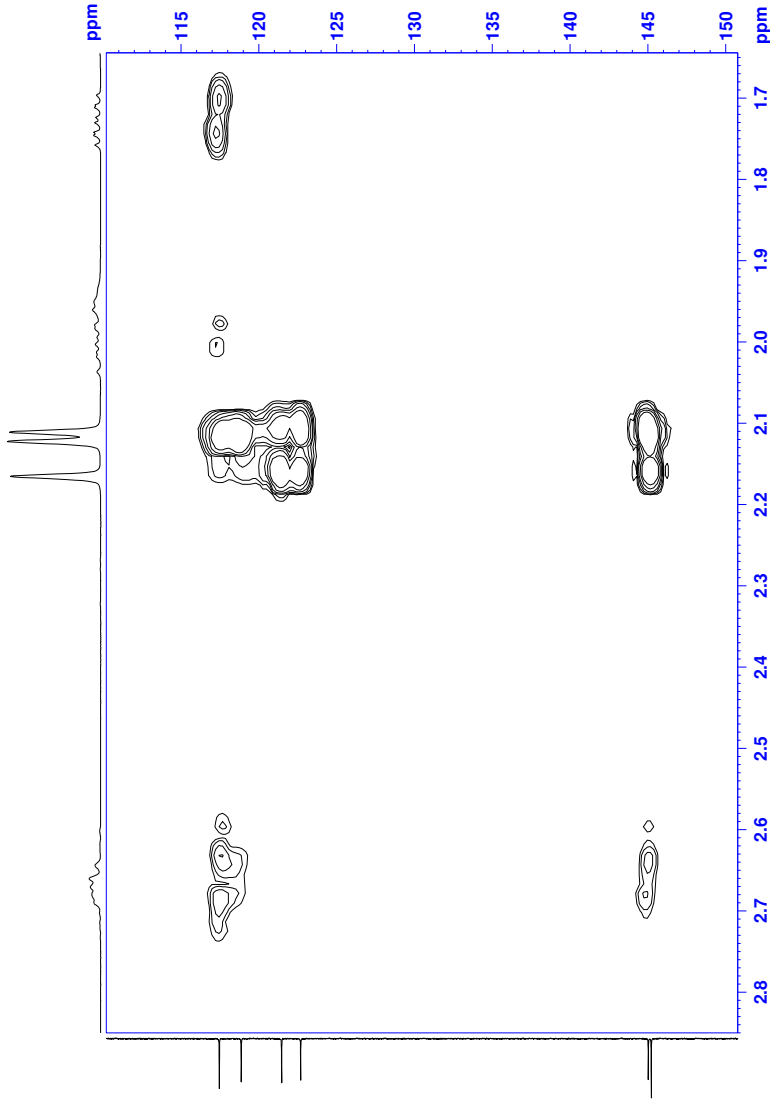

Figure A.6: Enlargement of HMBC NMR spectrum of **8**.

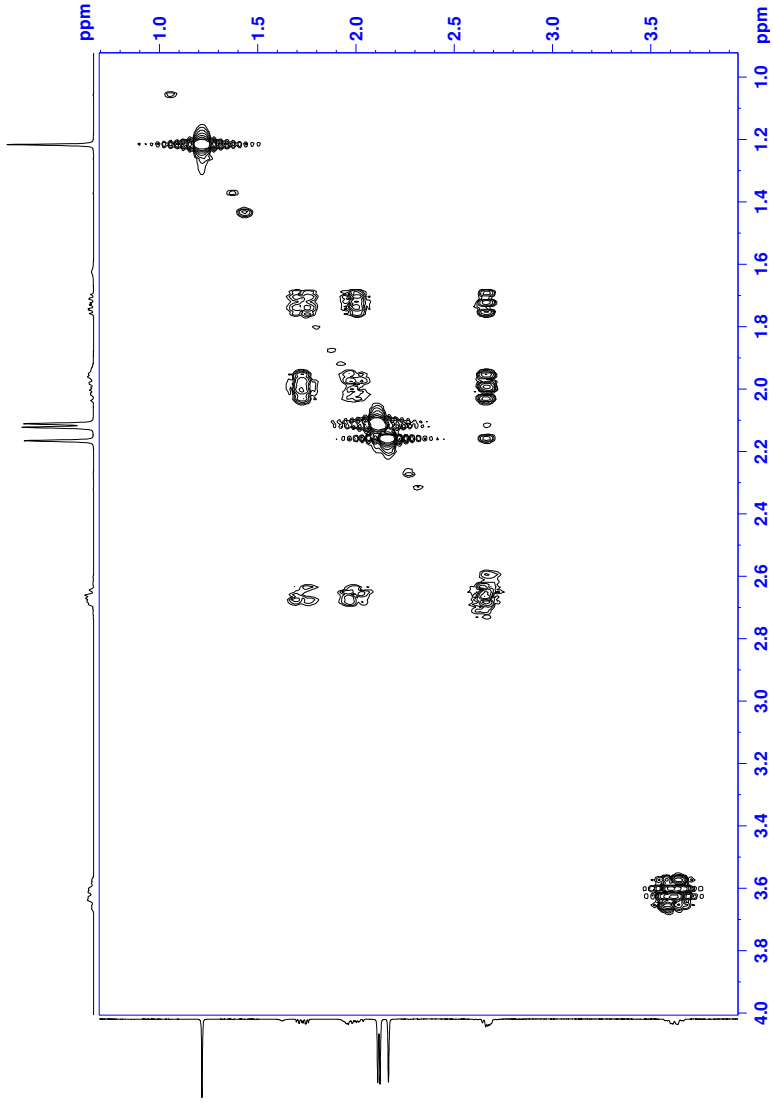

Figure A.7: COSY NMR spectrum of **8**.

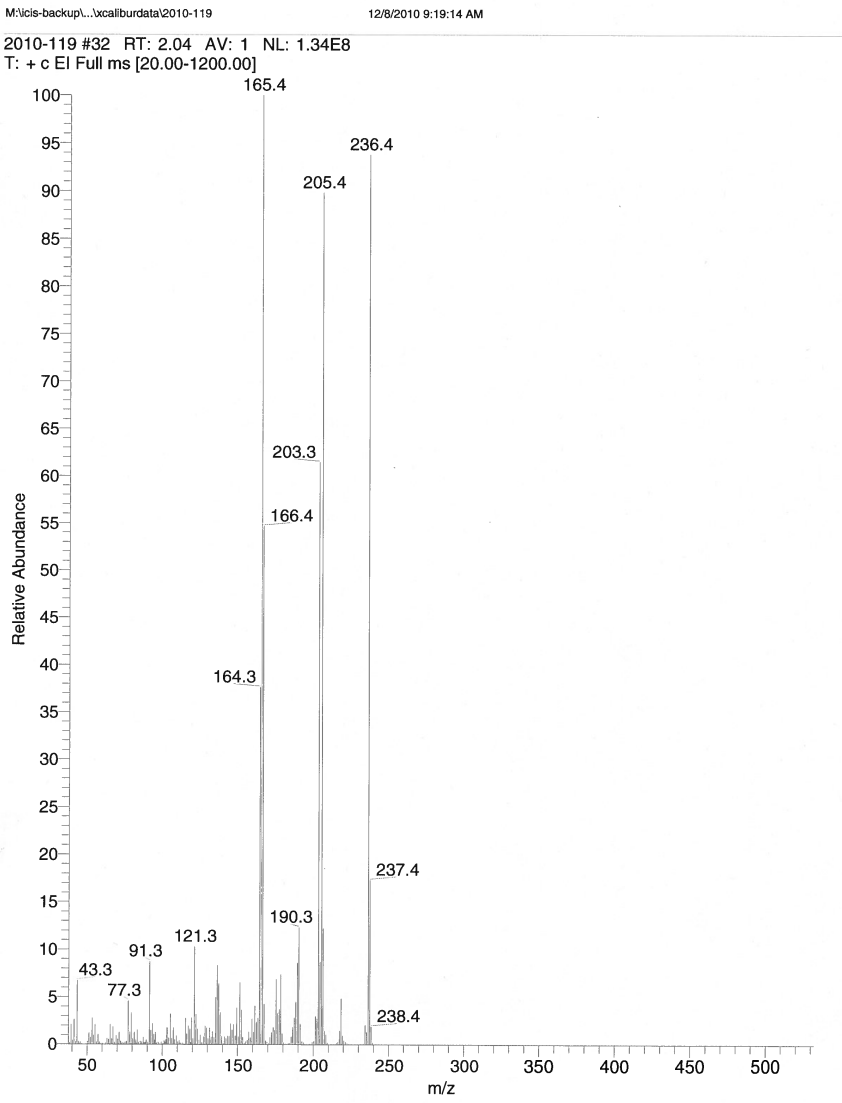

Figure A.8: LRMS spectrum with EI ionization of **8**.

B Spectroscopic data of 8B

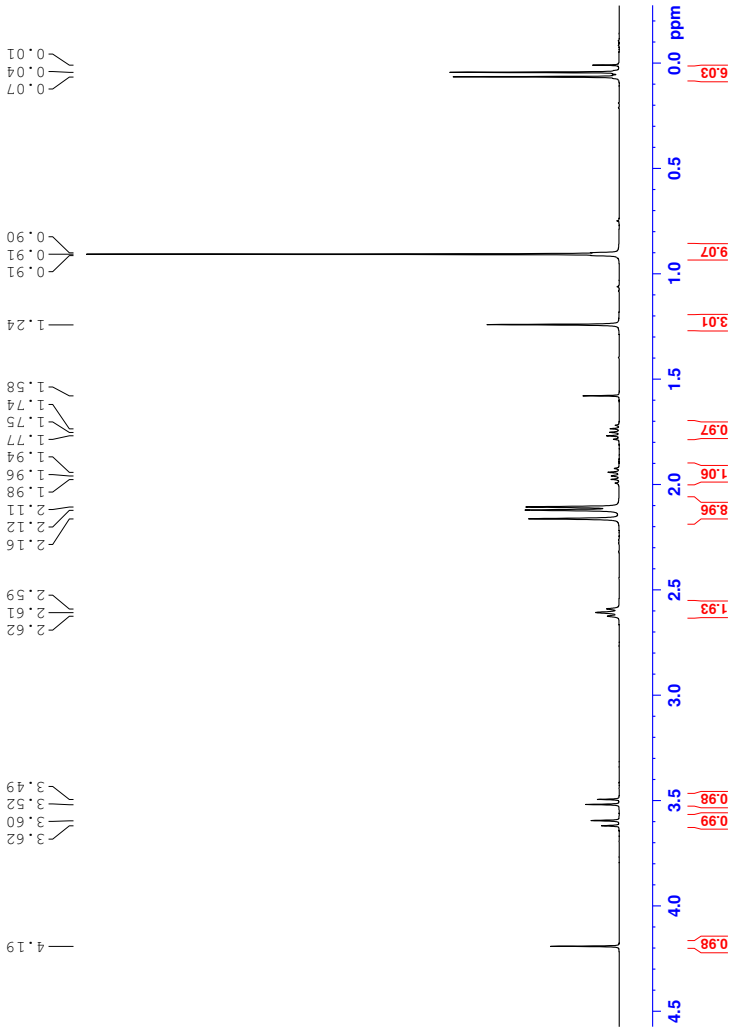

Figure B.1: ^{1}H NMR spectrum of **8B**.

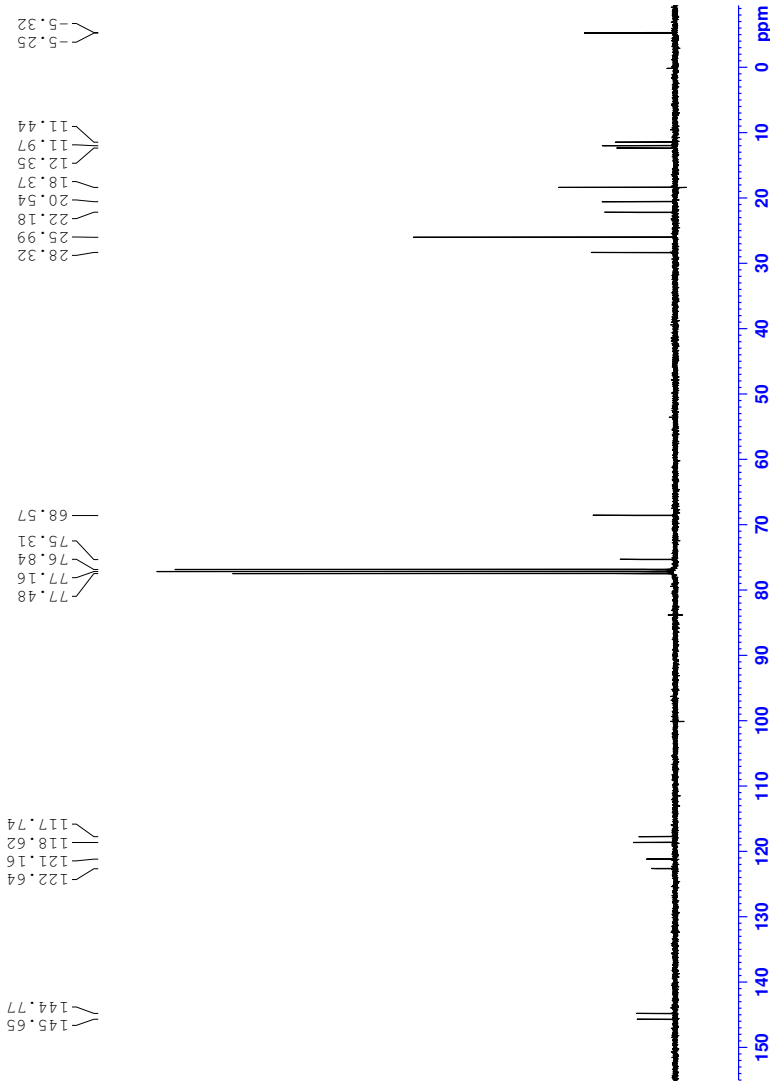

Figure B.2: ^{13}C NMR spectrum of **8B**.

C Spectroscopic data of 27

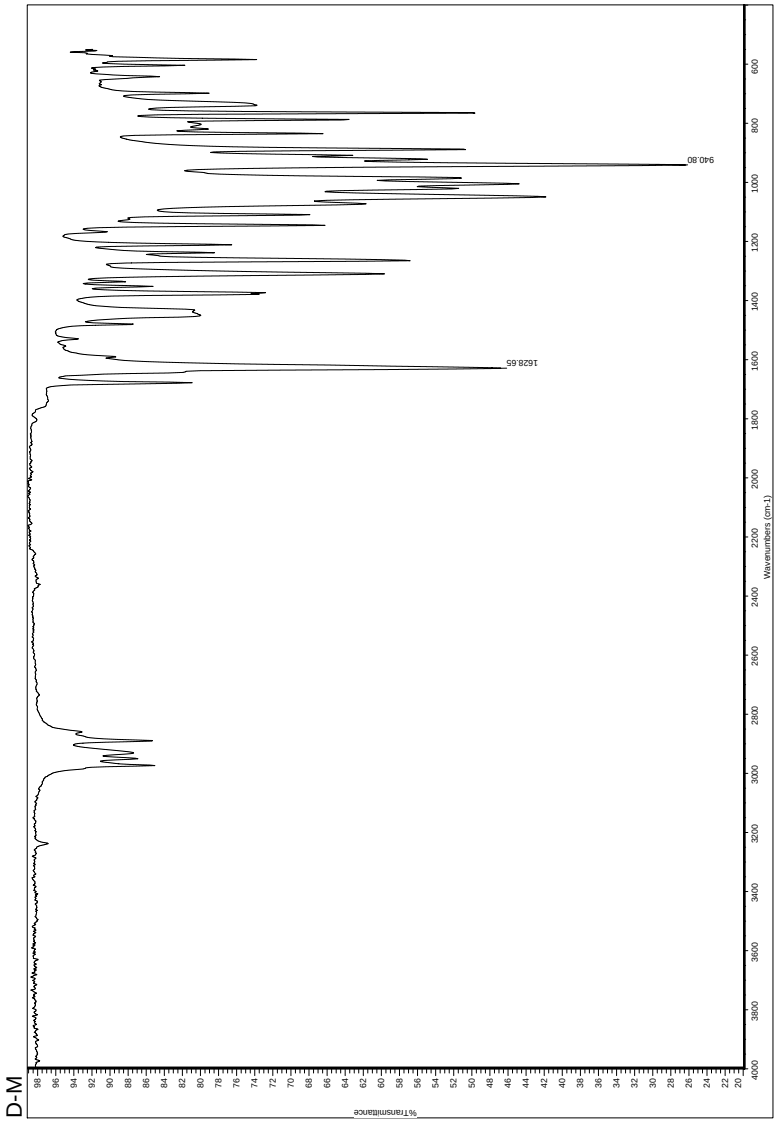

Figure C.1: IR spectrum of **27**.

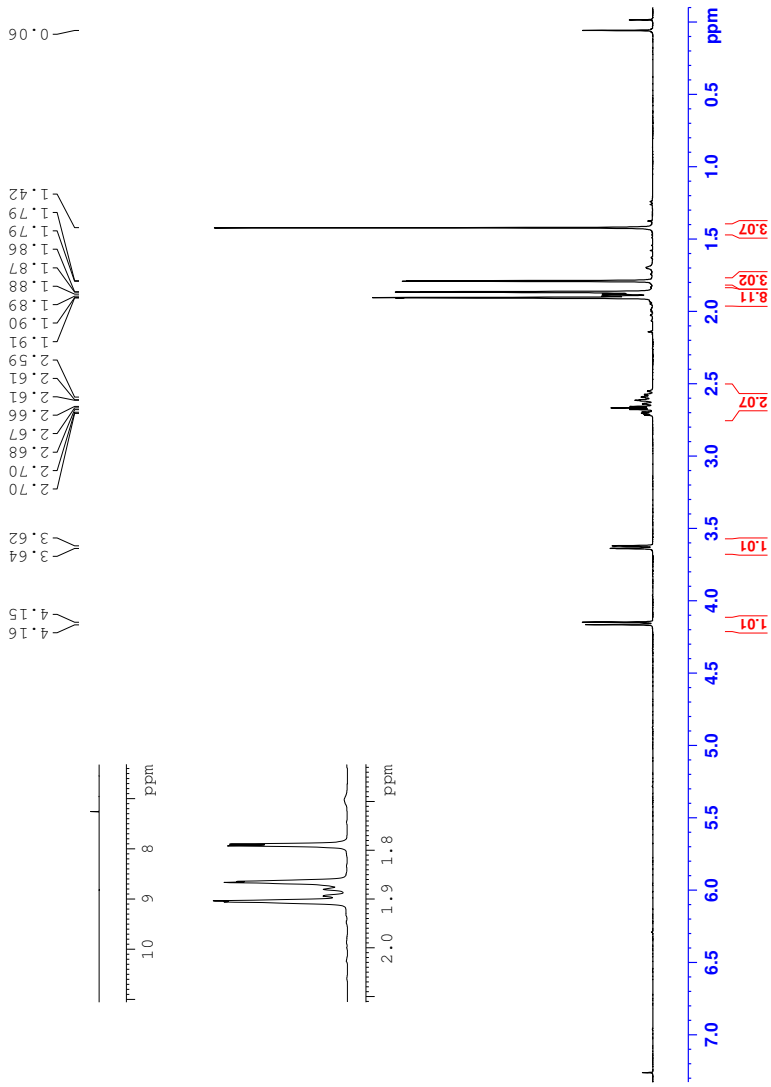

Figure C.2: ^{1}H NMR spectrum of **27**.

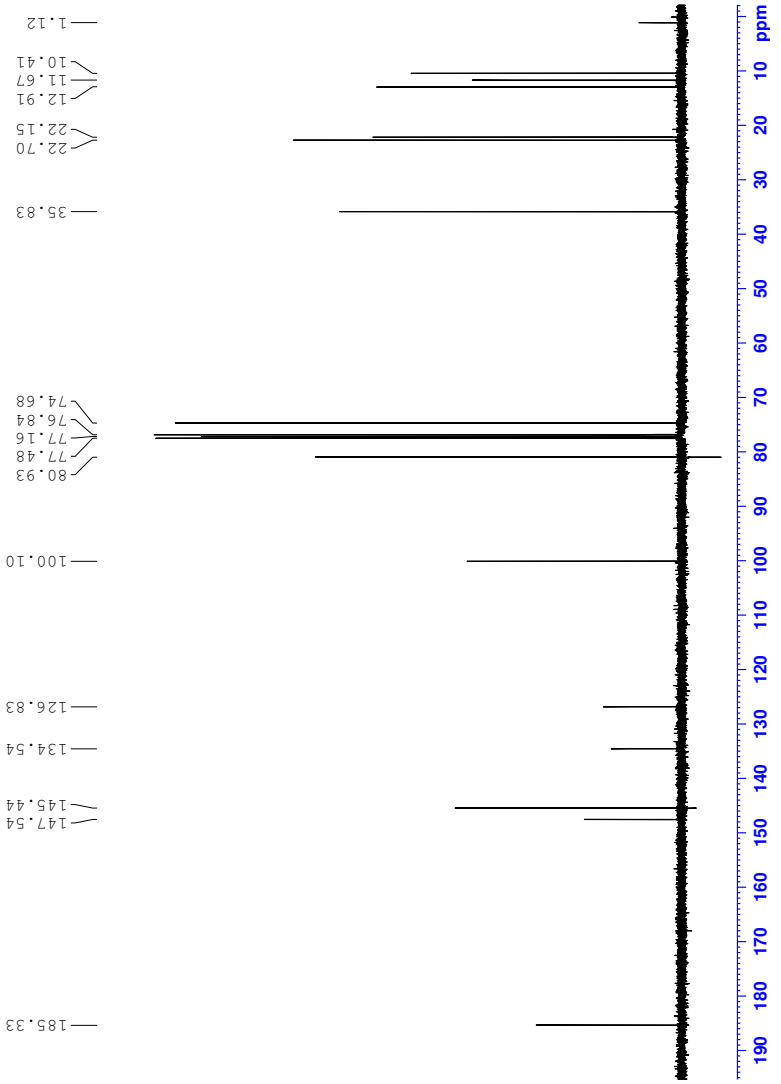

Figure C.3: ^{13}C NMR spectrum of **27**.

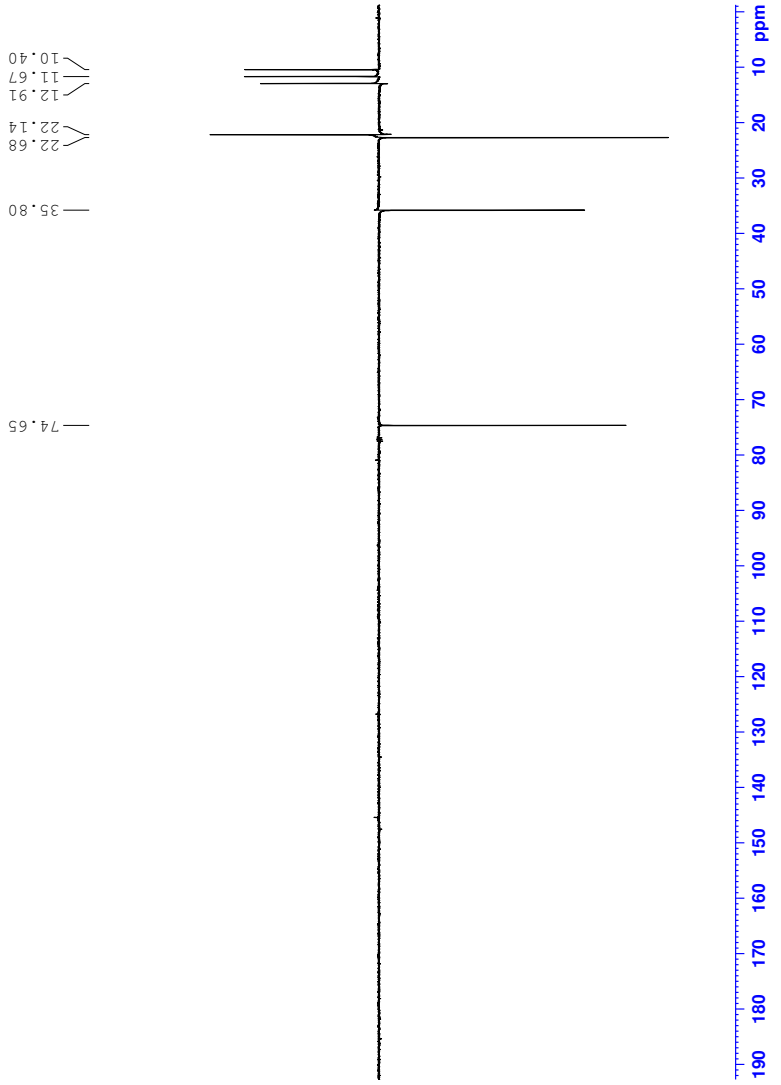

Figure C.4: DEPT135 NMR spectrum of **27**.

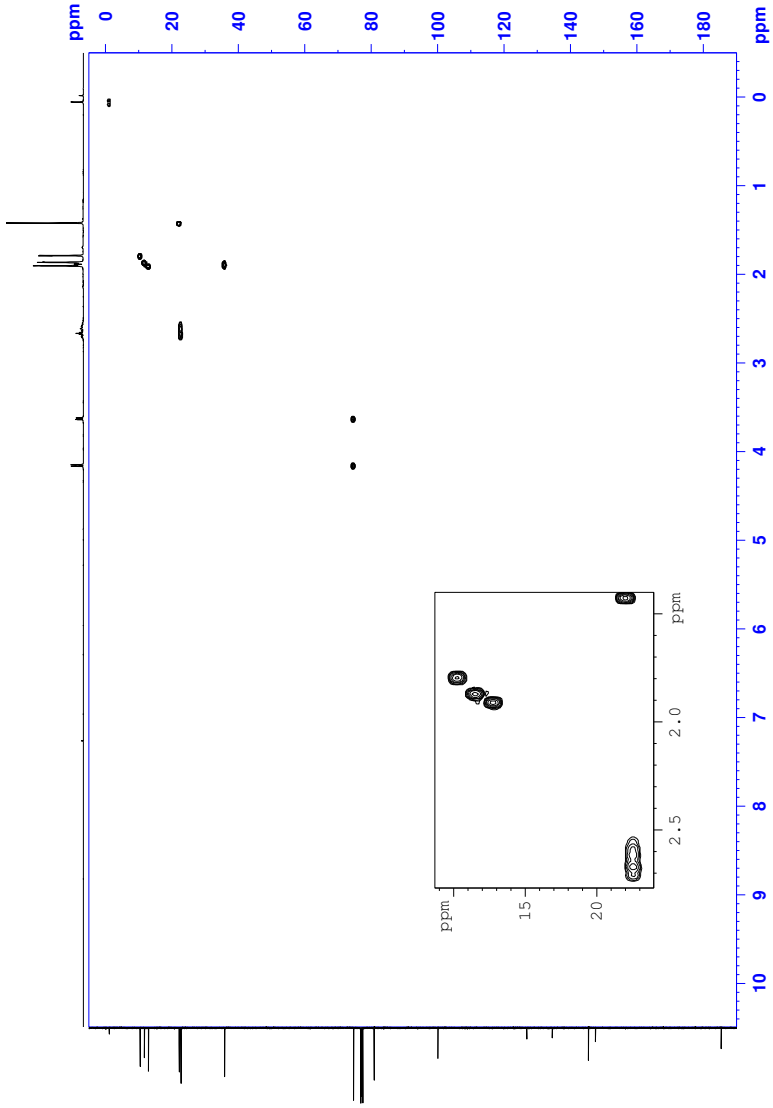

Figure C.5: HSQC NMR spectrum of **27**.

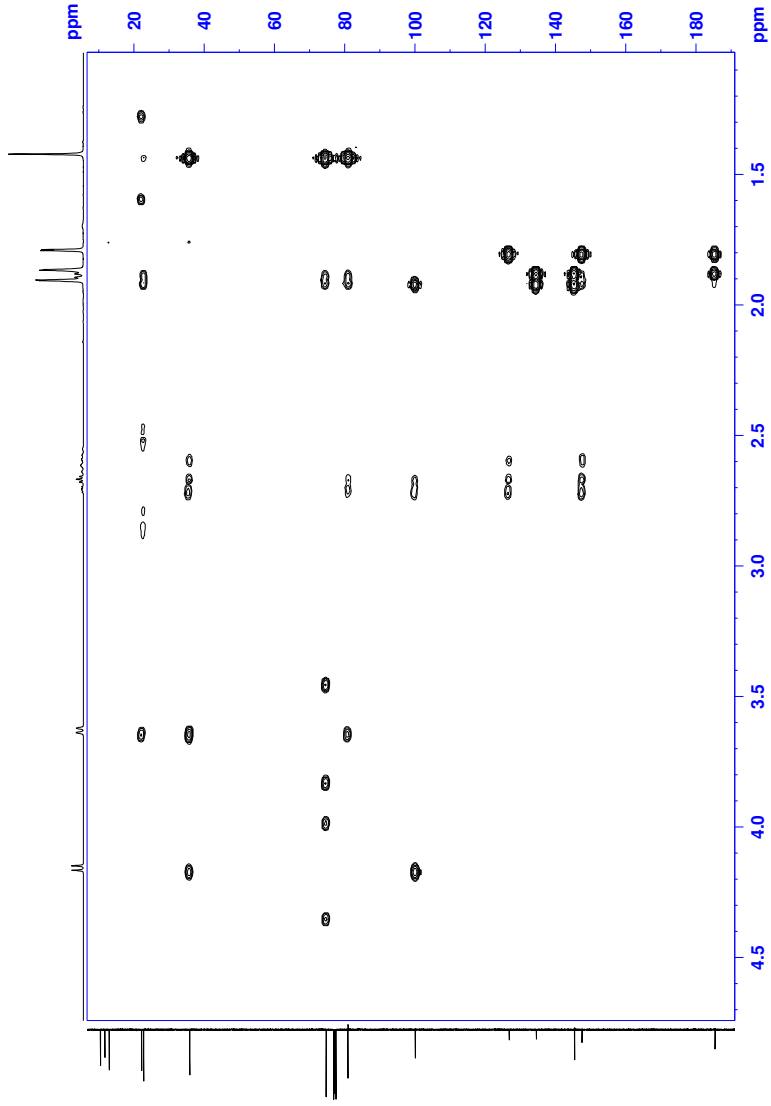

Figure C.6: HMBC NMR spectrum of **27**.

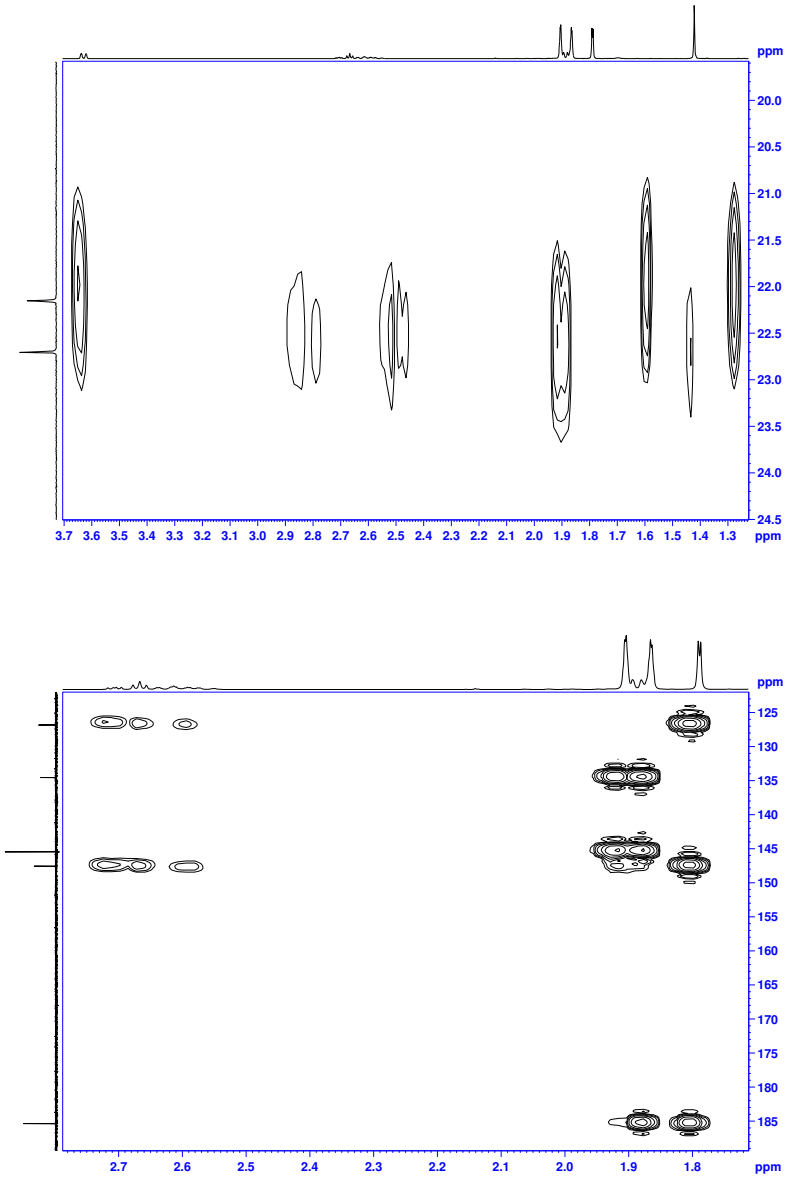

Figure C.7: Enlargements of the HMBC NMR spectrum of **27**.

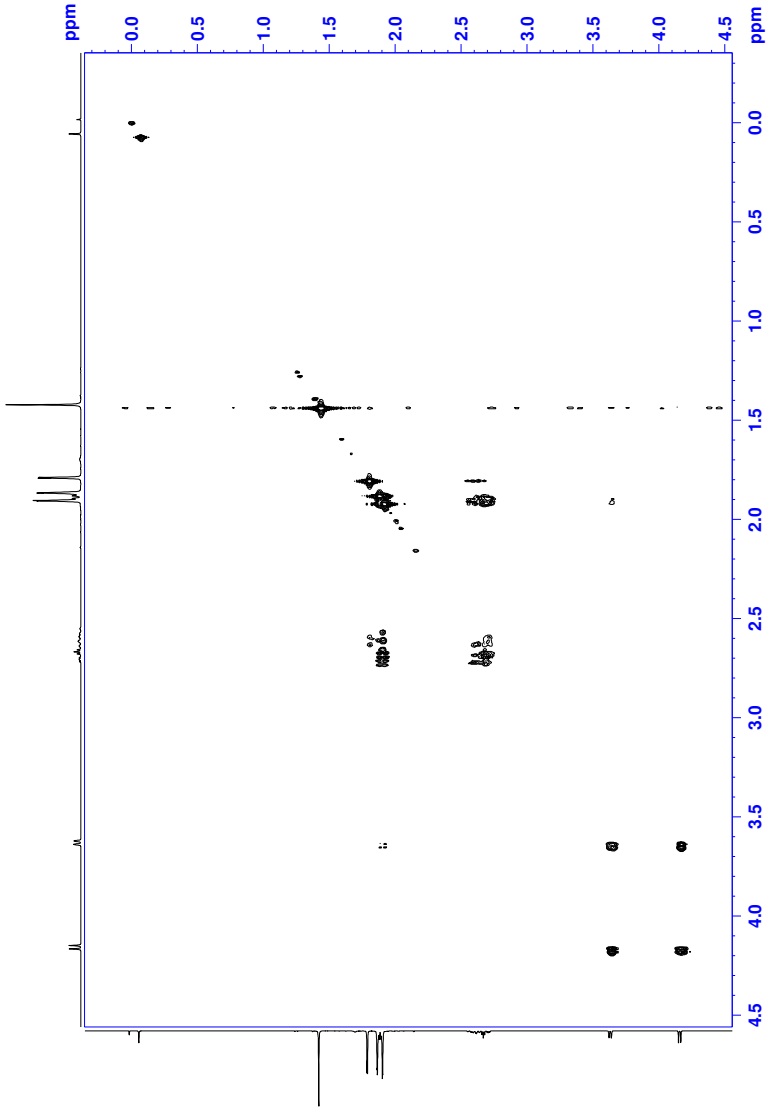

Figure C.8: COSY NMR spectrum of **27**.

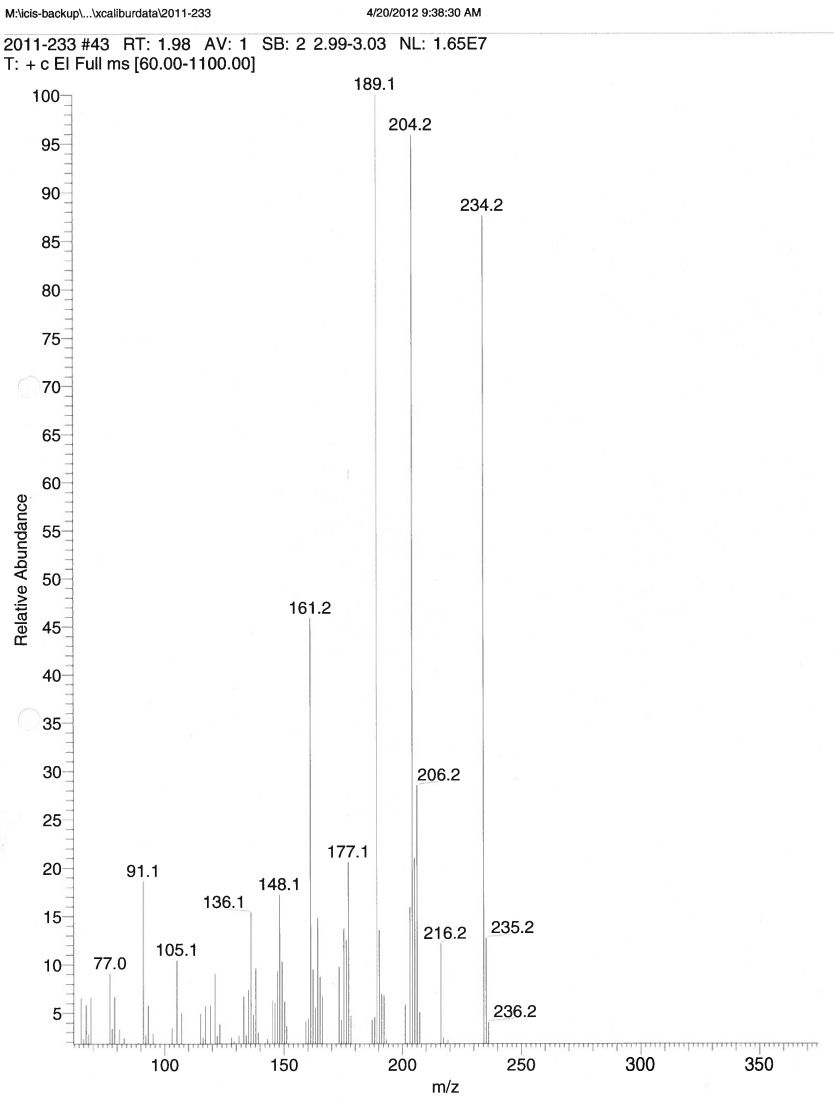

Figure C.9: LRMS spectrum with EI ionization of **27**.

D Spectroscopic data of 9

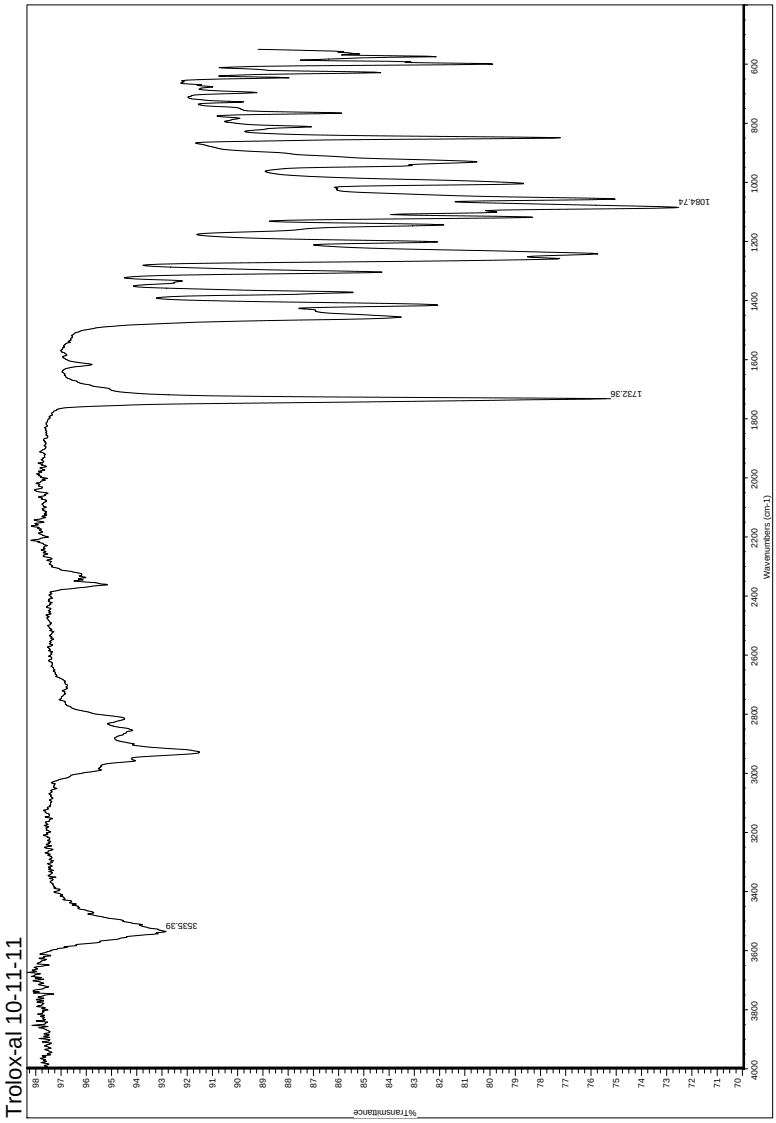

Figure D.1: IR spectrum of **9**.

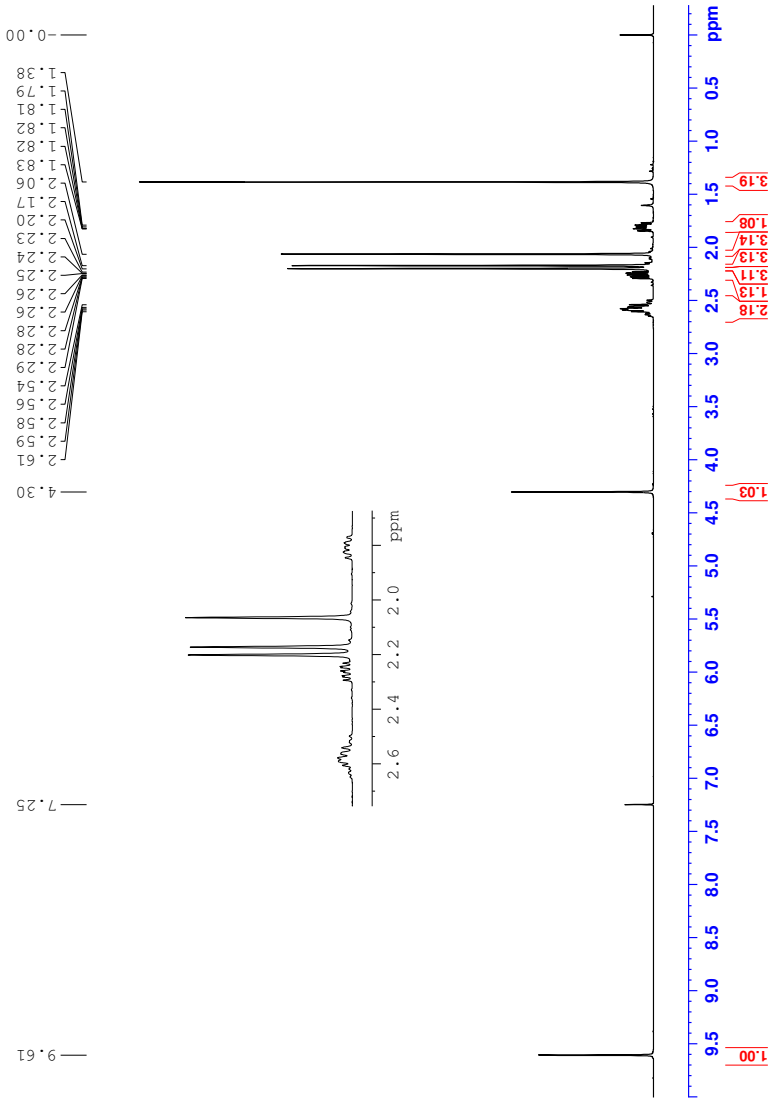

Figure D.2: ^{1}H NMR spectrum of **9**.

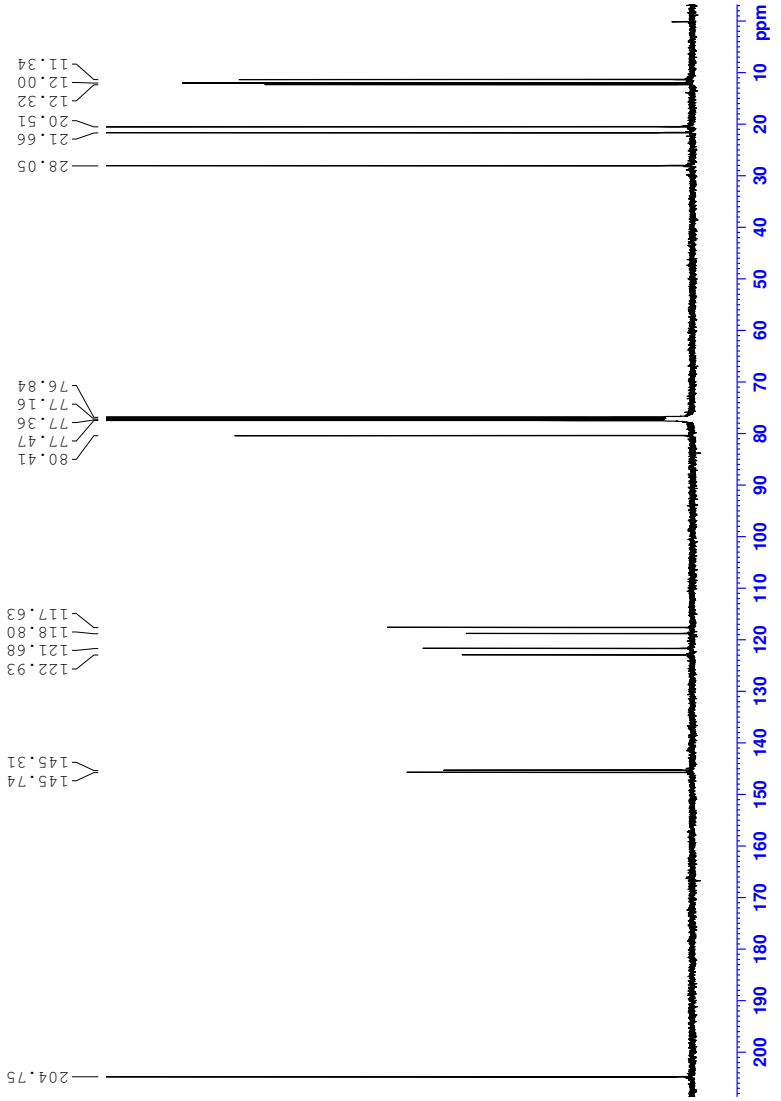

Figure D.3: ^{13}C NMR spectrum of **9**.

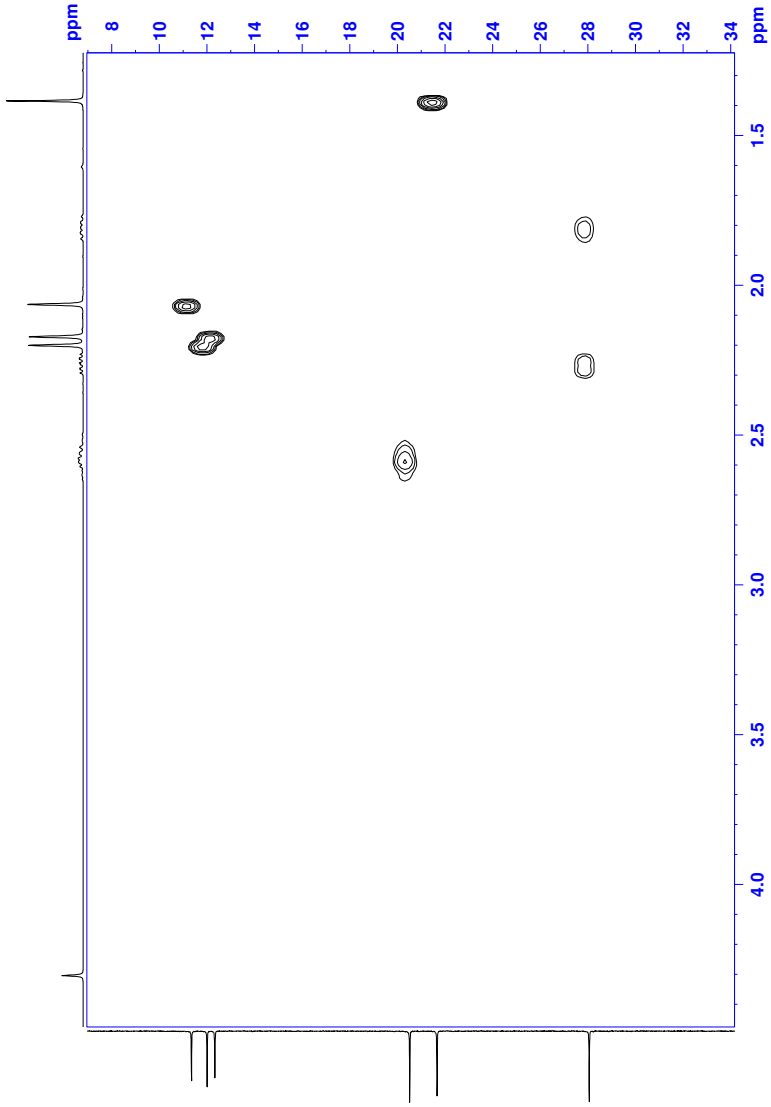

Figure D.4: HSQC NMR spectrum of **9**.

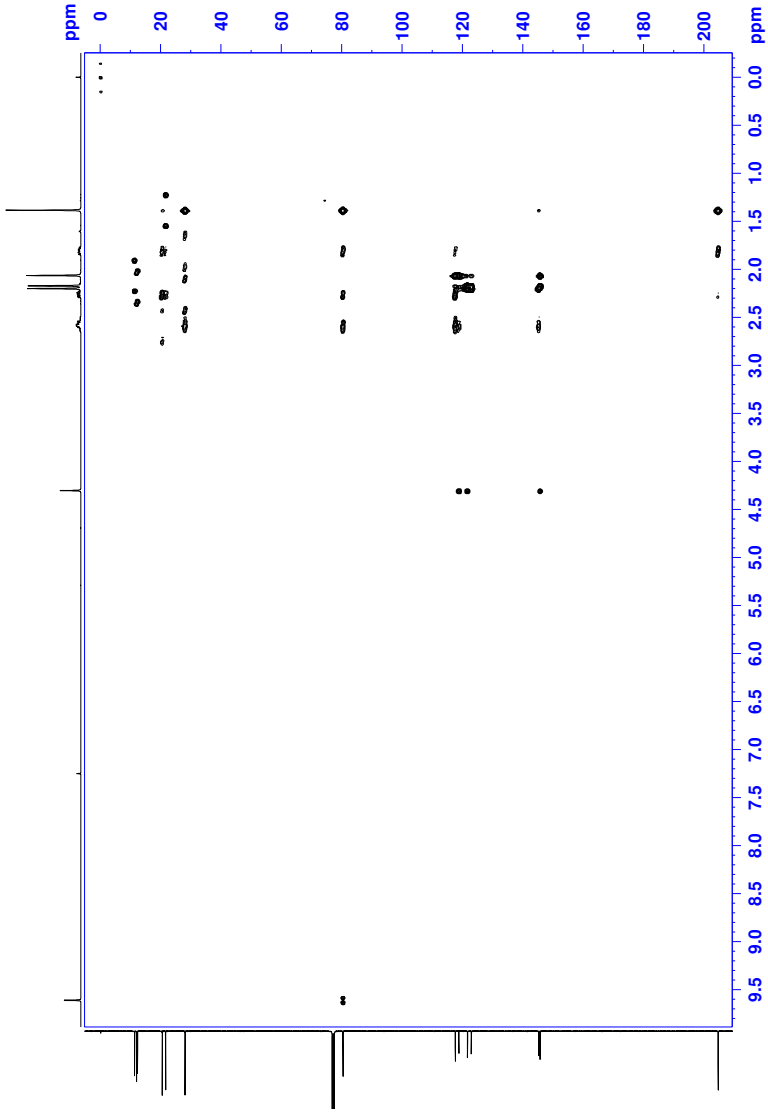

Figure D.5: HMBC NMR spectrum of **9**.

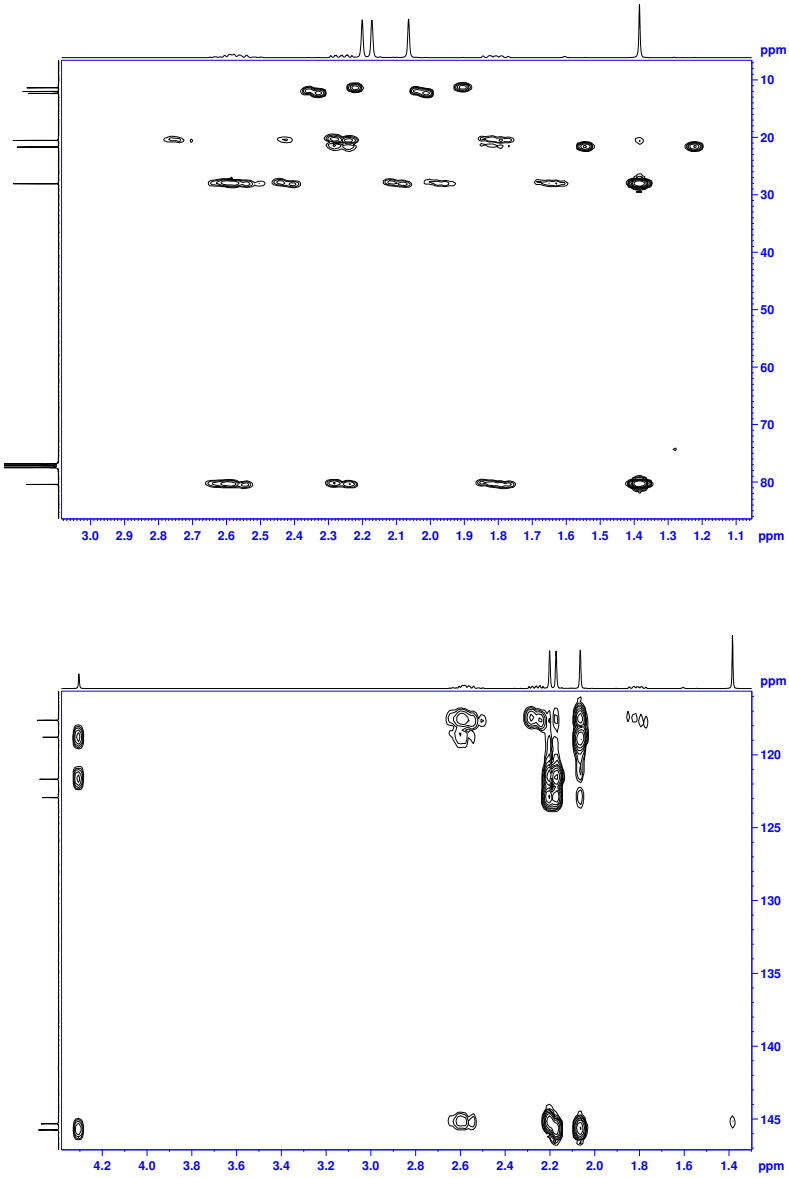

Figure D.6: Enlargements of the HMBC NMR spectrum of **9**.

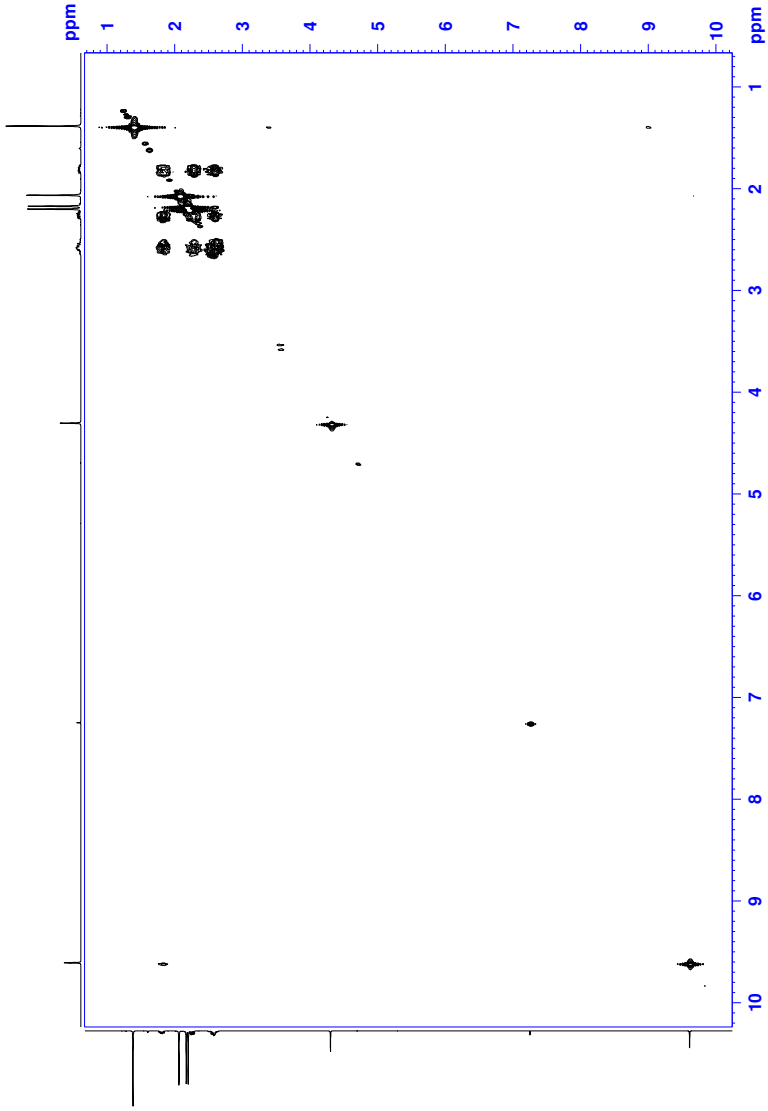

Figure D.7: COSY NMR spectrum of **9**.

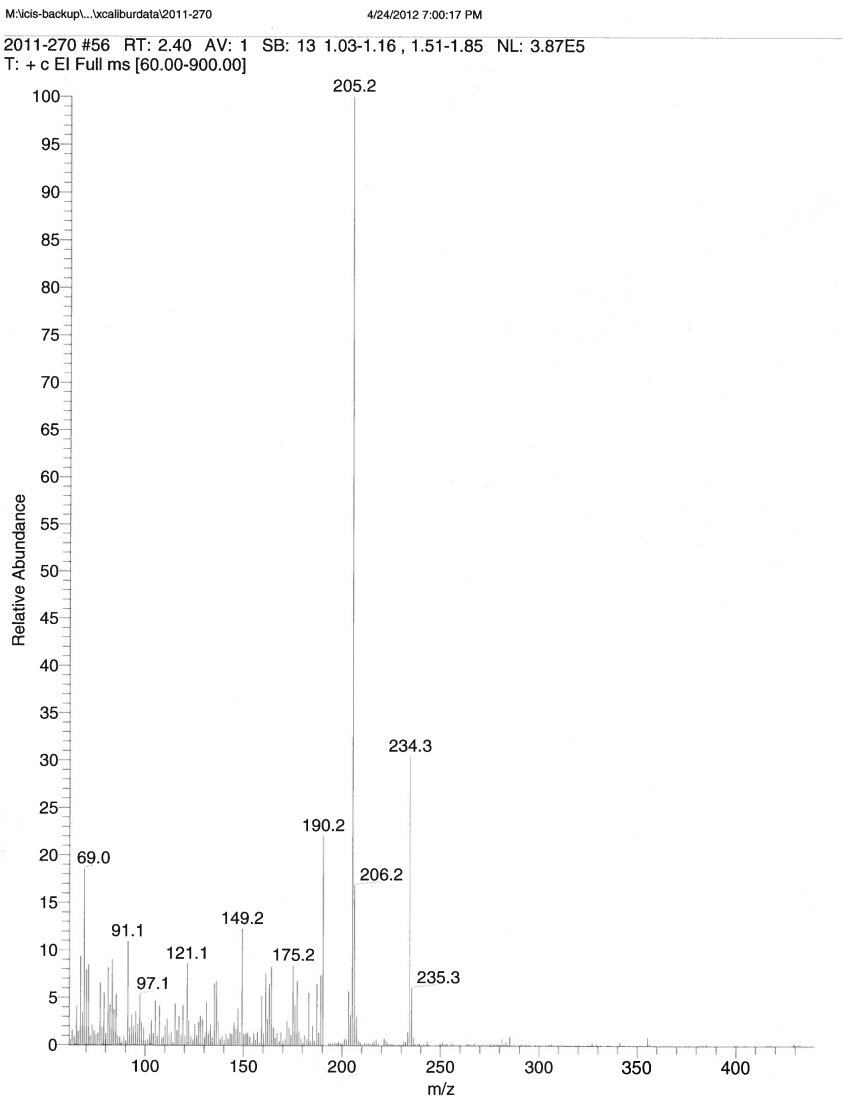

Figure D.8: LRMS spectrum with EI ionization of **9**.

E Spectroscopic data of 11

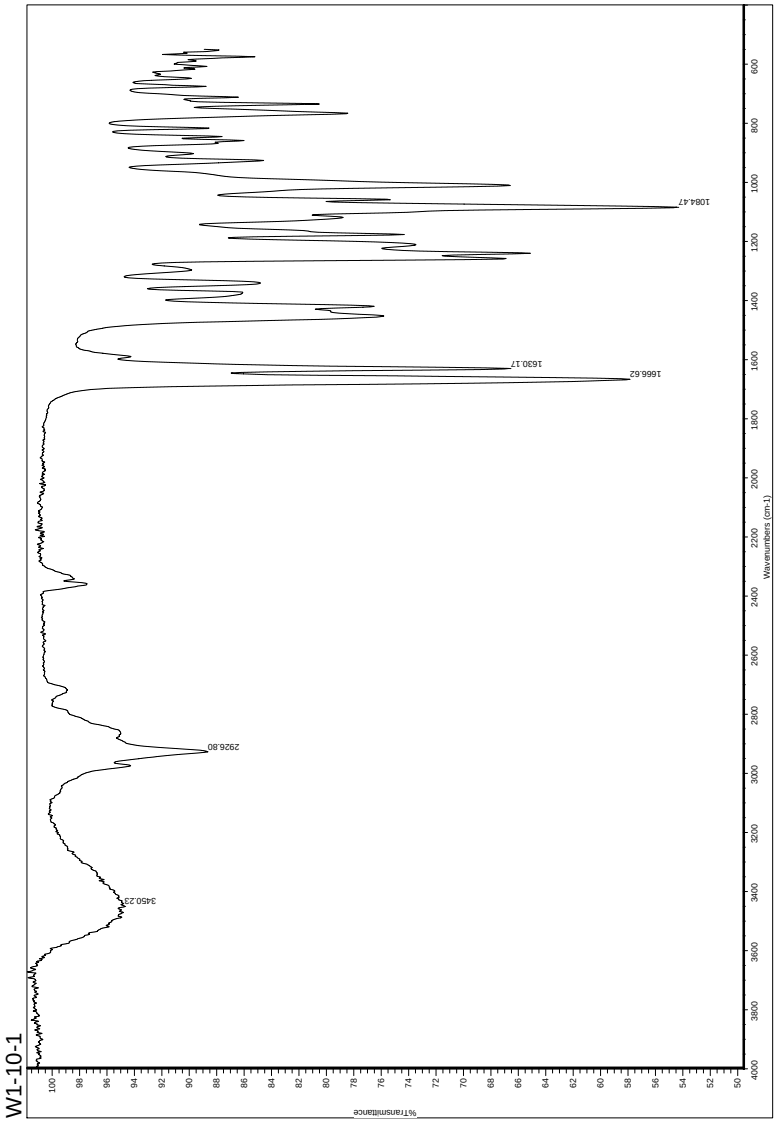

Figure E.1: IR spectrum of **11**.

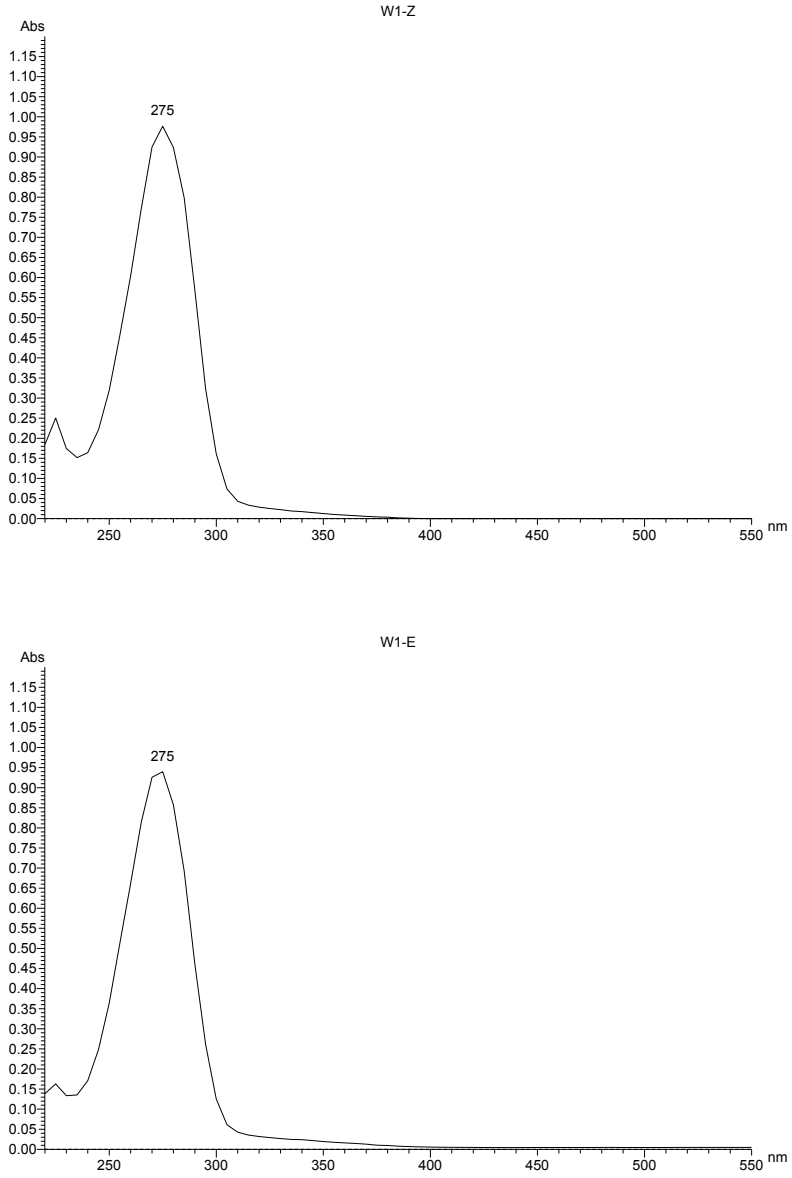

Figure E.2: UV/Vis spectra of (4*Z*)-**11** (top) and (4*E*)-**11** (bottom).

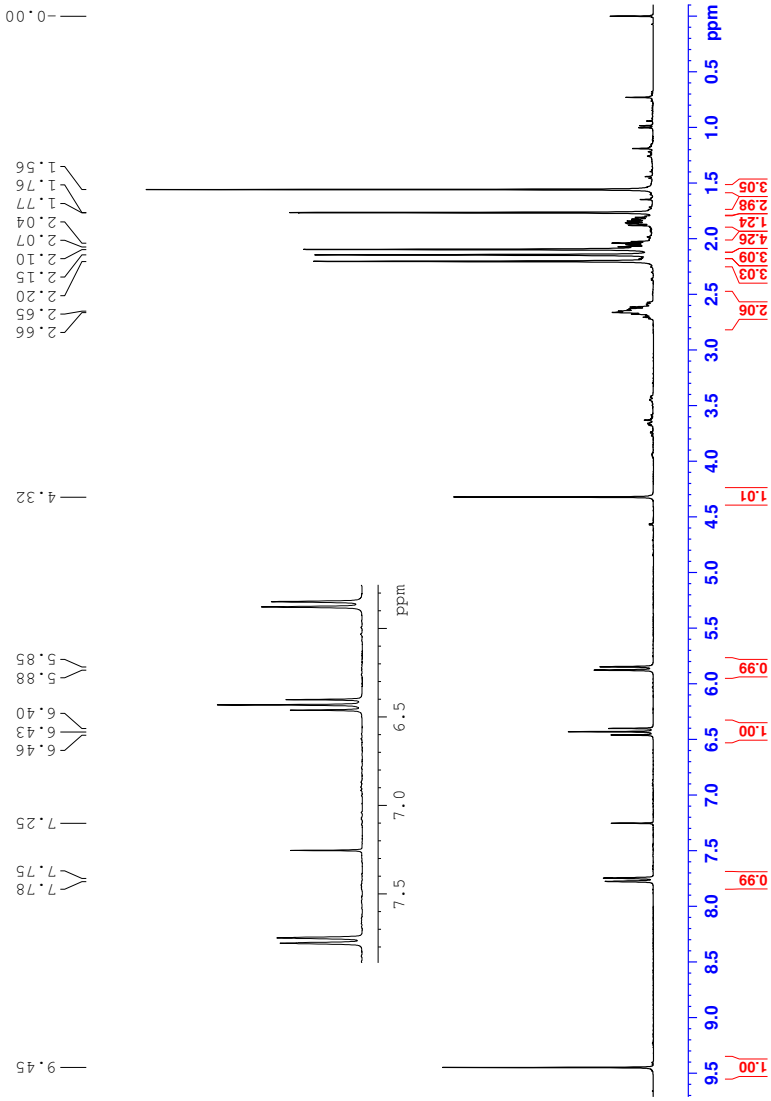

Figure E.3: ^{1}H NMR spectrum of (4*Z*)-**11**.

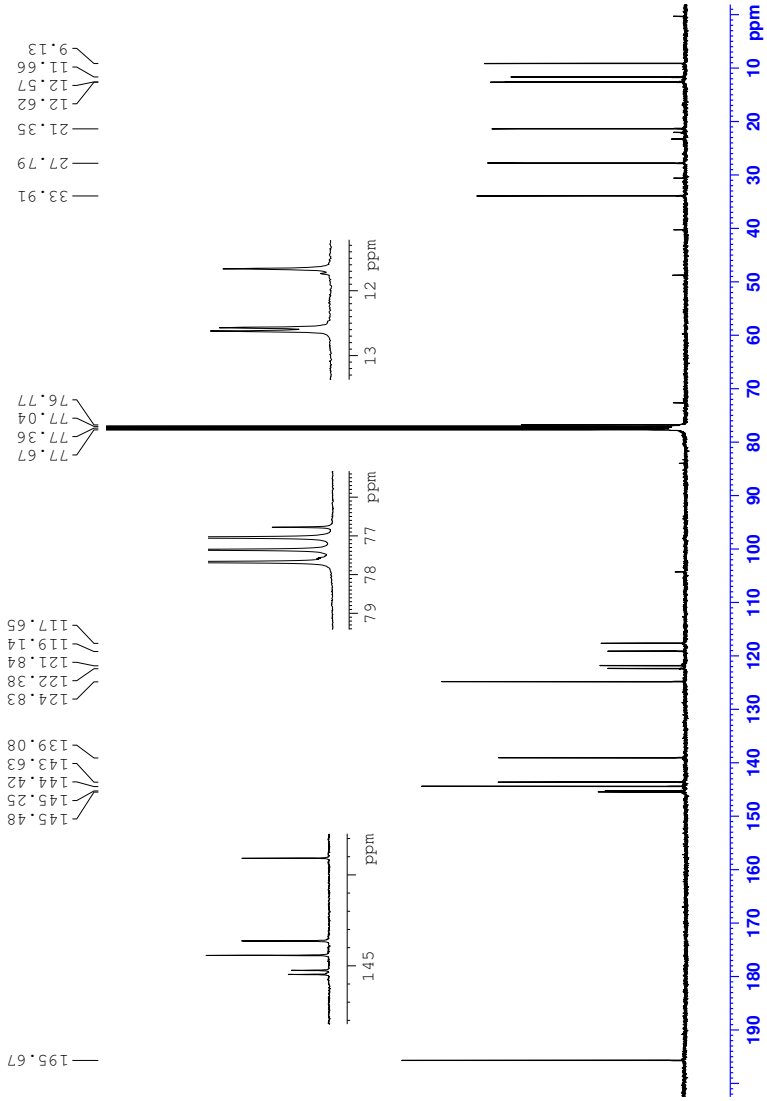

Figure E.4: ^{13}C NMR spectrum of (4*Z*)-**11**.

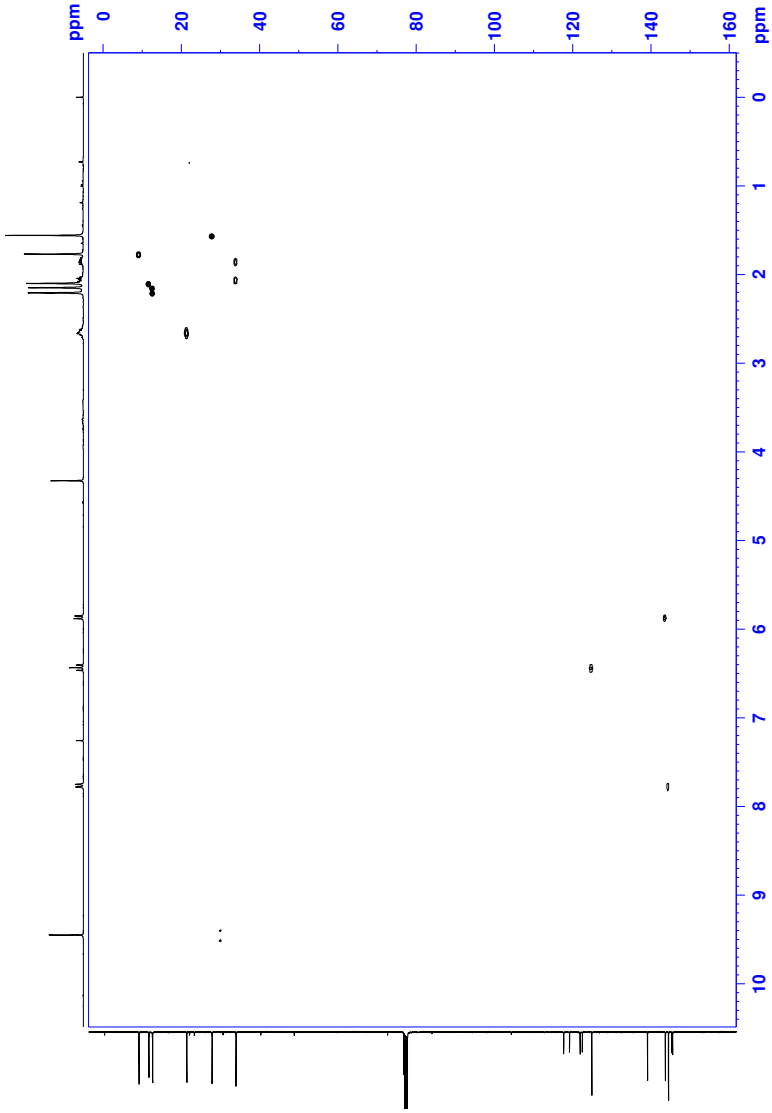

Figure E.5: HSQC NMR spectrum of (4*Z*)-**11**.

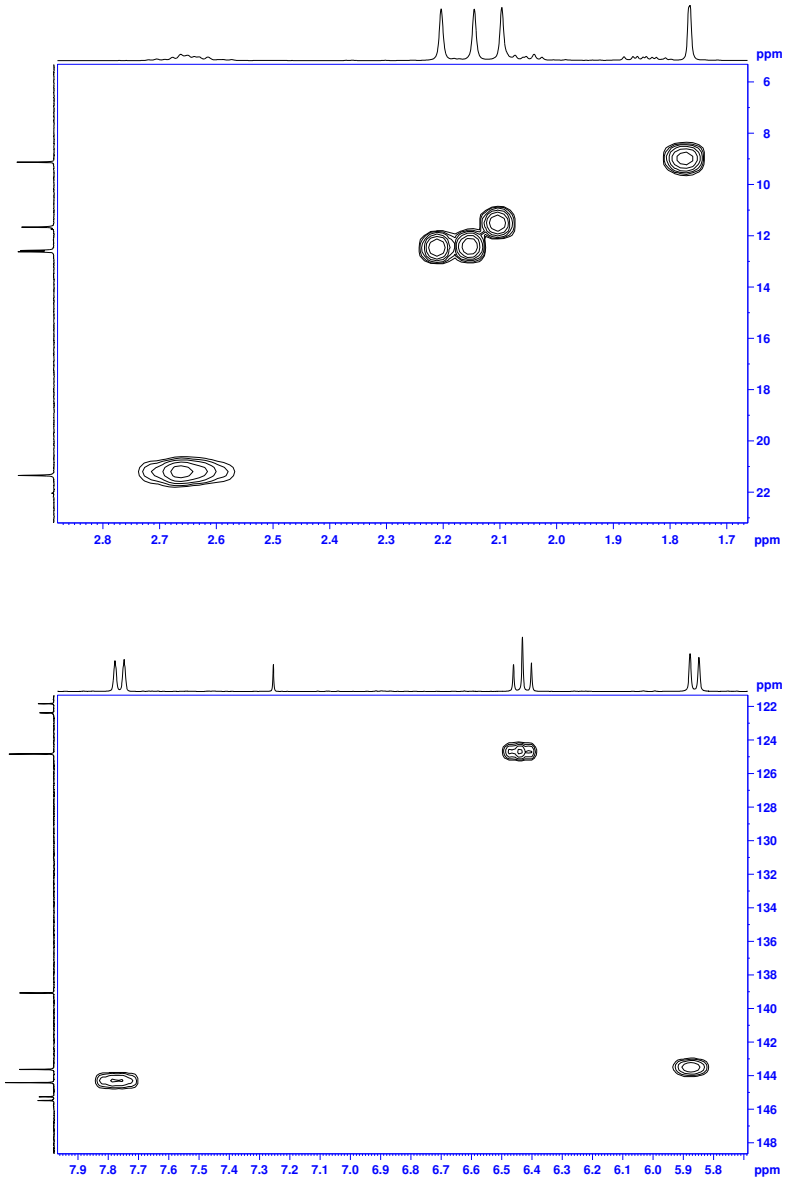

Figure E.6: Enlargements of the HSQC NMR spectrum of (4*Z*)-**11**.

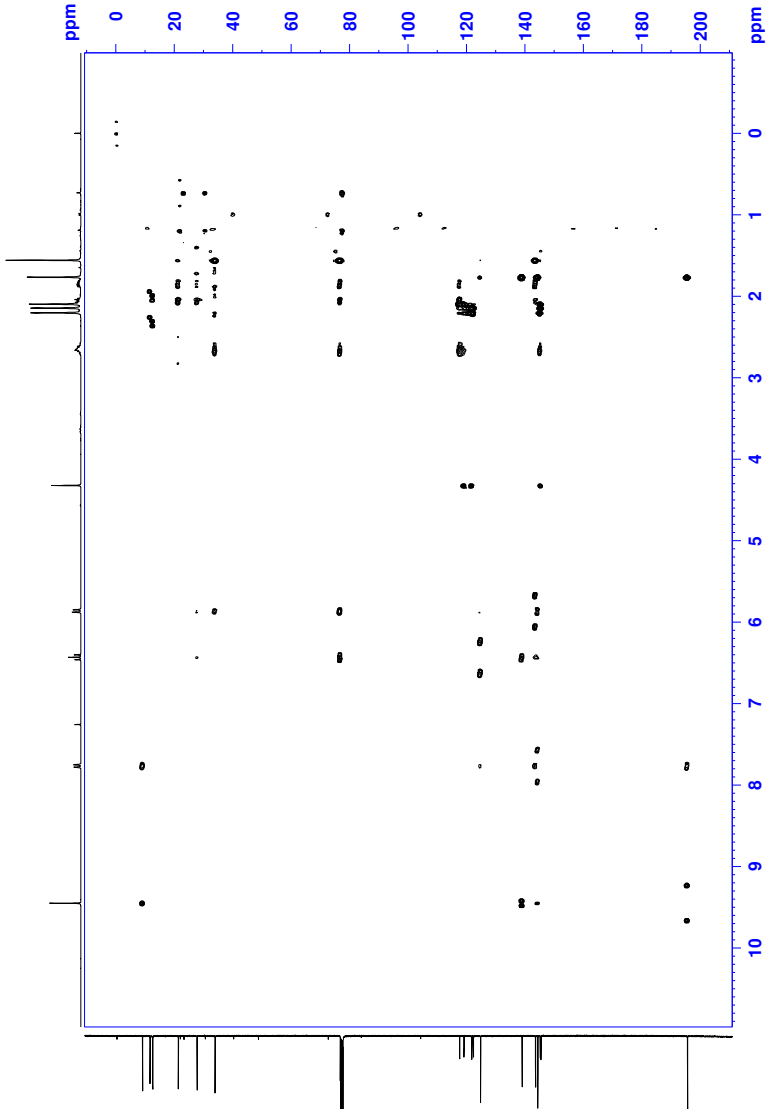

Figure E.7: HMBC NMR spectrum of (4*Z*)-**11**.

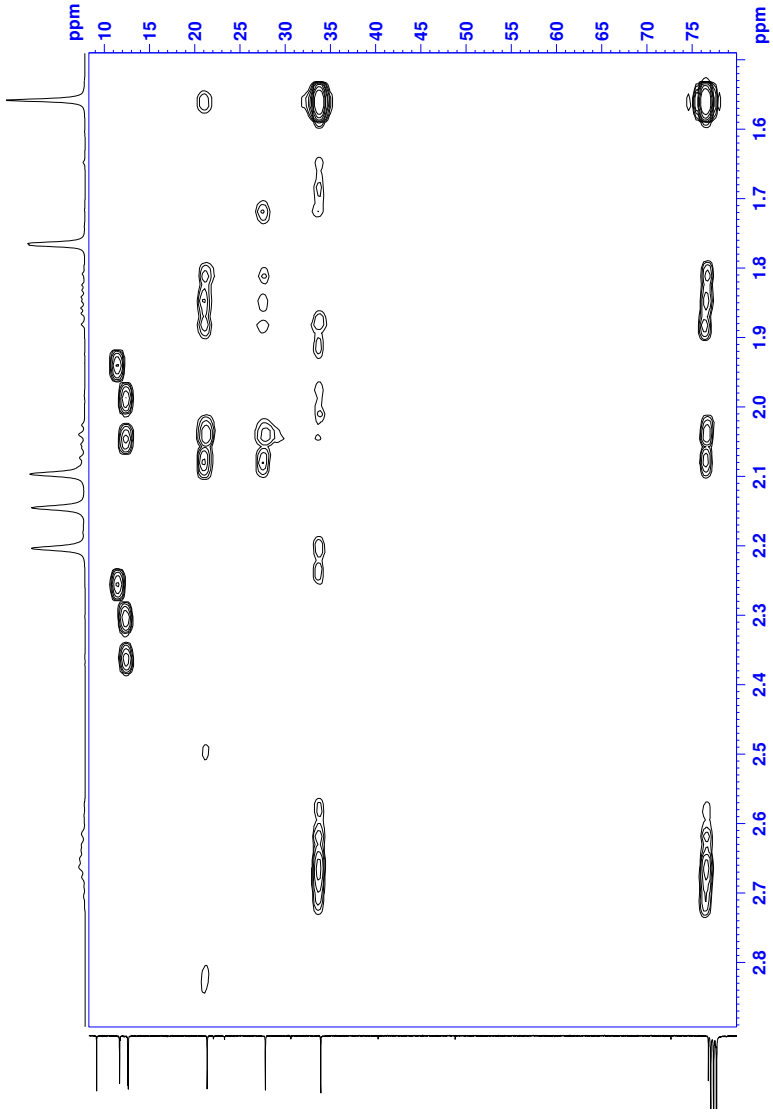

Figure E.8: Enlargements of the HMBC NMR spectrum of (4*Z*)-**11**.

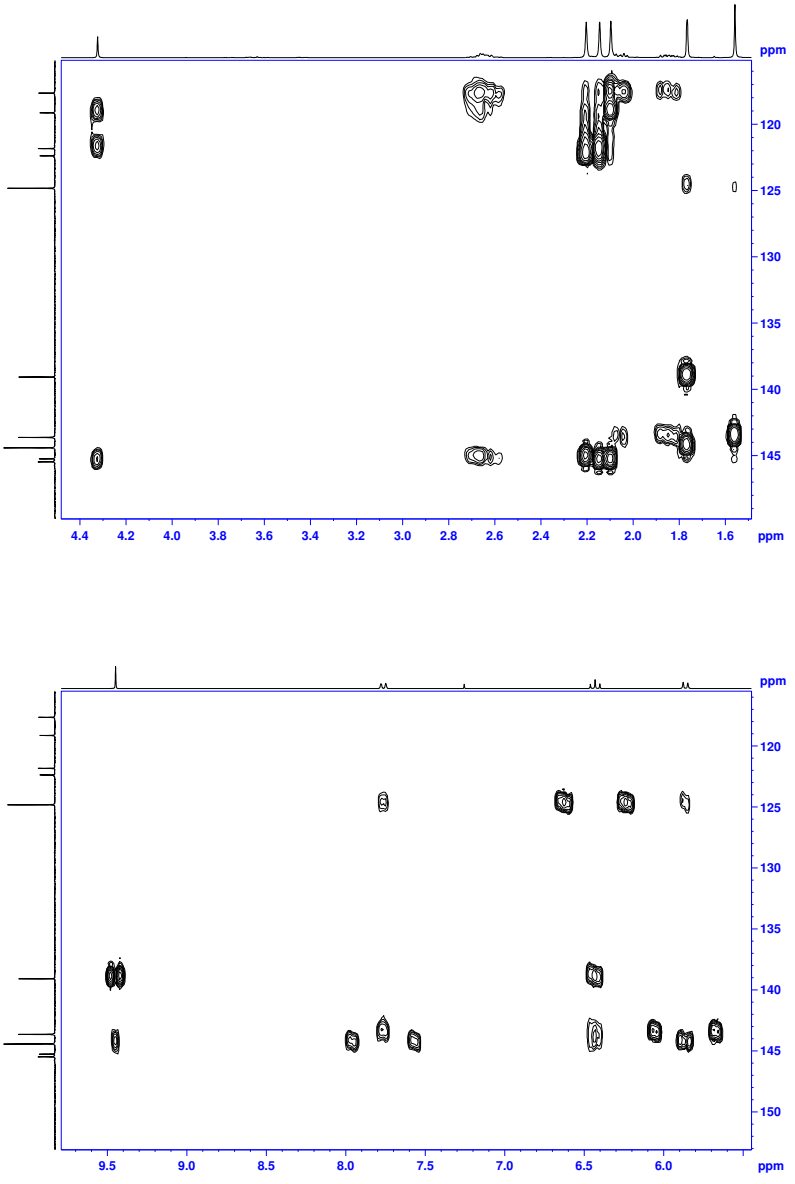

Figure E.8: Enlargements of the HMBC NMR spectrum of (4*Z*)-**11** (cont.).

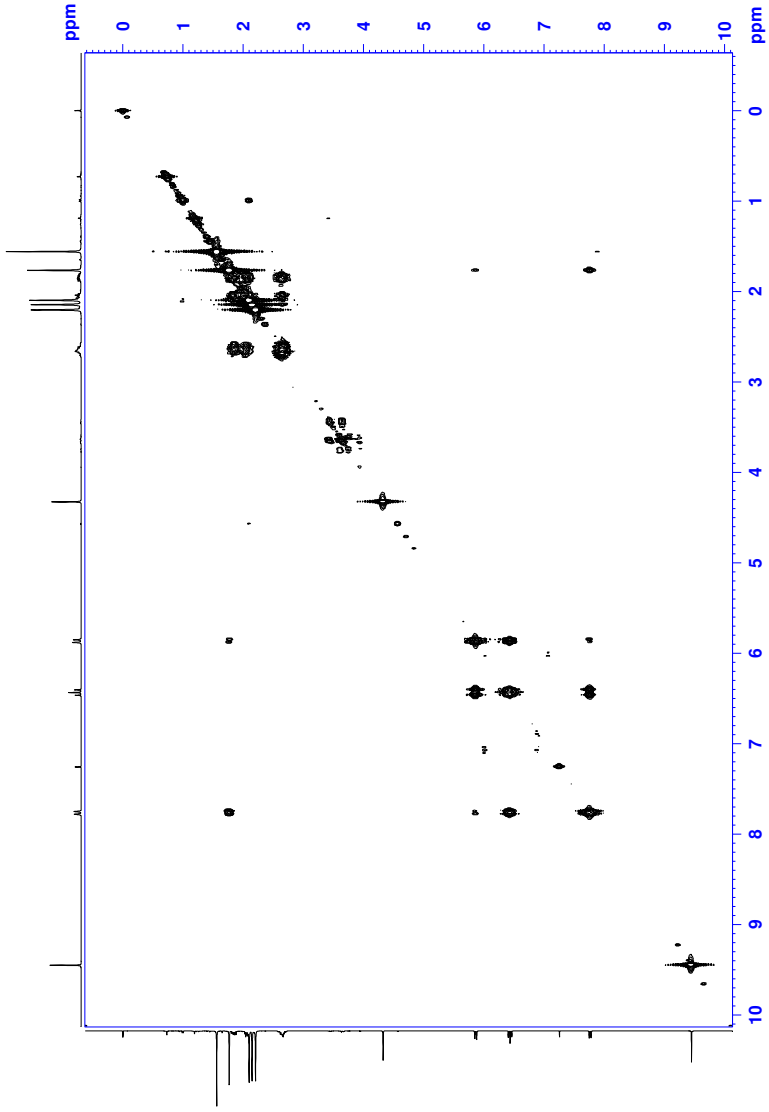

Figure E.9: COSY NMR spectrum of (4*Z*)-**11**.

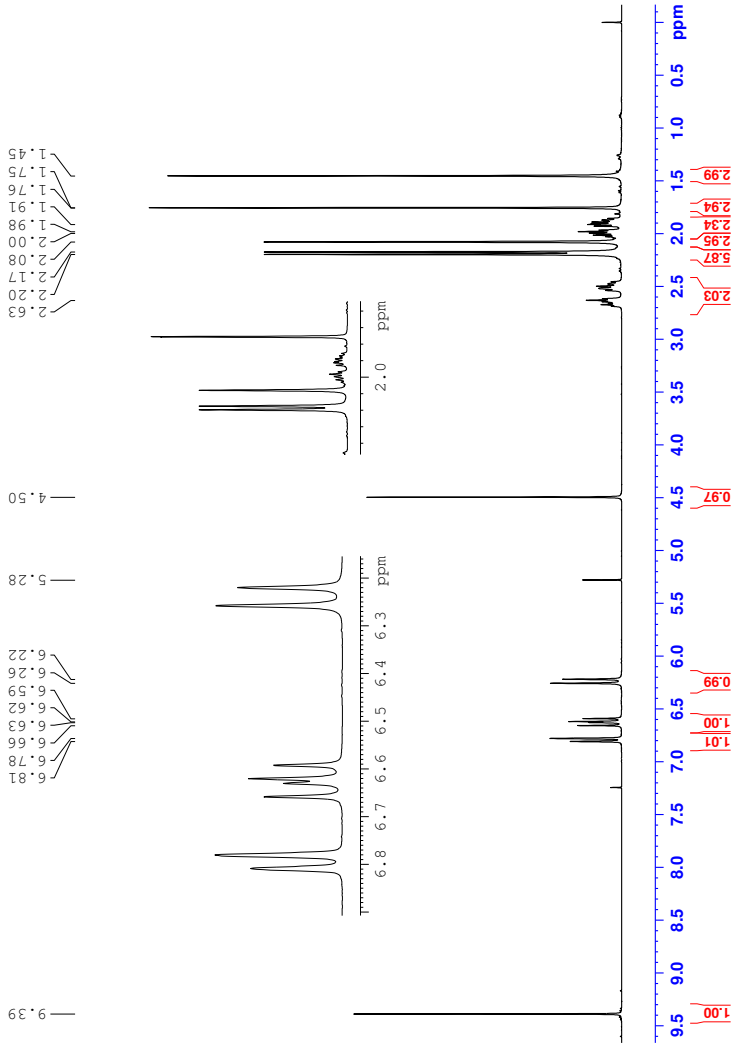

Figure E.10: ^{1}H NMR spectrum of (4*E*)-**11**.

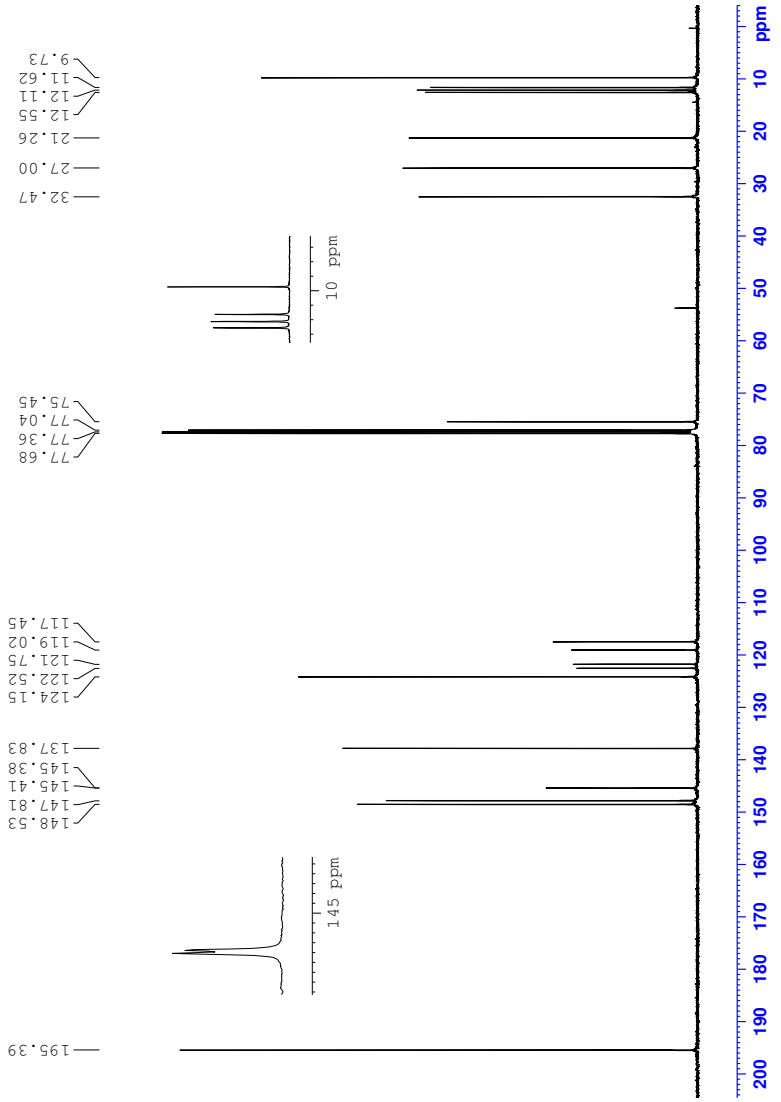

Figure E.11: ^{13}C NMR spectrum of (4*E*)-**11**.

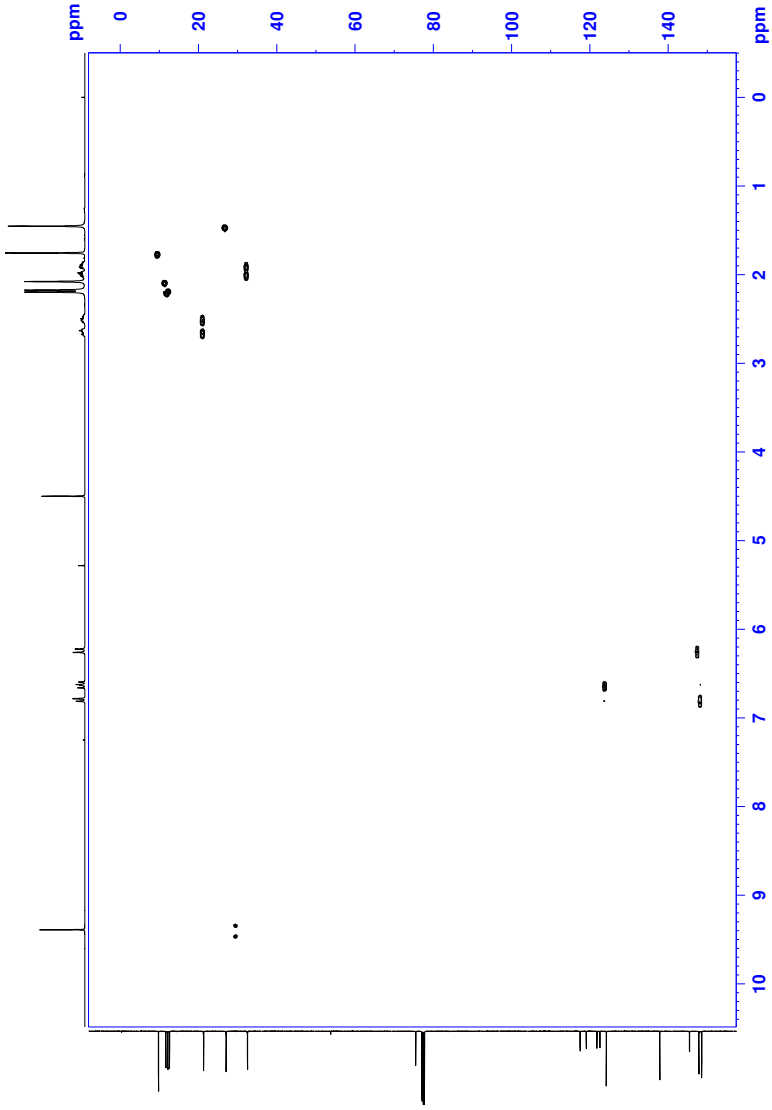

Figure E.12: HSQC NMR spectrum of (4*E*)-**11**.

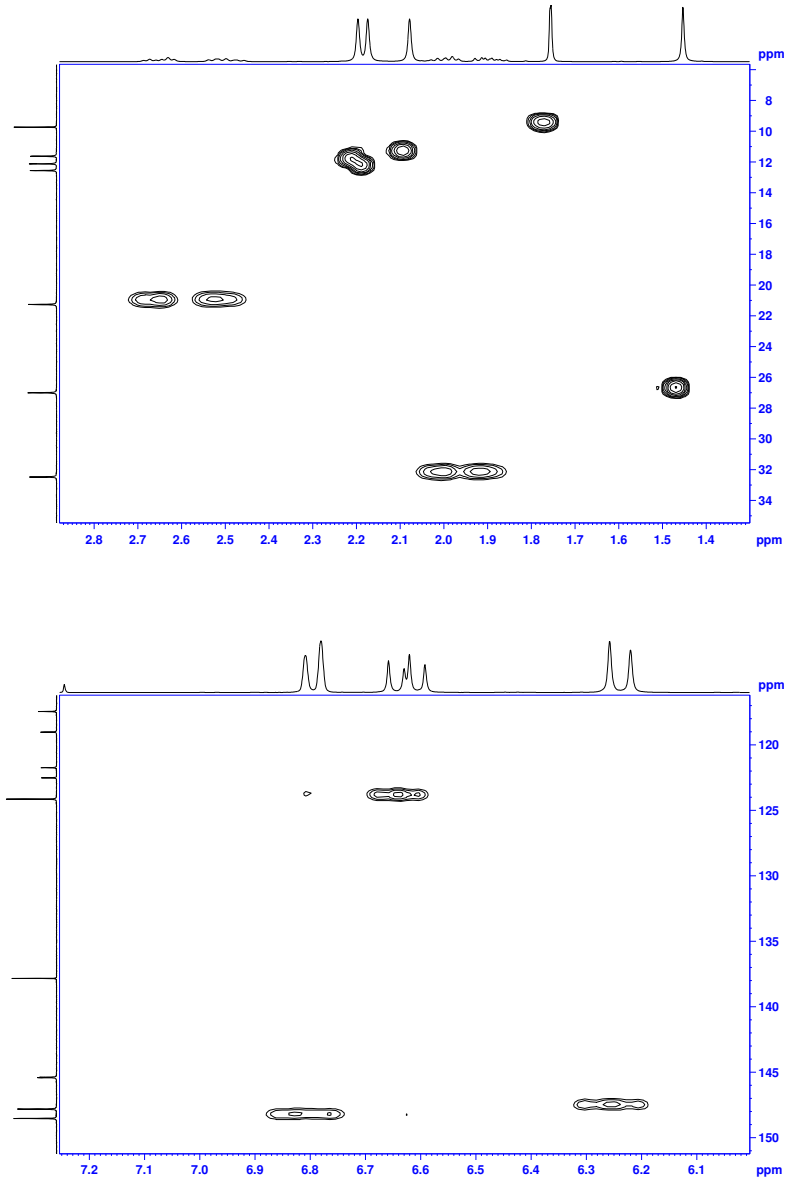

Figure E.13: Enlargements of the HSQC NMR spectrum of (4*E*)-**11**.

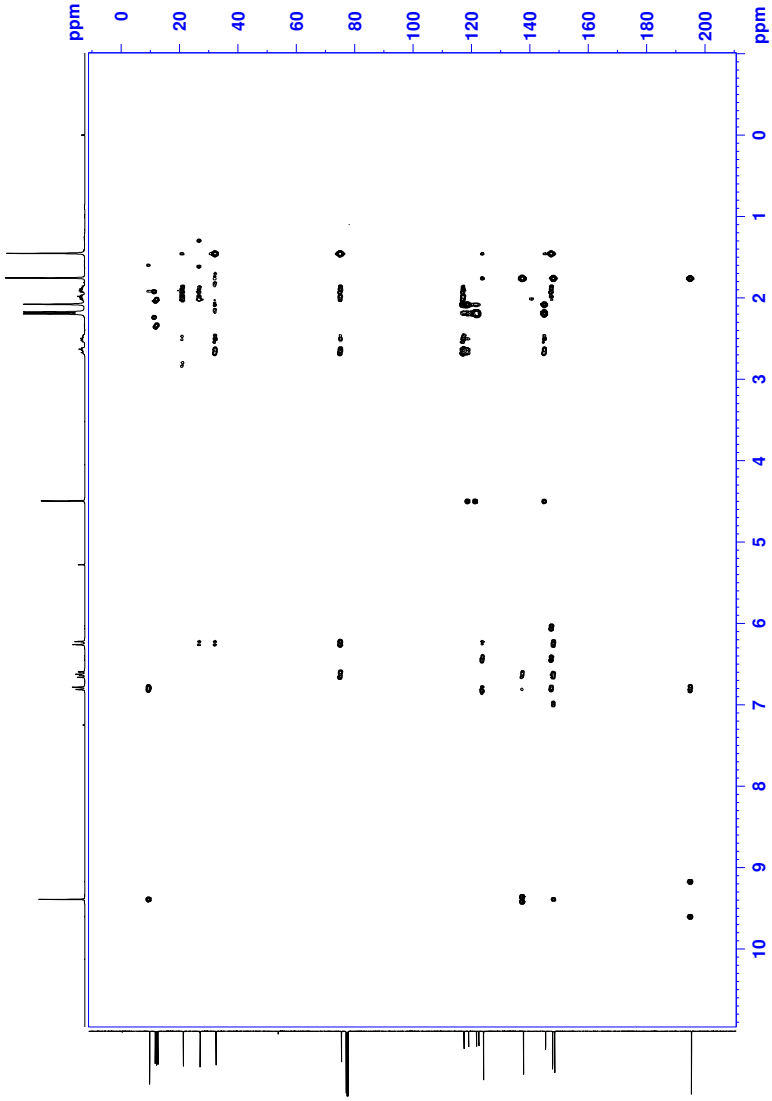

Figure E.14: HMBC NMR spectrum of (4*E*)-**11**.

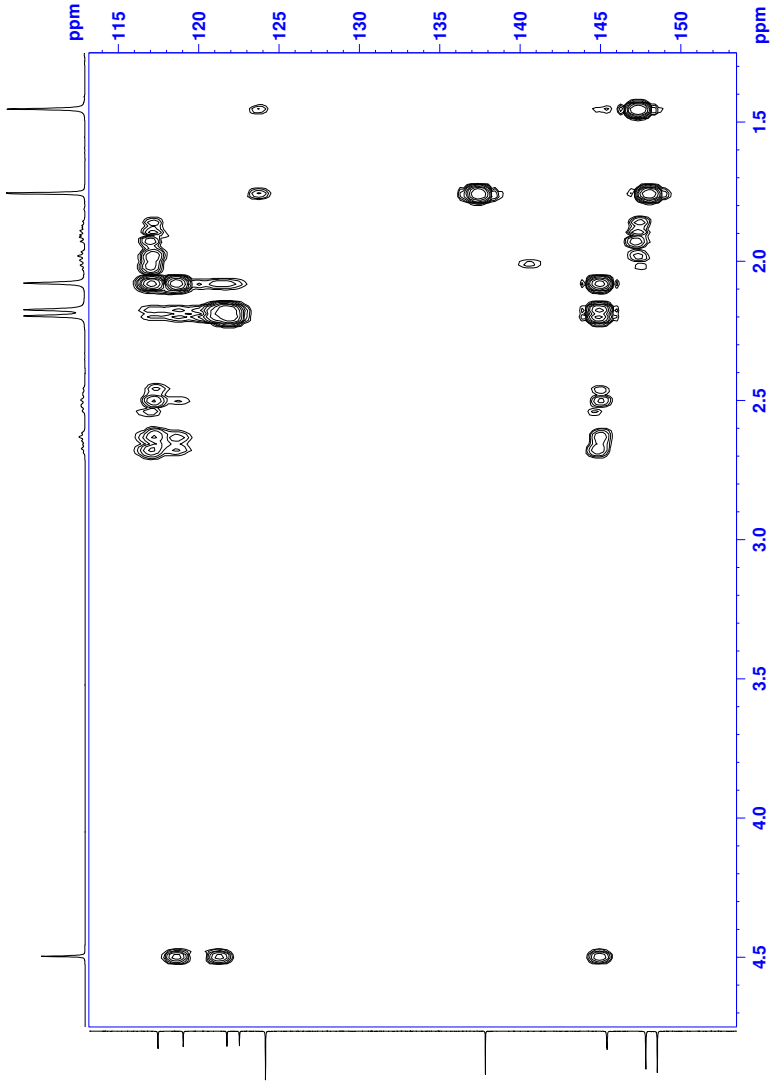

Figure E.15: Enlargements of the HMBC NMR spectrum of (4*E*)-**11**.

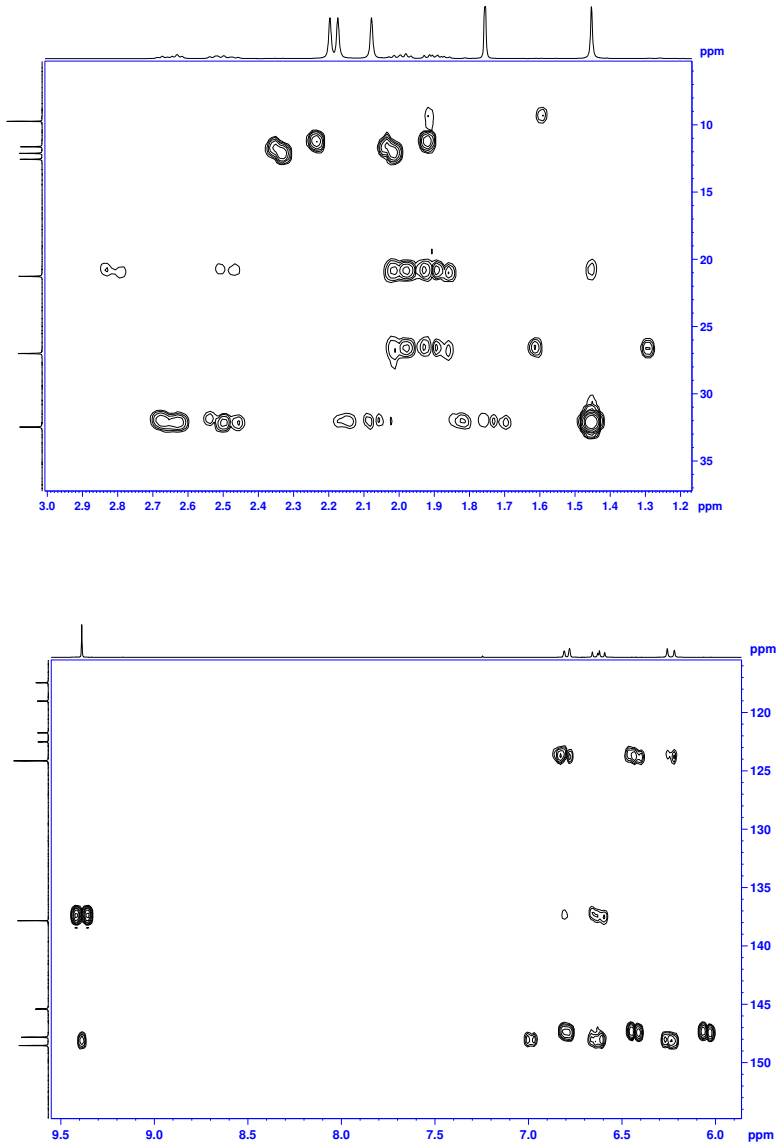

Figure E.15: Enlargements of the HMBC NMR spectrum of (4*E*)-**11** (cont).

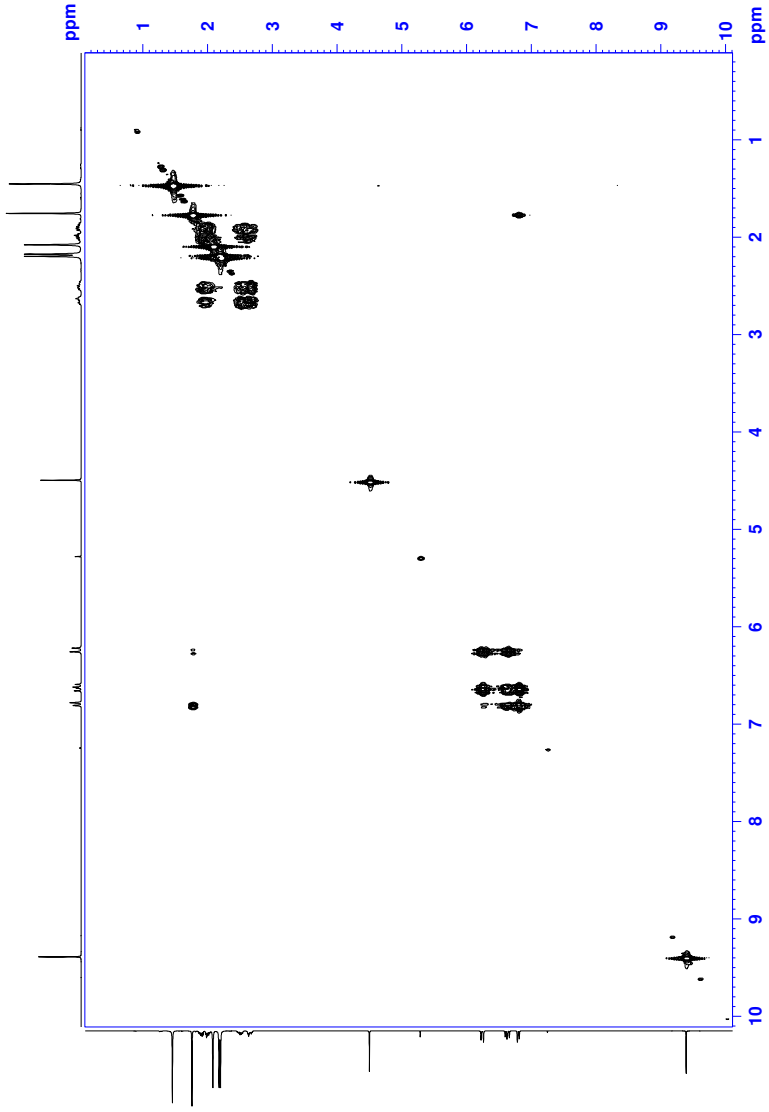

Figure E.16: COSY NMR spectrum of (4*E*)-**11**.

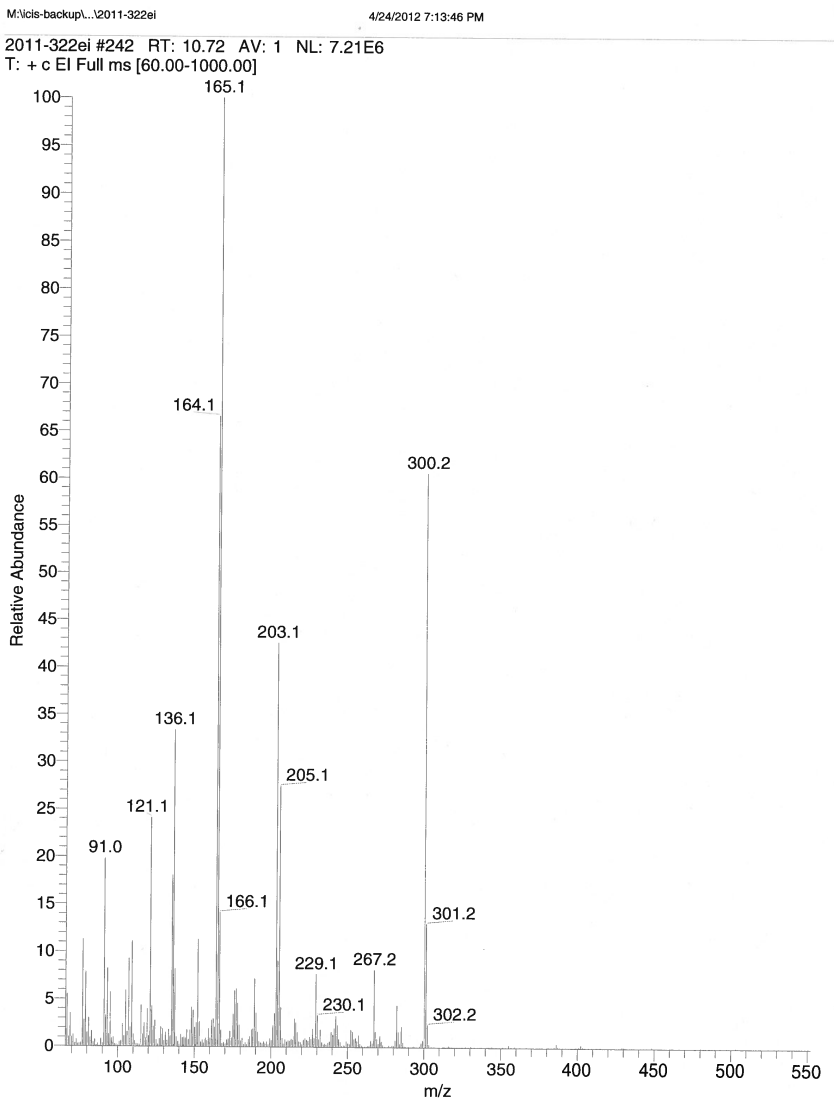

Figure E.17: LRMS spectrum with EI ionization of **11**.

F Spectroscopic data of 12

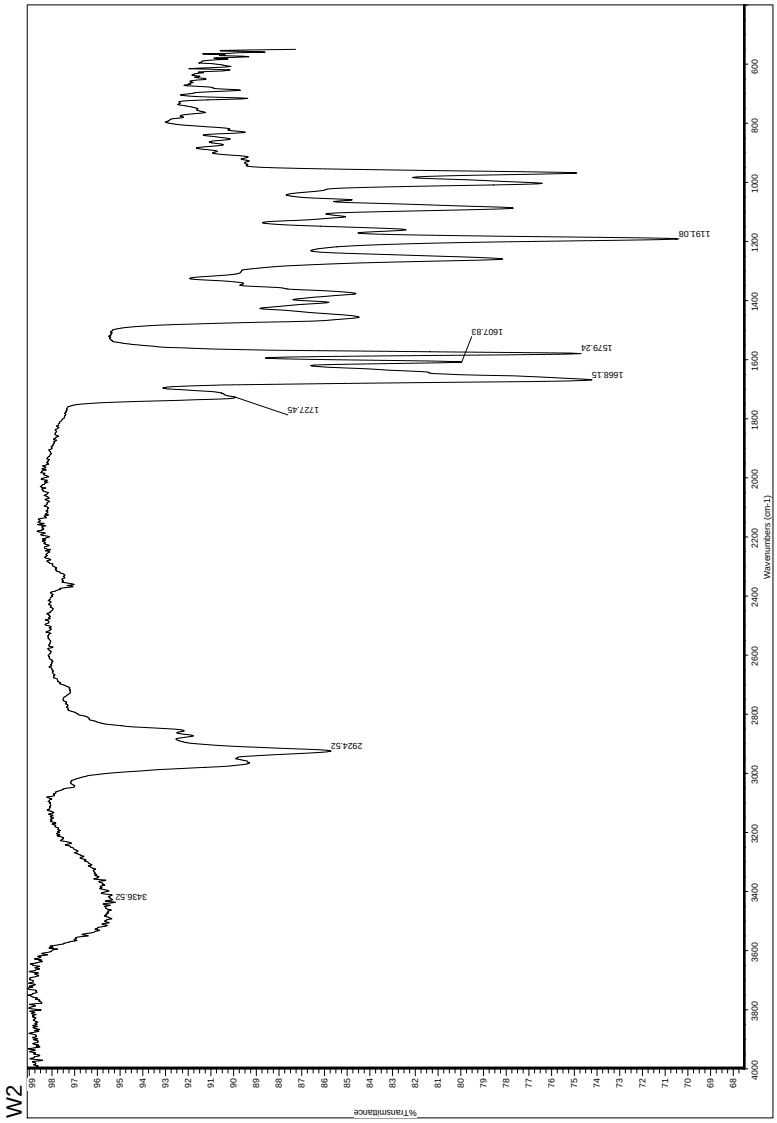

Figure F.1: IR spectrum of **12**.

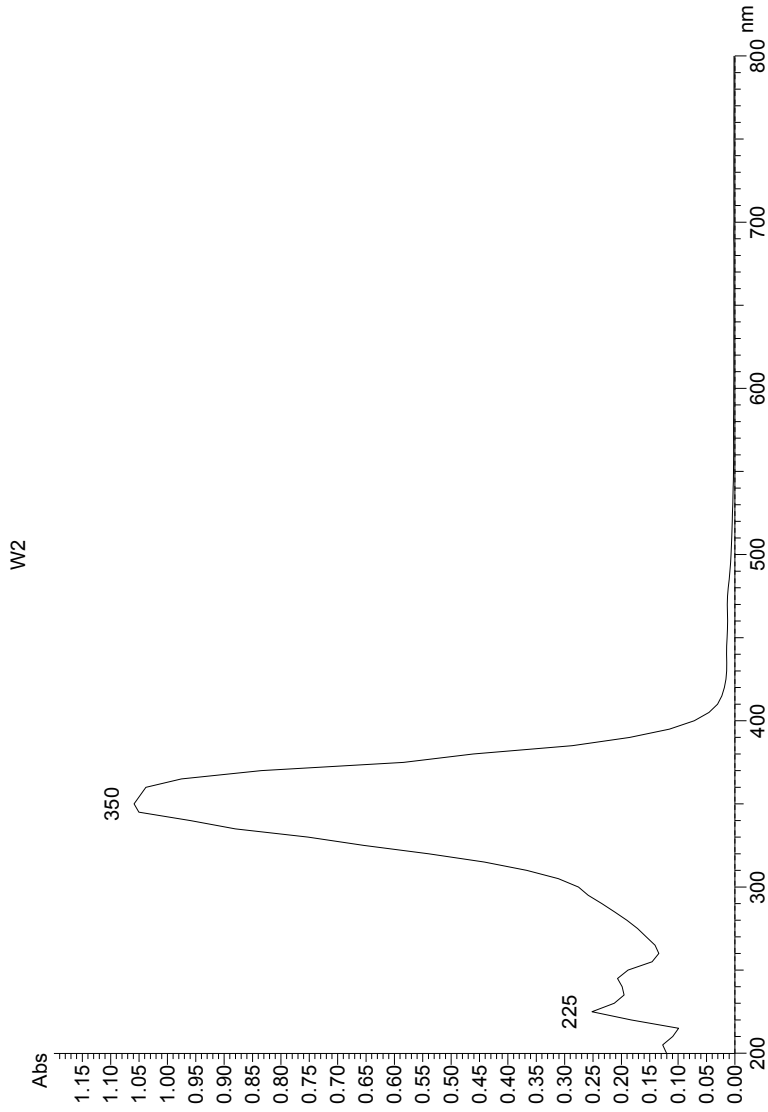

Figure F.2: UV/Vis spectrum of **12**.

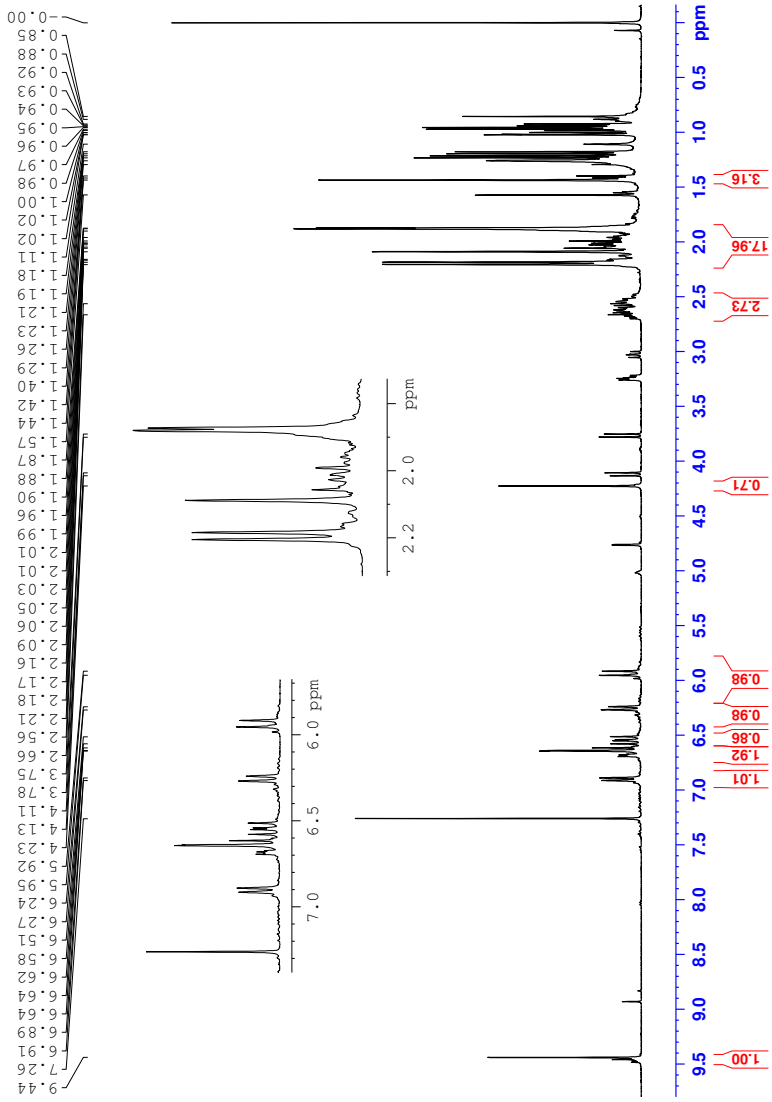

Figure F.3: ^{1}H NMR spectrum of **12**.

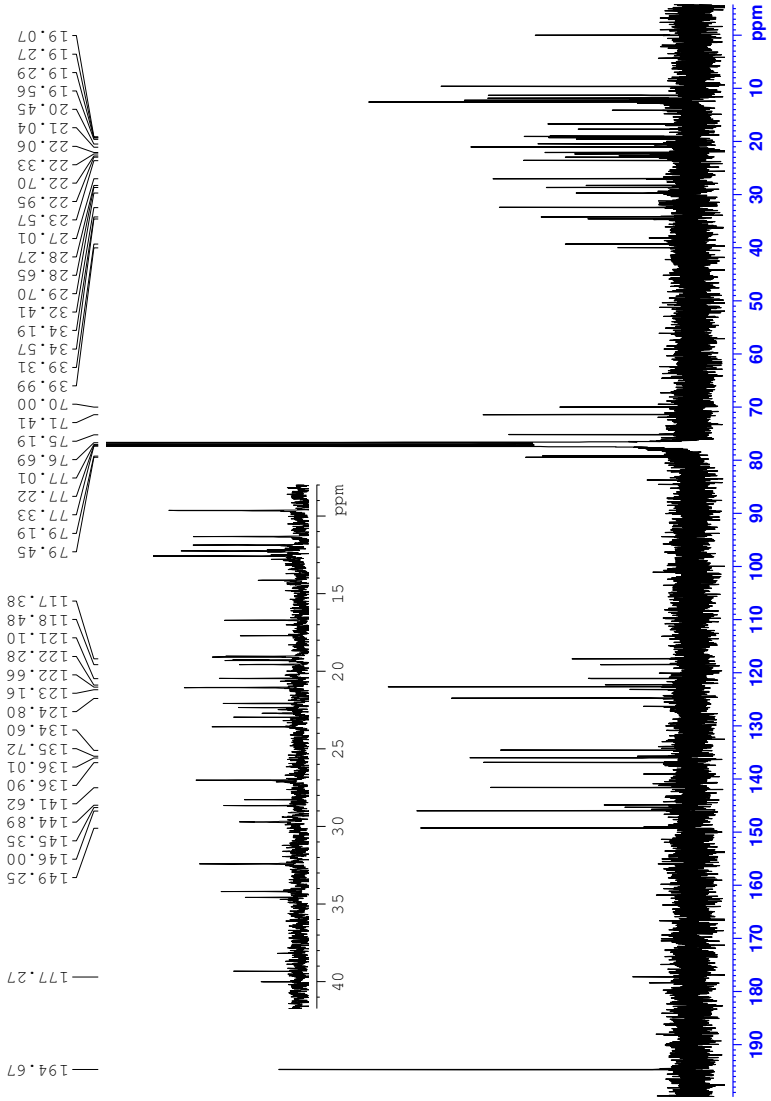

Figure F.4: ^{13}C NMR spectrum of **12**.

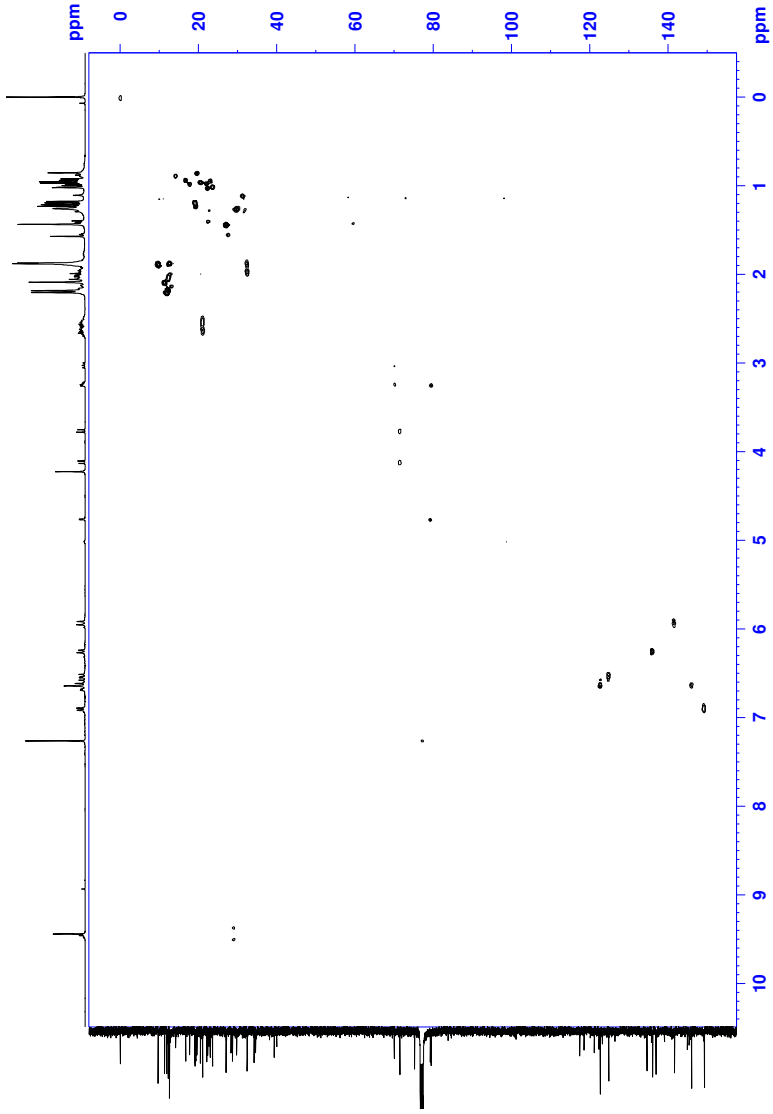

Figure F.5: HSQC NMR spectrum of **12**.

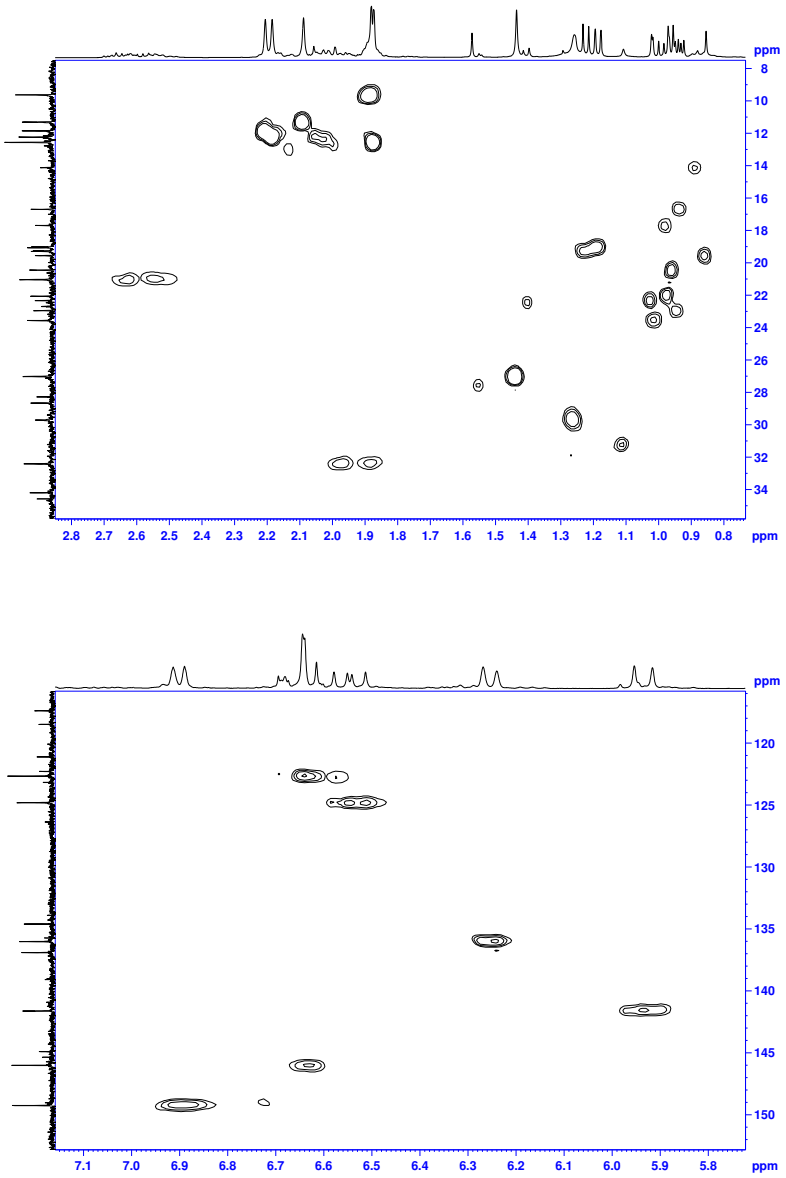

Figure F.6: Enlargements of the HSQC NMR spectrum of **12**.

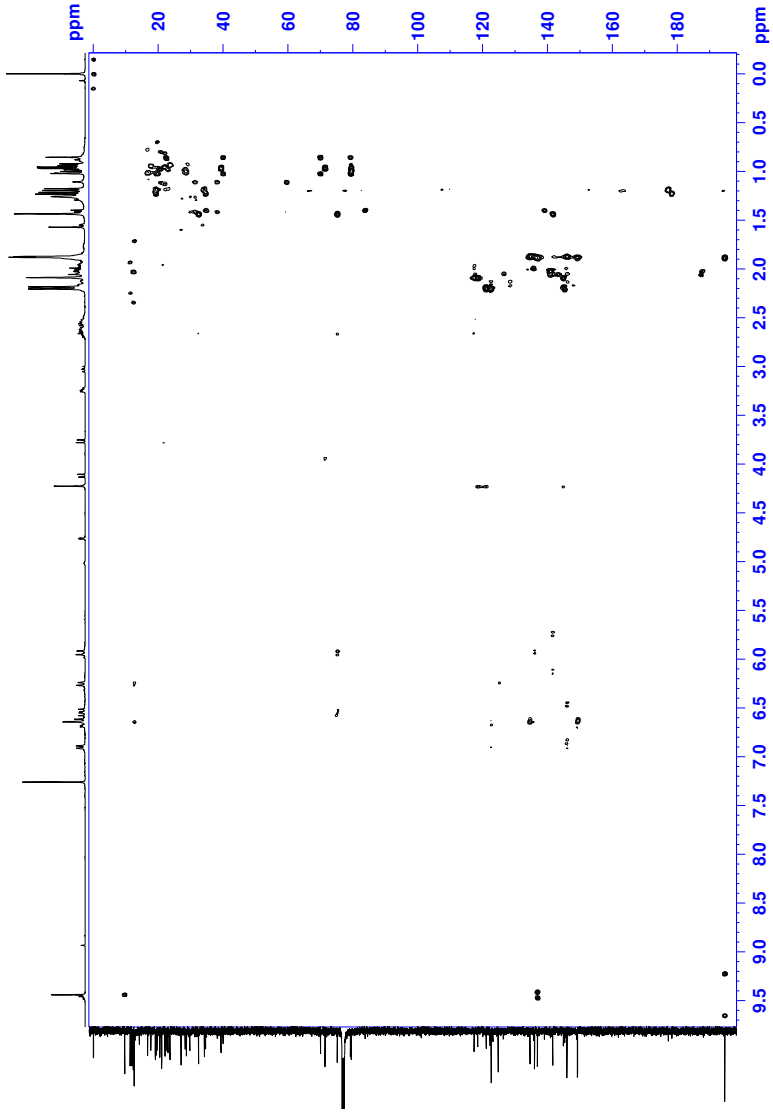

Figure F.7: HMBC NMR spectrum of **12**.

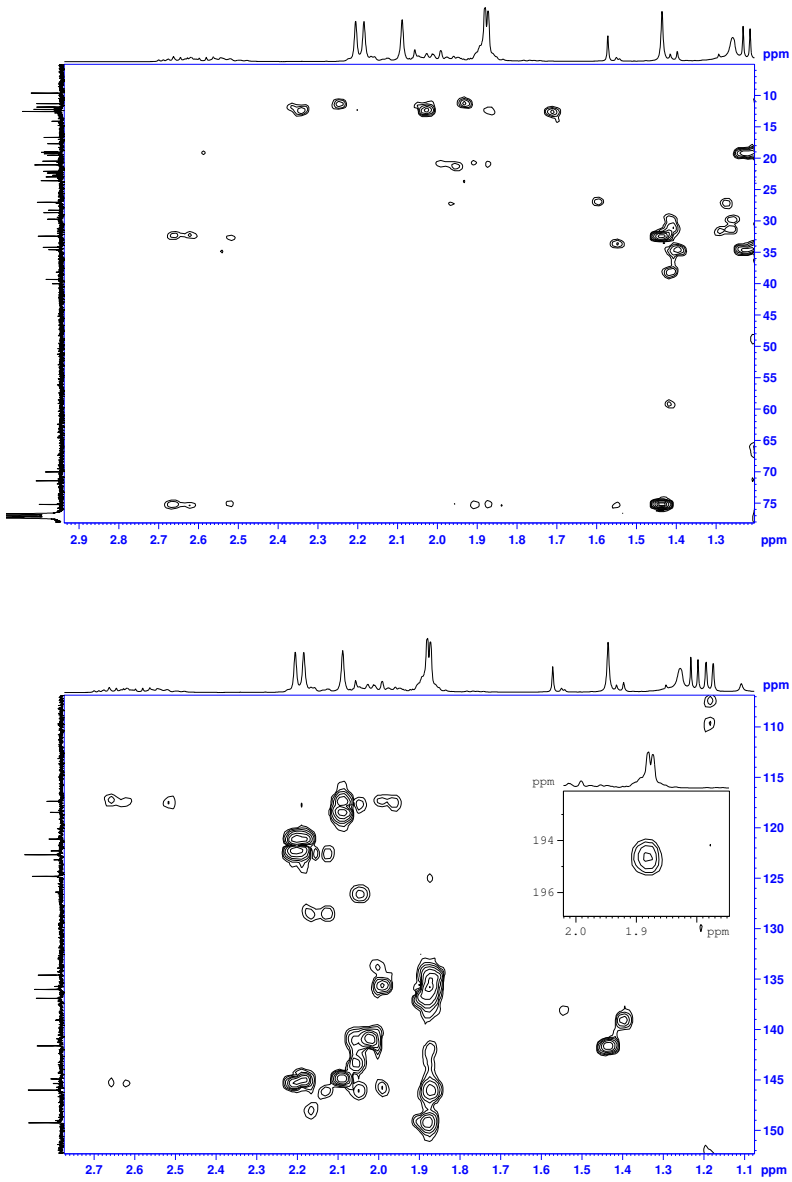

Figure F.8: Enlargements of the HMBC NMR spectrum of **12**.

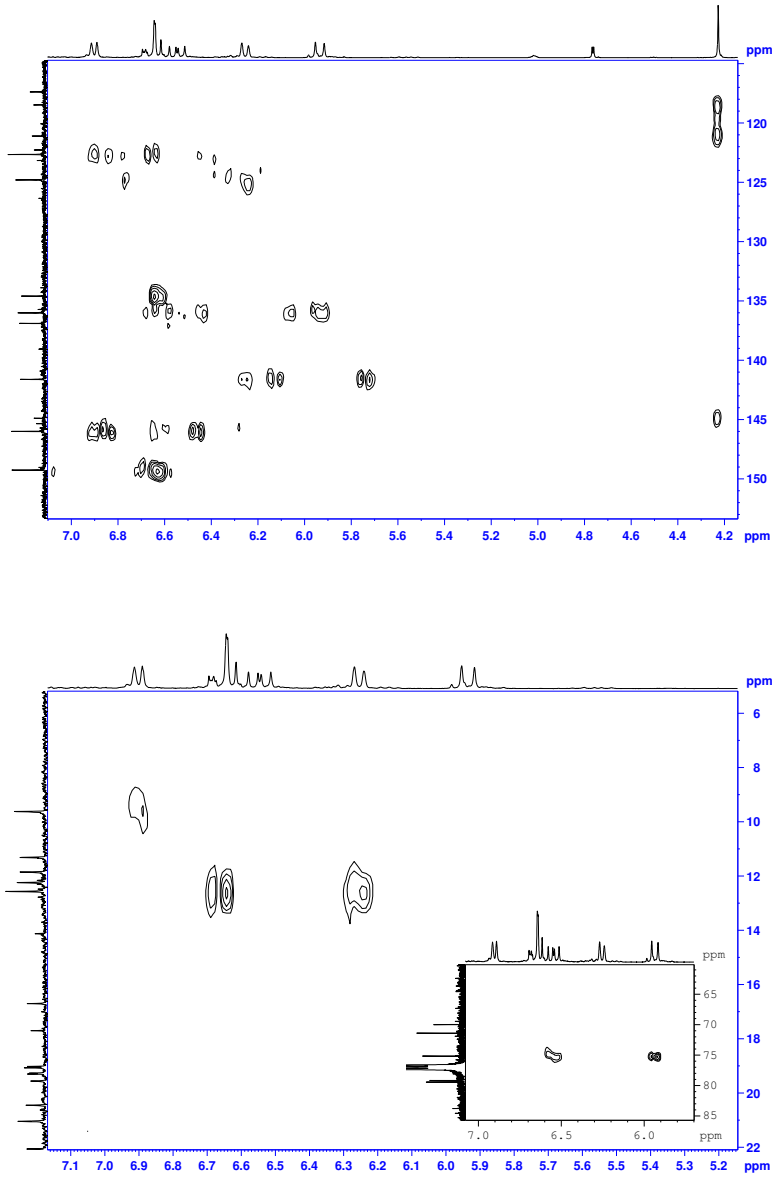

Figure F.8: Enlargements of the HMBC NMR spectrum of **12** (cont.).

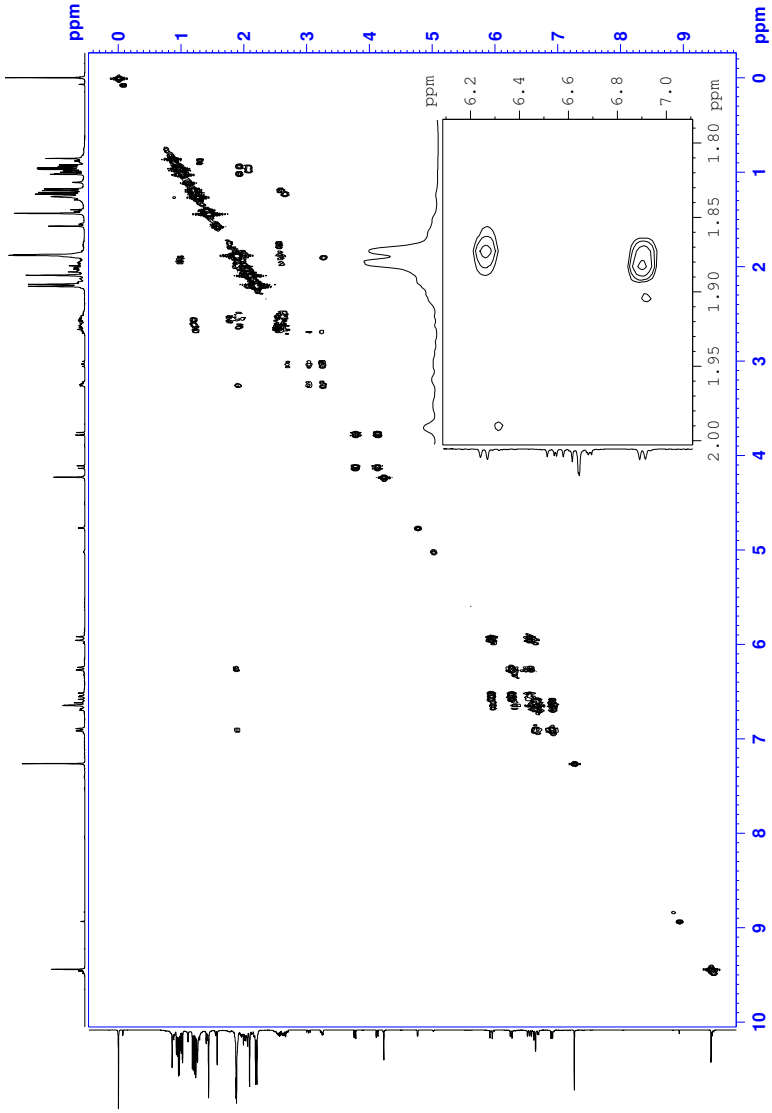

Figure F.9: COSY NMR spectrum of **12**.

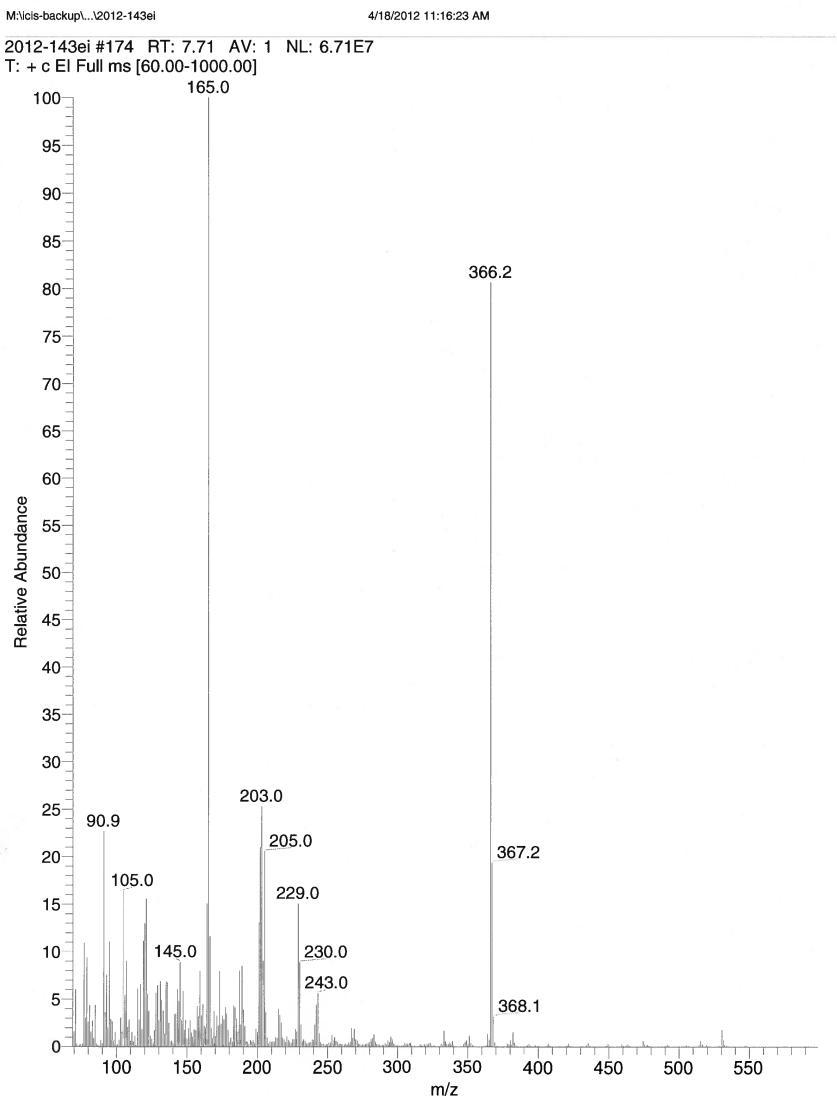

Figure F.10: LRMS spectrum with EI ionization of **12**.

G Spectroscopic data of 9A

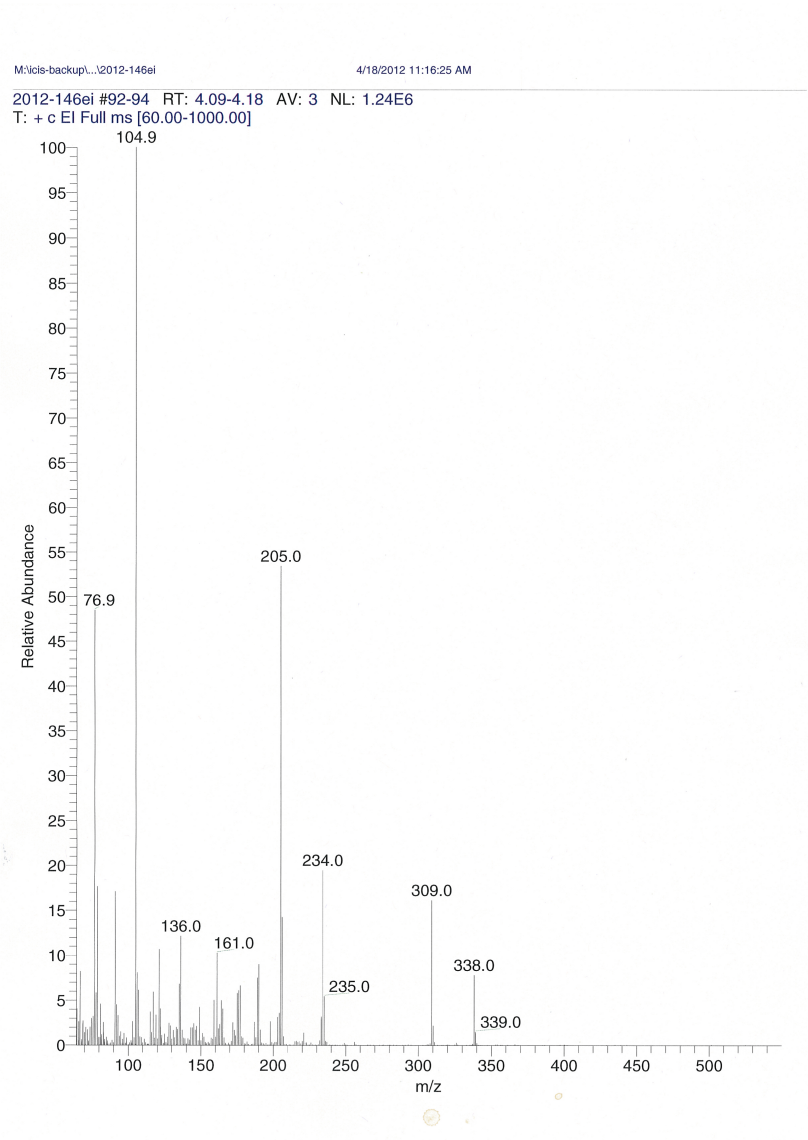

Figure G.1: LRMS spectrum with EI ionization of **9A**.